THE UNIVERSITY OF OKLAHOMA

GRADUATE COLLEGE

EXPERIMENTAL AND NUMERICAL SIMULATION STUDY OF MICROBIAL ENHANCED OIL RECOVERY USING BIO-SURFACTANTS

A DISSERTATION

SUBMITTED TO THE GRADUATE COLLEGE FACULTY

In partial fulfillment of the requirements for the

Degree of

DOCTOR OF PHILOSOPHY

By

SAIKRISHNA MAUDGALYA

Norman, Oklahoma

2005

UMI Number: 3203287

UMI Microform 3203287

ProQuest Information and Learning Company
300 North Zeeb Road
P.O. Box 1346
Ann Arbor, MI 48106-1346

EXPERIMENTAL AND NUMERICAL SIMULATION STUDY OF MICROBIAL ENHANCED OIL RECOVERY USING BIO-SURFACTANTS

A DISSERTATION

APPROVED FOR THE MEWBOURNE SCHOOL OF PETROLEUM AND GEOLOGICAL ENGINEERING

By

_____

DR. ROY M. KNAPP

_____

DR. RICHARD G. HUGHES

_____

DR. MICHAEL J. McINERNEY

_____

DR. DEAN S. OLIVER

_____

DR. MICHAEL L. WIGGINS

DEDICATION

To my parents, sister and teachers

ACKNOWLEDGEMENTS

I would like to first thank Dr. Roy Knapp for guiding me through my Masters and Doctoral studies program. It is through his patience and teaching that I could reach where I am today. I thank Dr. Richard Hughes for the profound influence he has had on me. I leave this program having gained a great mentor and a life long friend because that is the way he always treated us students. I also thank Dr. McInerney and am grateful for his advice and encouragement at important junctures of my studies here at the university. I thank Dr. Oliver and Dr. Wiggins for being on my doctoral advisory committee.

Others who deserve my gratitude are Dr. Nagle and Martha Folmsbee. I am especially grateful to Martha for having assisted me in taking laboratory measurements and credit for the experimental work presented here should be shared with her. I thank Mike Shaw for helping while constructing the experimental setup and providing invaluable assistance whenever the apparatus experienced breakdowns.

Some individuals who insisted that I acknowledge them in my dissertation are Dharti, Susmith, Kevin and Matt. I appreciate their encouragement and wishes through the duration of my studies. And lastly, I thank the United States Department of Energy for providing financial assistance for conducting this research.

TABLE OF CONTENTS

LIST OF TABLES

LIST OF FIGURES

Figure **Page**

ABSTRACT

An experimental and numerical study were conducted to investigate the ability of bio-surfactant produced by the microbe *Bacillus mojavensis* strain JF-2 to recover residual oil from consolidated porous media. Experiments showed that the bio-surfactant at concentrations as low as 40.0 ppm (0.04 mg/scc) and viscosified with 1000.0 ppm of polymer could recover 10.0 % to 40.0 % of residual oil when injected through sandstone cores at typical field rates.

A 2-phase, 10-component microbial enhanced oil recovery numerical simulator was modified to include reservoir salinity and facilitate surfactant and polymer injection. The effects of reservoir brine salinity and divalent ion effects on bio-surfactant and polymer adsorption, polymer retention, polymer viscosity, bio-surfactant interfacial tension and the shear rate effect on polymer viscosity were added to the simulator. Core flood experiments where JF-2 bio-surfactant viscosified with partially hydrolyzed polyacrylamide was injected into Berea cores at waterflood residual oil saturation were simulated. The effects of brine salinity and hardness on surfactant and polymer behavior were tested and the core flood simulation results compared with the experimental results.

After the laboratory and simulation studies, a residual oil recovery method based on non-aqueous phase liquid (NAPL) contaminant removal from aquifers is discussed and functional form of the transport equation presented. In this method, residual oil is treated as another chemical species dispersed in porous media instead of a phase that is uniformly distributed across the media.

EXPERIMENTAL AND NUMERICAL SIMULATION STUDY OF MICROBIAL ENHANCED OIL RECOVERY USING BIO-SURFACTANTS

CHAPTER 1

INTRODUCTION

Microbial enhanced oil recovery (MEOR) has long been considered by scientists and microbiologists as a relatively cheap method to recover tertiary oil from reservoirs[1]. MEOR can recover tertiary oil by improving macroscopic sweep efficiency through microbially induced permeability profile modification; or reducing interfacial tension between oil and water with microbial bio-surfactants to lower the capillary trapping forces; or stimulating the reservoir porosity and permeability with microbial products such as acids, or combining all three mechanisms[1]. This dissertation focuses on the application of bio-surfactants produced by microbes to recover residual oil trapped within the pores of a rock.

At the end of waterflooding of reservoirs, a large quantity of oil may remain trapped within the reservoir. The oil is retained by capillary forces acting on oil globules within the porous medium. Surfactants reduce capillary forces by lowering the interfacial

tension between oil and water. This allows any displacing force such as the viscous force of injected or flowing surfactant to recover some of this oil. Microbial bio-surfactants are similar to synthetic surfactants in terms of the oil recovery mechanism. What differentiates them from synthetic surfactants is that they are generated *in situ*, inside the reservoir, by microbes when sufficient nutrients and suitable conditions are present.

1.1 Laboratory experiments and numerical simulation of bio-surfactant based tertiary oil recovery.

For this dissertation, the ability of the bio-surfactant produced by a microbe called *Bacillus mojavensis* (earlier known as *Bacillus subtilis*) strain JF-2 to recover residual oil was investigated[2]. Studies[3,4] have reported that this bio-surfactant can reduce the interfacial tension between oil and water to nearly 0.001 dynes/cm as compared to 29-40 dynes/cm for normal oil-water IFT without any surfactant. Laboratory experiments have reported that the JF-2 bio-surfactant when viscosified with a polymer achieved high oil recoveries from sand packs that were at waterflood residual oil saturation[5]. In this work, the bio-surfactant flooding studies were extended to Berea sandstone cores to investigate the bio-surfactant's ability to recover residual oil from consolidated porous media.

Since laboratory core experiments are time consuming, it is not feasible to conduct them every time a new microbial recovery process is tested. For testing and development, an accurate numerical simulator can be a valuable tool for researchers. Simulation provides the ability to test different recovery processes under varying conditions without having to resort to time consuming laboratory experiments. A MEOR simulator previously developed by Xhang[6] was modified to improve its ability to predict oil recovery by bio-surfactant treatment. Changes made to the simulator included modifying

the interfacial tension bio-surfactant concentration relationship, incorporating a polymer flow model, modeling polymer retention and the resulting permeability reduction and introducing brine salinity and modeling salinity effects on surfactant and polymer behavior.

This dissertation is divided into two parts. In the first part, experiments with JF-2 bio-surfactant are reported. First, studies to develop a model between interfacial tension (IFT) and JF-2 bio-surfactant concentration and model brine salinity effects on IFT are described. Laboratory scale JF-2 bio-surfactant floods conducted on Berea sandstone cores at waterflood residual oil saturation are analyzed and reported next.

In the second part of the dissertation, the core flooding experiments were numerically simulated using a modified MEOR simulator. To be able to simulate the experiments, the simulator was modified to include salinity and shearing effects on surfactant and polymer behavior. These are the two most important mechanisms that adversely impact polymers and surfactants. Shearing occurs when the polymer flows through a rock resulting in the loss of viscosity. Brine salinity increases surfactant and polymer adsorption, increases the oil-water IFT and reduces polymer viscosity. High brine salinity is a primary cause for the loss of surfactant effectiveness and polymer solution viscosity in a reservoir[7,8]. Since field conditions involve the flow of micellar-polymer solutions through brine saturated porous media, it was important that the effects of aqueous phase salinity on bio-surfactant adsorption, IFT, polymer viscosity, polymer adsorption and the effect of shearing on solution viscosity be included in the simulator when modeling real reservoirs. The simulator was tested and the core flood experiments were simulated after the modifications were made.

As part of the modifications, the mathematical relationships derived earlier in the experiments section between JF-2 bio-surfactant concentration and IFT and between change in IFT and aqueous phase salinity were added to the simulator. The simulator was also modified to use the trapping number instead of the capillary number to calculate new residual oil saturations and phase relative permeability. Studies indicate that the trapping number is a more useful measure of the forces that retain oil than just the capillary number[9]. The trapping number has been used and tested in other chemical flood numerical simulators[10].

1.2 A new model for surfactant based tertiary oil recovery.

A method to simulate residual oil mobilization in tertiary oil recovery as organic chemical contaminant removal from an aquifer is discussed. This method is motivated by the approach used by hydrologists and environmental engineers to simulate non-aqueous phase liquid contaminant (NAPL) removal from aquifers and soils[11]. It is believed that simulating tertiary recovery as a contaminant transport problem in a single aqueous phase would represent the physics of the process more realistically and could be simpler than the multiphase multicomponent finite difference simulation approach. An advantage of this method is that it can be used to simulate component transport by streamlines resulting in better reservoir description and reduced computation times[12] .

1.3 Chapter descriptions and summary.

Following the introductory first chapter, chapter two surveys the previous work reported on MEOR laboratory and field studies and the efforts to numerically model MEOR processes. Chapter three describes the laboratory experiments conducted to test the JF-2 bio-surfactant on Berea sandstone cores and generate data to develop

mathematical models to modify the MEOR simulator. In chapter four, development of the numerical models is described and in chapter five, the modifications to the simulator are tested. Some of the core flood experiments are simulated and results compared with their experimental values. In chapter six, the new approach to tertiary oil recovery simulation where residual oil recovery is treated as a chemical species transport problem is discussed. And in the last chapter, chapter seven, the conclusions and recommendations are presented.

CHAPTER II

LITERATURE REVIEW

In this chapter, a survey of existing literature on microbial enhanced oil recovery (MEOR) processes and processes related to micellar/surfactant-polymer flooding is presented. This survey will focus on laboratory experiments, mathematical modeling and numerical simulation of surfactant based MEOR and enhanced oil recovery (EOR).

2.1 MEOR experimental work.

Donaldson *et* al.[1] report that microbial enhanced oil recovery was first studied by Beckman in 1926 who discovered that certain microbes when grown in the presence of nutrients could free oil from oil saturated porous media. Zobell[13,14], who experimentally demonstrated the release of oil from oil sands by certain sulfate reducing bacteria, continued Beckman's work. Yarborough and Coty[15] report that the first ever MEOR field test was conducted by the Mobil Research Laboratory in 1954. Significant improvements in oil recovery were not observed but it provided scientists with an understanding of the interaction between different microbes in a reservoir and the importance of proper and sufficient nutrients. Since then, many field trials and laboratory studies have been done to study the mechanisms and processes in microbial enhanced oil recovery. Lazar[16] and

Moses[17] present comprehensive surveys of field trials around the world and analyze reasons for their success and failures.

2.2 *Bacillus mojavensis* strain *JF-2*.

Different bacteria are considered in MEOR. Lazar's[16] survey of field trials indicated that the main species of MEOR bacteria are *Clostridia*, *Pseudomonas* and *Bacillus*. Marsh et al.[18] studied and compared the properties of *Clostridium* and *Bacillus* bacteria. *Clostridium* was a good acid and gas producer and *Bacillus* was a good bio-surfactant producer. Lin et al.[3] observed that one of the strains of *Bacillus* called *Bacillus licheniformis* strain JF-2 anaerobically produced bio-surfactant that lowered interfacial tension between crude oil and brine from 29-35 dynes/cm to nearly 0.001 dynes/cm. Jenneman et al.[19] studied the use of the JF-2 bio-surfactant to recover residual oil from sandstone cores. Folmsbee et al.[2] renamed the bacterium to *Bacillus mojavensis* strain JF-2. Lin et al.[3] also reported that the critical micellar composition (CMC) of the JF-2 bio-surfactant was equal to 11.0 ppm. The CMC is the surfactant concentration where the lowest IFT could be observed. Mulligan et al.[20] reported that the JF-2 bio-surfactant is anionic in nature. This simplifies JF-2 bio-surfactant analysis because its behavior would be similar to well characterized synthetic anionic surfactants. Subsequently, Maudgalya[5] showed in laboratory flooding experiments that low concentrations of the JF-2 bio-surfactant when mixed with a mobility reducing agent and a co-surfactant alcohol to increase the bio-surfactants salinity tolerance could recover significant fractions of residual oil from unconsolidated porous media.

2.3 Surfactants and enhanced oil recovery.

Rosen[21] has written a very detailed text on surfactant behavior. Surfactants are used for oil recovery because of their ability to reduce the interfacial tension between oil and water and thereby mobilize the oil. Pursley et al.[22] reported one of the earliest field tests that employed surfactants to recover oil from a waterflooded oil reservoir in the Loudon field, Illinois. The test used a sulfonate surfactant and resulted in a small improvement in the oil fraction of the produced fluids stream suggesting that the surfactant successfully mobilized some residual oil. Green and Willhite[23] provide an extensive list of surfactant based field tests. Laboratory testing of surfactants for oil field applications is also widely reported in literature. Green and Willhite[23] stated that anionic and non-ionic surfactants were more suitable for oil field recovery applications since they are relatively stable and have low adsorption tendencies. Winsor as reported by Lake[24], Healy and Reed[25] and Nelson and Pope[26] extensively studied the effect of brine salinity on surfactant behavior. Winsor, according to Lake[24] was the first person to show the shifting of a crude oil-water-surfactant microemulsion from a water external state to an oil external state as brine salinity increased. Healy and Reed[25] described the change in micro-emulsion systems with increasing salinity in terms of Type I, II and III systems. This classification helped relate surfactant behavior to salinity and design surfactants that would work better under different reservoir salinities. Nelson and Pope[26] showed the importance of having a salinity gradient in reservoirs. They explained how different salinities along the surfactant flow path could improve oil recoveries. The salinity gradient approach led to the use of treatment preflush to reduce salinity ahead of the surfactant and to improve surfactant performance. An important outcome of these studies

was the definition of an optimal salinity where the IFT between the microemulsion, oil and water was the lowest. The optimal salinity was an important design parameter for surfactant based enhanced oil recovery and helped estimate surfactant performance. Salter[27] investigated the role of co-surfactant alcohols in surfactant treatments. He showed that adding water soluble low molecular weight alcohol to surfactant solutions increased their optimal salinity.

Surfactant adsorption has been studied by many researchers. An important work was by Meyers and Salter[28] who studied the role of salinity in increasing adsorption of anionic surfactants. Their work led to the use sacrificial chemical agents to lower brine salinity ahead of the surfactant. Wang[29] showed that anaerobic conditions within porous media reduced surfactant adsorption. This was important because reservoirs usually are an anaerobic environment and more accurate estimates of surfactant requirements can be calculated through properly designed laboratory experiment with field cores. Healy et al.[7] studied surfactant flooding behavior in field cores. They explained the effect of flow rates and salinity on oil production and cumulative oil recovery. Smith and Malmberg[30] conducted experiments to measure adsorption losses during surfactant flow through porous media and Lawson[31] explained the differences between anionic and nonionic surfactant adsorption.

2.4 Polymers in micellar-polymer flooding.

Polymers are added to surfactant micellar solutions to reduce the adverse effects of reservoir heterogeneity and improve surfactant sweep efficiency. Green and Willhite[32] report the use of polymers to improve the surfactant sweep efficiency in numerous field tests. Mungan[8], Gogarty[33], Smith [34], and Dauben and Menzie[35] studied polymer

application as a mobility control agent in waterflooding and surfactant flooding. Hirasaki and Pope[36] investigated polymer retention and adsorption in porous media. They described mathematical models for retention and adsorption and how they caused permeability reduction. Gogarty[37] investigated the effects of shearing and mobility control on polymer flow through porous media and showed that close to the wellbore shearing could be high and result in the permanent loss of viscosity of the polymer solution. Dawson and Lantz[38] investigated an important phenomenon in polymer flooding called inaccessible porevolume which caused earlier than expected breakthrough of polymer solutions. Martin and Kantamukkala[39] concluded through laboratory experiments that the level of hydrolysis of polymers, especially polyacrylamides affected the level of adsorption and that calcium and sodium chloride salts adversely affected polymer viscosity and mobility control. Camilleri et al.[40] presented mathematical models that incorporated the work described above and other phenomena.

2.5 Mathematical simulation.

Knapp et al.[41] developed a numerical model to simulate a microbial plugging process. The model investigated the growth and retention of microbes as a stationary phase leading to reduction of permeability of the porous media. The model assumed that development of the stationary phase was due to biomass retention and convective transport was the dominant method of microbial transport. Later, Zhang et al.[42] developed a one dimensional multi-component model that simulated biomass growth, metabolic product formation and nutrient consumption in a MEOR process. The model used a modified Monod equation to describe bacterial growth when two nutrients (substrates) were present. Permeability reduction was assumed to be caused by pore surface retention

and pore throat plugging by the microbes. Sarkar et al.[43] presented a one dimensional, two phase compositional numerical model for bacteria transport in a MEOR process where oil recovery was by bio-surfactant based interfacial tension reduction and selective plugging of higher permeability regions by biomass generated by microbial growth. Islam[44] then presented a mathematical formulation that described microbial movement in a multidimensional system where microbe and nutrient transport equations were coupled to phase flow equations. A drawback of this formulation was that it neglected physical dispersion as a transport mechanism.

Chang et al.[45] incorporated the governing equations for microbial and nutrient transport into a three dimensional, three phase black oil model. It simulated microbial activities from the net flux of microbes by convection and dispersion, microbial growth and decay, chemotaxis, nutrient consumption and deposition of microbes on rock grain surfaces. An IMPES simulator solved for pressure and phase saturations and a direct sparse matrix solver was used to obtain solutions for component transport equations.

As an extension of his previous work where a multicomponent transport model was developed[42], Zhang[6] developed a three dimensional multiphase MEOR simulator. Along with Monod type growth of microbes in the presence of two or more nutrients, the simulator incorporated a model for alcohol induced microbe and product generation inhibition. Component transport was simulated by the fifth order Runge- Kutta-Fhelberg (RKF) or Method Lines (MOC) integration method.

The use of the trapping number instead of the capillary number was first reported by Hornof and Morrow[46]. They performed laboratory experiments to evaluate the effect of buoyancy on residual oil saturation. The defined a dimensionless number called the

Bond number as the ratio between gravity and capillary forces. Jin[47] then combined the Bond and the capillary numbers into another non-dimensional entity called the transport number. Jin[47] also incorporated the transport number into a three dimensional reservoir simulator called UTCOMP.

2.6 A new model for surfactant based tertiary oil recovery.

Stegemier[48] conducted experiments to visualize residual oil distribution in waterflooded oil saturated porous media and related porous media properties to the distribution and morphology of residual oil. Stegemier[48] showed residual oil in water wet reservoirs was distributed as isolated ganglia surrounded by water. Conrad et al.[49] showed through laboratory experiments with packed glass beads and different porous media that organic chemical contaminant distribution in aquifers and soils was similar to residual oil saturation in reservoirs.

A number of scientists have studied contaminant transport for many years. Chevalier and Jason[50] conducted a literature review of two dimensional displacement experiments of non-aqueous phase liquids (NAPLs) in porous media. They report the important studies in the field of lighter and denser organic pollutant removal. Lake et al.[51] presented a fundamental mass balance equation for chemical transport through porous media. The equation was useful to develop models that described surfactant and polymer transport for improved oil recovery. In their work, Lake et al.[51] presented variations of the equation and described the conditions in which the variations were valid. Zheng and Bennet[52] have written a detailed text on chemical species transport and recovery useful for hydrologists and engineers. They derived models for transport of chemical species that included chemical reactions and physical adsorption and desorption of species from

the porous media. Kaluarichchi[53] has also written a detailed text on contamination of groundwater resources by organic pollutants such as benzene and toluene. Kaluarichchi[53] explained groundwater contaminant remediation or removal in laboratory experiments and the numerical methods used to model the process.

Application of finite difference simulation for chemical species transport in petroleum engineering was discussed in the previous section. In the field of streamline simulation for component transport, Thiele et al.[54] developed a three dimensional compositional streamline reservoir simulator. In the model, Thiele et al.[54] did not include physical dispersion in the chemical species transport model but showed that stream line solutions were just as accurate as finite difference solutions but computationally more efficient. Blunt et al.[55] developed a streamline code that included chemical dispersion that had generally been neglected earlier. The chemical dispersion was included as an additive term to the advection equation. Crane and Blunt[12] showed that streamline simulation can simulate advection type transport with no dispersion through porous media using and compared their solutions to those from ECILIPSE, a commercial black oil simulator. Crane and Blunt[12] also presented models that simulated adsorption, chemical reactions and secondary species generation along with chemical transport.

CHAPTER III

EXPERIMENTAL STUDIES

The experiments and data analysis to develop models for predicting JF-2 bio-surfactant based oil recovery and verify that the JF-2 bio-surfactant can recover oil from consolidated porous media are described in this chapter. Experiments for generating data for developing models that describe the relationship between JF-2 bio-surfactant, salinity and oil-water IFT are first described. Data from a bio-polymer characterization study was also analyzed to calculate model parameters that describe polymer flow through porous media. The models will be incorporated in a MEOR simulator to simulate polymer-bio-surfactant based tertiary oil recovery processes.

Polymer and JF-2 bio-surfactant flooding experiments through Berea sandstone cores are described next. Oil recovery was analyzed to determine the ability of JF-2 bio-surfactant to recover waterflood residual oil from consolidated porous media under typical field flowrates. Results of these experiments served as models to verify the MEOR simulator. Conclusions and recommendations follow the experiment description.

3.1 Interfacial tension (IFT) with JF-2 bio-surfactant concentrations and salinity.

3.1.1 Introduction. The variation of interfacial tension (IFT) between crude oil and brine as a function of JF-2 bio-surfactant concentration and salinity was studied in this

experiment. The study was done because the IFT model in the MEOR simulator was based on a decane-brine-sulfonate surfactant system[56] and had not been verified with JF-2 bio-surfactant - IFT measurements. Salinity effect on IFT was studied because it was not included in the MEOR simulator[6]. This study was done to verify the IFT model and modify it if necessary. Since the JF-2 bio-surfactant is an anionic surfactant, salinity should have an adverse impact on IFT and bio-surfactant adsorption[20,21,26]. Compared to synthetic surfactant concentrations in field tests[23], the JF-2 bio-surfactant concentrations produced in the laboratory are at least two orders of magnitude lower. These relatively low concentrations are likely to make the salinity effect more adverse. To understand the relationship between bio-surfactant concentration, salinity and IFT, the change in IFT with JF-2 bio-surfactant concentration was studied at constant salinity. This was followed by a study of IFT variation with salinity at constant bio-surfactant concentrations.

3.1.2. Theory. Brine salinity and surfactant concentration are the most important properties that affect synthetic surfactants because they increase IFT, surfactant adsorption and hasten surfactant degradation. All these effects reduce oil recoveries[20,21,26,27]. These factors could have the same impact on bio-surfactants making it necessary to qualitatively understand the impact of bio-surfactant concentration and salinity on IFT for the JF-2 or any other bio-surfactant.

According to Lake[24], Winsor was the first person who showed that salt ions tend to repel the anionic surfactant ions from the aqueous phase towards the oil-water interface. This resulted in a change in surfactant-oil microemulsion phase behavior. Rosen[21] described this as ‘salting out’. Rosen[21] also explained that the measured IFT was between the oil and brine in the ‘micro emulsion phase’. This was a phase where the oil, water and

the surfactant co-existed in a microemulsion. If the salinity was greater than the optimal salinity, the IFT between the oil and brine increased with increasing salinity. The optimal salinity for the JF-2 bio-surfactant is 0.3 % by wt. NaCl[57]. Normal reservoir salinities greatly exceed this value. So it was necessary to understand the effect of salinity on IFT when the JF-2 bio-surfactant was used.

The model used by the MEOR simulator for calculating IFT was an exponential function that was based on the behavior of a decane-water-sulfonate surfactant system[56]. Two concerns regarding the model were that it was never validated with JF-2 data and it did not incorporate salinity effects. These two concerns were addressed in this study.

3.1.3 Experimental Procedure. Separate samples of JF-2 bio-surfactant were prepared as described in **Appendix A1**. Bio-surfactant concentration was measured with a high performance liquid chromatograph and the IFT was measured using a spinning drop tensiometer. The IFT measurement procedure is given in **Appendix A2**. The crude oil was 32^0 API oil from McClain County, Oklahoma with a viscosity of 6.0 cp. Tensiometer readings were taken at temperatures between 25^0 and 27^0 C. The readings for each bio-surfactant concentration or brine salinity were repeated with three or four different samples for greater accuracy. IFT was measured at 1.0x, 0.5x and 0.25x times the original bio-surfactant concentrations. Surfactants at 0.5x and 0.25x the original bio-surfactant concentration were prepared by diluting the original solution with supernatant media solution. The composition of the supernatant solution was similar to the bio-surfactant solution but with no bio-surfactant. For studying the effect of increasing salinity, IFT was measured at 5.0 %, 7.5 % and 10.0 % NaCl by wt. (50000 ppm, 75000 ppm and 100000 ppm). Since all bio-surfactant samples were originally prepared in a 5.0

% NaCl solution, samples with lower salinity could not be prepared for testing. Higher salinity concentrations were prepared by dissolving additional sodium chloride in the samples.

3.1.4.1 Observations. IFT **vs.** JF-2 bio-surfactant concentration.

In this study, IFT measurements were taken at a constant salinity of 5.0 % NaCl. The IFT values are tabulated in **Table 3.1.1** and plotted against the bio-surfactant concentration in **Figure 3.1.1**. The plot shows a stepwise decrease of IFT with increasing bio-surfactant concentration. The first IFT value on the plot is at 0.0 ppm of bio-surfactant and is equal to 29.0 dynes/cm. The IFT decreases to 1.0 dynes/cm as the bio-surfactant concentration increases to 11.0 ppm. Between 11.0 and 41.0 ppm, the IFT appears constant and close to 1.0 dynes/cm. Beyond 41.0 ppm, the IFT again reduces until a minimum value of 0.1 dynes/cm is reached at the maximum concentration between 54.0-58.0 ppm. To be conservative at concentrations above 58.0 ppm it was assumed that the IFT remained unchanged at concentrations higher than 58.0 ppm. This was not confirmed because 58.0 ppm was the highest available bio-surfactant concentration.

Discussion. An oil-brine IFT equal to 29.0 dynes/cm was within the normal range of IFT's for different oil-water systems[4]. Three critical bio-surfactant concentrations were identified on the plot in **Figure 3.1.1**. The first was 11.0 ppm where the IFT was 1.0 dynes/cm. This was identified as the critical micellar concentration (CMC) for JF-2 bio-surfactant solution because it was close to 10.0 ppm, the CMC of synthetically purified JF-2 bio-surfactant[3]. At concentrations greater than the CMC, micelle formation stops or greatly slows the decrease in IFT[21]. The IFT remained unchanged until the bio-surfactant

concentration reached 41.0 ppm where it decreased again and reached a minimum of 0.1 dynes/cm at the maximum bio-surfactant concentration between 54.0 and 58.0 ppm. It is believed that a third phase containing oil, water and a microemulsion with very low IFT's had formed in this concentration range[58]. The average value of the concentrations or 56.0 ppm, was defined as the critical microemulsion concentration (CMEC) for the JF-2 bio-surfactant. Surfactant literature reports a region with ultra-low IFT's but it is not classified as the CMEC. It is observed when salinities vary instead of varying surfactant concentrations. In conclusion, three characteristic concentrations identified from the data were the CMC or 11.0 ppm, 41.0 ppm and the CMEC at 56.0 ppm and were used for modeling purposes. They have been circled on **Figure 3.1.1**.

Original model for predicting IFT. The experimental data were compared with the values predicted by the original IFT model. The original mathematical Equation to predict IFT as a function of bio-surfactant concentration is[56]:

$$Log(\sigma_{ow}) = Log(\sigma_{\max}) + Log\left(\frac{\sigma_{\max}}{\sigma_{\min}}\right)\left(\frac{C_{surf,\max} - C_{surf}}{Delsuf}\right)^{ES} \tag{3.1}$$

where,

C_{surf} = Bio-surfactant concentration (ppm).

σ_{ow} = IFT at bio-surfactant concentration $C_{surf,}$ (Dynes/cm).

$\sigma_{\max}$, $\sigma_{\min}$ = Maximum and minimum interfacial tension (Dynes/cm).

$C_{surf,\max}$, $C_{surf,\min}$ = Maximum and minimum bio-surfactant concentrations (ppm).

$Delsuf = C_{surf,\,Max} - C_{surf,\,Min}$ (ppm).

ES = Concentration exponent.

The exponent factor *ES* controls the dependence of IFT on bio-surfactant concentration. The concentration exponent is less than unity at low concentrations[56].

Table 3.1.1 IFT and JF-2 bio-surfactant concentration.

Bio-surfactant Concentration (ppm)	IFT (Dynes/cm)
58.0	0.35
29.0	0.38
11.6	1.88
54.0	0.168
27.0	0.42
10.8	0.37
57.0	0.10
28.5	1.50
11.4	2.50
11.0	2.54
41.0	1.21
38.0	1.48
21.0	1.50
10.5	2.00
11.0	0.93
5.5	3.00
2.75	4.20

Figure 3.1.1 IFT **vs.** Bio-surfactant concentration

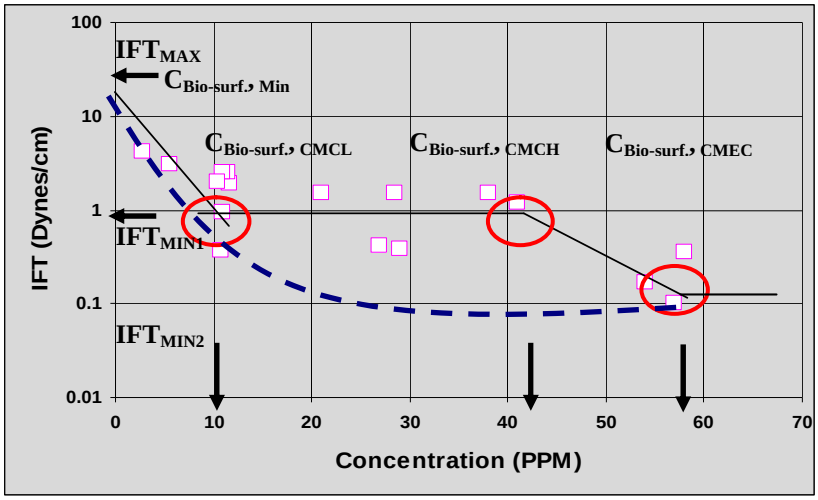

Laboratory readings

IFT values predicted by Equation 3.1 are plotted as the dotted line in **Figure 3.1.1**. It can be observed that they differ from the experiment data. The predicted values were equal to the experimental data until about 11.0 ppm of bio-surfactant. Beyond that, the experimental data diverged from the values predicted by Equation 3.1. Two important observations were made. First, IFT was very sensitive to bio-surfactant concentration since it decreased by a factor of 100 when the bio-surfactant concentration increased by a factor of 10. Second, the predicted IFT data trend was similar to the experimental IFT trend. The sensitivity meant that a more accurate model than Equation 3.1 was needed to correctly predict IFT. The second observation meant that the form of Equation 3.1 could still be used but the parameters in the equation must depend on the bio-surfactant concentration and change with it. Since the experimental data showed two distinct concentration regions; Region 1 between 0.0 ppm and 41.0 ppm of bio-surfactant and Region 2 between 41.0 ppm and greater bio-surfactant concentrations, Equation 3.1 was used with different parameters for the two regions. Extra terminology was defined for this and is explained below.

Modified mathematical model. In Region 1, the IFT was 1.0 dynes/cm at the bio-surfactant CMC of 11.0 ppm and this was defined as the lower critical micellar concentration CMCL. Since IFT remained constant after 11.0 ppm until the bio-surfactant concentration was 41.0 ppm, 41.0 ppm was called the higher critical micellar concentration or CMCH. In region 2, IFT decreased from 1.0 dynes/cm at 41.0 ppm to 0.1 dynes/cm at 56.0 ppm. This concentration, 56.0 ppm, was called the critical microemulsion concentration or CMEC and the IFT value was assumed as the minimum

possible IFT or IFT_{Min}. The maximum concentration, CMAX was assumed equal to or greater than 56.0 ppm. The modified equations are:

For bio-surfactant concentrations between 0.0 ppm and 41.0 ppm**,**

$$Log(\sigma_{ow}) = Log(\sigma_{\min 1}) + Log\left(\frac{\sigma_{\max}}{\sigma_{\min 1}}\right)\left(\frac{C_{surf,CMCH} - C_{surf}}{Delsuf1}\right)^{ES1} \quad (3.2)$$

For bio-surfactant concentrations between 41.0 ppm to 56.0 ppm,

$$Log(\sigma_{ow}) = Log(\sigma_{\min}) + Log\left(\frac{\sigma_{\min 1}}{\sigma_{\min 2}}\right)\left(\frac{C_{surf,\max} - C_{surf}}{Delsuf2}\right)^{ES2} \quad (3.3)$$

where,

C_{max} = Maximum bio-surfactant concentration = 56.0 ppm

C_{min} = Minimum bio-surfactant concentration = 0.0 ppm.

C_{CMCL} = Lower bio-surfactant critical micellar concentration (ppm) = 11.0 ppm

C_{CMCH} = Higher bio-surfactant critical micellar concentration (ppm) = 41.0 ppm

C_{CMEC} = Bio-surfactant critical microemulsion concentration (ppm) = 56.0 ppm

$Delsuf1 = C_{CMCH} - C_{min}$ (ppm).

$Delsuf2 = C_{max} - C_{CMCH}$ (ppm).

σ_{ow} = IFT at bio-surfactant concentration $C_{Bio\text{-}surf,}$ (Dynes/cm).

$\sigma_{\min 1}$ = Interfacial tension at $C_{surf,\ CMCL}$ (ppm) = 1.0 Dynes/cm

$\sigma_{\min 2}$ = Interfacial tension at $C_{surf,\ CMEC}$ (ppm) = 0.1 Dynes/cm

$\sigma_{\max}$ = Interfacial tension at $C_{surf,\ Min}$ = 29.0 Dynes/cm

ES1, *ES2* = 7.0 and 3.0

IFT values predicted by the new model are shown in **Figure 3.1.2**. It can be observed in **Figure 3.1.2** that the two equations were an improvement over a single equation because the result is closer to the predicted values and is based on the experimental data. The concentration exponent, '*ES*' has a value greater than one for both

cases. Though their values should be less than unity for low concentrations, 2.0 and 7.0 were considered appropriate since they provided a good fit.

Figure 3.1.2 IFT predicted by modified equations

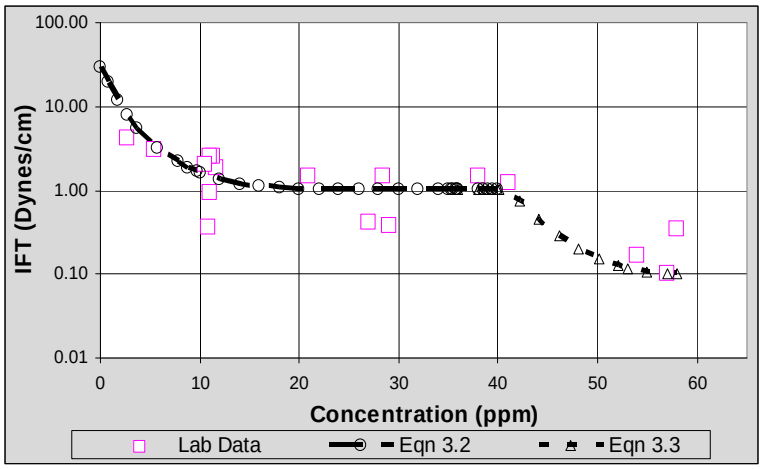

3.1.4.2. Observations. IFT and aqueous phase salinity.

To analyze the effect of salinity on IFT, IFT measurements at constant bio-surfactant concentrations but different salinities were analyzed. Experimental IFT data measured at bio-surfactant concentrations between 54.0-58.0 ppm were averaged and analyzed at 5.0, 7.5 and 10.0 % NaCl. This bio-surfactant concentration range was narrow enough to assume that the bio-surfactant concentration was constant. Averaged IFT data at different salt concentrations are shown in **Table 3.1.2**. The data shows increasing IFT with salinity.

Table 3.1.2 Average IFT values at different salinities.

Salinity (ppm)	$\Delta Conc._{Salt}$ (ppm)	IFT (Dynes/cm)	ΔIFT (Dynes/cm)
50000	0	0.155	0
75000	25000	0.855	1.29
100000	50000	2.035	1.88

Discussion. Change in IFT or ΔIFT was studied as a function of the change in salt concentration or $\Delta Conc._{Salt}$. Underlying assumptions that could not be verified from available data were that change in IFT does not depend on the initial brine salinity or bio-surfactant concentration and that change in IFT was reversible. In other words, it meant that ΔIFT would be the same function of $\Delta Conc._{Salt}$ for all initial brine salinities or bio-surfactant concentrations. If the original 5.0 % NaCl brine was replaced by 2.0 % brine, IFT would decrease because of reduced brine salinity. This was a reasonable assumption because the IFT for JF-2 bio-surfactant is a monotonically increasing function above its optimum salinity of 0.3 % NaCl[57] and most reservoirs have higher salt concentrations.

Defining the IFT at the original salt concentration of 50000 ppm NaCl (5.0 %) as the base value, ΔIFT was plotted against $\Delta Conc._{Salt}$ in **Figure 3.1.3**. The plot shows that ΔIFT was nearly linear to $\Delta Conc._{Salt}$. Using a regression routine, a linear plot was fit through the data points. The equations relating the two variables and to calculate the corrected IFT are:

$$\Delta\sigma = 0.404\left(\Delta Conc._{salt}\right) \tag{3.4}$$

$$\sigma_{new} = \sigma_{initial} + 0.404\left(\Delta Conc._{salt}\right) \tag{3.5}$$

where,

$\Delta\sigma_{new}$ = Change in IFT or ΔIFT (dynes/cm)

σ_{new} = IFT after correcting for salinity (dynes/cm)

$\sigma_{initial}$ = The value calculated by Equations 3.2 or 3.3 at 5.0 % ppm NaCl

$\Delta Conc._{salt}$ = Salt concentration in surfactant/aqueous phase – 50.0 (mg/scc)

Figure 3.1.3 ΔIFT **vs.** $\Delta Conc._{salt}$

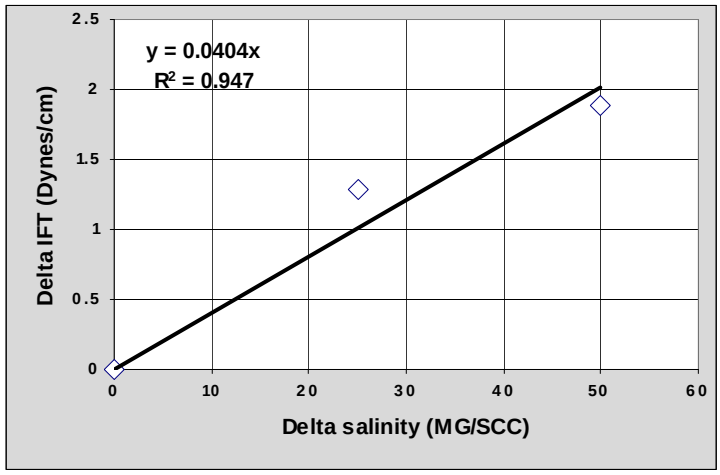

Model limitations. Some limitations of the IFT model are:

1. Since only three points were used to define the model, the model may not be accurate.
2. If brine salinity became less than 0.3 % NaCl, the proposed model will predict a lower than true IFT. This is because the IFT increases when the salinity decreases below 0.3 % while the model assumes that the IFT decreases as long as salinity is below 5.0%.
3. The assumption that the change in IFT is independent of the initial conditions should be verified through additional IFT measurements for different salinities and bio-surfactant concentrations.
4. The assumption of IFT reversibility should also be verified through more experiments because the bio-surfactant molecules may undergo permanent changes when salinity changes.

3.1.5 Conclusions.

1. A modified version of the original IFT- bio-surfactant model has been presented. It was shown that the original IFT – surfactant concentration model could not predict the stepwise reduction in IFT with increasing bio-surfactant concentration. Two sets of Equation parameters dependant on bio-surfactant concentration were required. Using separate parameters ensured a better IFT prediction compared to the original model. The new model was more reliable because it was based on laboratory IFT measurements of JF-2 bio-surfactant.
2. A linear relationship was developed to predict the change in IFT as a function of aqueous phase salinity.

3.2. Bio-polymer characterization

3.2.1. Introduction. In micellar polymer flooding, polymer is added to the surfactant to reduce its mobility and improve its macroscopic sweep efficiency[8]. Laboratory studies with sand packs have shown the importance of adding polymers to reduce bio-surfactant viscosity and improve oil recoveries[5]. Generally, the polymers added to surfactants are polysaccharides such as xanthan gum and polyacrylamides. Polysaccharides are biological in origin. Acrylamides are synthetic in nature and are used in the hydrolyzed form. Both types of polymers can degrade in reservoirs; either by microbial action or salinity degradation[32]. Another problem that affects polymer performance is shearing as it flows through porous media[33]. Shearing can be permanent in nature if the polymer's elastic limit is exceeded. Bio-polymers are affected less than polyacrylamides by shearing and salinity. To overcome these problems, high concentrations of polymers can be added

to the surfactant, but at the field scale, this makes the process uneconomic. For an economic MEOR process, losses due to shearing and salinity must be minimized.

Losses may be reduced if polymers are generated in the oil reservoir along with the bio-surfactant. Certain polymer producing bacteria may grow along with the bio-surfactant producing microbes. This can be advantageous because the nutrients that are used to generate bio-surfactant can also be used to produce biopolymer. And losses associated with polymer injection and flow can be mitigated. Field studies have shown that bio-polymers can be effectively used to alter reservoir permeabilities to divert water into poorly swept low permeability zones[59].

The SP-018 microbe is known to produce bio-polymer under anaerobic conditions[60]. The use of this bio-polymer was previously investigated for MEOR applications[6]. In the studies here, SP-018 bio-polymer was used as the polymer component of the micellar bio-surfactant treatment being developed. In order to do so, it was necessary to characterize the polymer's behavior. Polymer characterization included predicting polymer solution viscosity as a function of polymer concentration and viscosity dependence on shear rate and salinity. Previous laboratory studies had taken measurements of SP-018 properties but the mathematical models that describe polymer flow in porous media were never tested on the available data. These mathematical Equations are used to characterize the bio-polymer and derive constants that could be used in predicting its behavior under reservoir conditions.

3.2.2. Theory. The most common relationship used for predicting polymer viscosity as a function of polymer concentration *C* (wt. %) in an aqueous solution is the Flory-Huggins relationship[61,62] and is give by:

$$\mu_p = \mu_w\left(1 + Ap_1C + Ap_2C^2 + Ap_3C^3\right) \tag{3.6}$$

Equation 3.6 has been used to predict solution viscosity for polyacrylamides and Xanthan for field scale simulations[63]. For the case where salt was present in the solution, Equation 3.6 was modified to[40,63]:

$$\mu_p = \mu_w\left(1 + \left(Ap_1C + Ap_2C^2 + Ap_3C^3\right)C_{sep}^{Sp}\right) \tag{3.7}$$

where, C_{sep} was defined as the effective salinity of the solution and the exponent *Sp* was a viscosity parameter equal to the slope of a solution viscosity vs. salinity plot on a log-log plot. The effective salinity was expressed in terms of meq/ml because it was simpler to represent the ionic contribution of both calcium and sodium chloride ions in these units instead of weight percent or any other mass concentration units. For polyacrylamides, *Sp* was reported as large and negative and for Xanthan, small and positive[40,63]. However, the relationship also assumed that the minimum effective salinity in the system is 0.1%[63]. This was necessary because, at low salinities and a negative *Sp*, the Equation would predict abnormally large solution viscosities.

The polymer experiences shearing as it flows through the reservoir and its viscosity decreases if the polymer is of a shear thinning type[34,35,36]. Meter and Bird present an equation to predict non-Newtonian fluid viscosity as function of shear rate[64]:

$$\mu_{\dot{\gamma}} = \mu_\infty + \frac{\mu_0 - \mu_\infty}{\left(\frac{\dot{\gamma}}{\gamma_{\frac{1}{2}}}\right)^{P_\alpha - 1}} \tag{3.8}$$

where,

μ_∞ = Solution viscosity at infinite shear rate: assumed to be that of water (cp)

$\mu_{\dot{\gamma}}$ = Viscosity at a shear rate $\dot{\gamma}$ (cp)

μ_0 = Viscosity at zero shear rate (cp)

$\dot{\gamma}$ = Shear rate (sec^{-1})

$\gamma_{\frac{1}{2}}$ = Shear rate where the solution viscosity was half the zero shear rate and infinite shear rate viscosities (sec^{-1})

P_α = Viscosity parameter that controlled the abruptness of the change in viscosity with shear. The relationship was verified by experiments conducted by Tsaur[65] and Martin et al.[66] as reported in Lake[61]. Shear rate was calculated using a formula derived by Hirasaki and Pope[36]:

$$\dot{\gamma} = \left(\frac{3n}{4n-1}\right)^{\frac{n}{n-1}} 4\frac{|u_t|}{\sqrt{8KK_{rl}\phi S_l}} \tag{3.9}$$

where,

n = Dimensionless fluid exponent

u_t = The water phase velocity (ft/day)

K = Absolute permeability (Darcy)

ϕ = Porosity of the medium (fr)

K_{rl} = Relative water permeability

S_l = Water saturation (fr)

The water saturation term was included because the shear on polymer increased when was present.

3.2.3. Experiment procedure. Measurement of experimental SP-018 bio-polymer data is reported in the paper by Pfiffner et al.[60]. The measured data were viscosity as a function of salinity, shear rate and polymer concentrations.

3.2.4. Observations. In **Tables 3.2.1**, **3.2.2** and **3.2.3**, viscosities of SP-018 in water at different polymer concentrations, brine salinity and shear rate are shown.

Table 3.2.1. SP-018 solution viscosity vs. polymer concentration (no salinity)[60]

Polymer conc. (wt. %)	Viscosity at zero shear rate (cp)
0.1	124.2
0.2	248.4
0.25	300.0
0.3	389.5
0.4	505.3
0.5	701.1

Table 3.2.2. SP-018 solution viscosity vs. salinity (SP-018 conc. 0.25%)[60]

Salinity (wt.%)	Effective salinity, C_{sep} (meq/ml)	Viscosity (cp)
0	0	140.6
2.5	0.43	7.5
5.0	0.85	5.6
7.6	1.29	5.6
9.8	1.70	5.6

Table 3.2.3. SP-018 solution viscosity vs. shear rate (SP-018 conc. 0.1 wt.%)[60]

Shear rate (sec^{-1})	Viscosity (cp)
3.86	118.6
7.5	114
8.19	94.3
20.15	62.9
37.49	44.6
79.43	32.9
156.91	21.4
386.33	8.6

3.2.5. Results.

3.2.5.1. **Viscosity vs. Concentration**. A linear model and the Flory-Huggins model were compared for predicting polymer solution viscosity. The linear model is not shown here because the Flory-Huggins provided a better fit on the laboratory data. The viscosity

values predicted by the Flory-Huggins equation are plotted alongside the laboratory values in **Figure 3.2.1** and tabulated in **Table 3.2.4**. Equation co-efficients are shown on the plot. The co-efficients A_{P1}, A_{P2} and A_{P3} for the SP-018 bio-polymer were 2506.6 wt^{-3} %, -1249.1 wt^{-2} % and 1396.3 wt^{-1} %. Other polymers will need their own co-efficients.

Table 3.2.4. SP-018 solution viscosity vs. polymer concentration (no salinity)

Polymer concentration (wt. %)	Viscosity (Lab.) (cp)	Viscosity (Flory Huggins eqn.) (cp)
0.1	124.2	127.4
0.2	248.4	245.0
0.25	300.0	311.2
0.3	389.5	371.6
0.4	505.3	515.8
0.5	701.1	698.3

Figure 3.2.1 Plot of Flory-Huggins equation fit to laboratory data

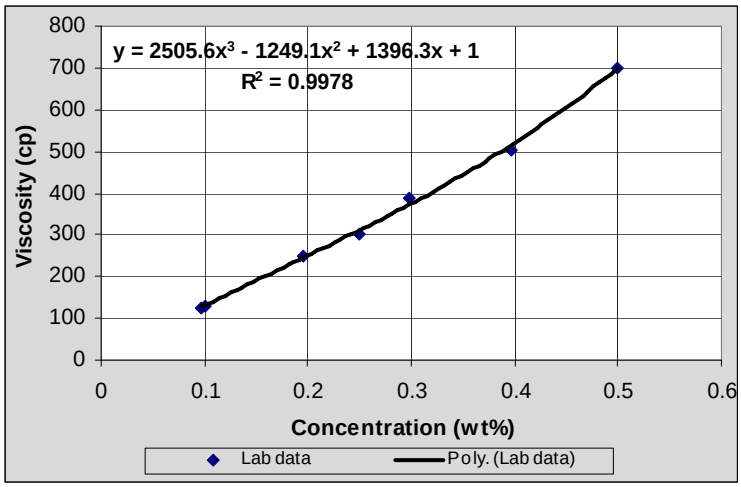

3.2.5.2. **Viscosity vs. Salinity**. The data in **Table 3.2.2** showed that salinity had an adverse effect on SP-018 solution viscosities. Solution viscosities decreased from 140.6 cp to 5.6 cp when salinity increased from 25000 to 98000 ppm NaCl (2.5 % to 9.8 %). As discussed earlier, the model that was proposed in Equation 3.7 to account for salinity effects does not accurately predict solution viscosity when the solution salinity is very

low and *Sp* is large and negative. It is reasonable to assume that reservoir brines likely exceed 0.1 % salt but it should be expected that a proposed model should be valid across the entire range of saline conditions. In the case of Xanthan gum, Equation 3.7 was likely to predict reasonably accurate viscosities at all salinities because viscosities increased with salinity and *Sp* was positive[63]. At low salinities the value of the term C_{sep}^{Sp} would be small and the solution viscosity would be low. But if using polymers such as polyacrylamides and SP-018 where the slope between viscosity and salinity is potentially large and negative, Equation 3.7 would be unsuitable even at 1.0 % or 2.0 % salt concentrations. This is because C_{sep}^{Sp} would be small and would result in an unrealistically large polymer solution viscosity.

To predict the viscosity of polyacrylamides and SP-018 polymer over a wider range of salinities a modification to Equation 3.6 is proposed

$$\mu_p = \mu_w\left(1+\left(Ap_1C + Ap_2C^2 + Ap_3C^3\right)\frac{1.0}{Abs\left(1.0 - SpC_{sep}\right)}\right) \tag{3.9}$$

Sp was defined as a constant that characterized the rate of change of viscosity to the effective salinity (similar to the parameter 'b' in the denominator of a Langmuir isotherm model) and had the unit ml/meq. The advantage of Equation 3.9 is that even at very low salinities (<0.1%) when *Sp* is negative, it will not give unrealistic values for polymer solution viscosities like 10^6 cp. Moreover it can be used for Xanthan gum for which *Sp* is positive. Equation 3.9 may give faulty values if the product of *Sp* and C_{sep} is positive and greater than one; a case that arises when Sp is positive and salinities are large. But when tested with values from an actual Xanthan gum field flood (Sp > 0), the product SpC_{sep} never exceeded 1.0. The model was tested on SP-018 and the result can be observed in **Figure 3.2.2** and the values are tabulated in **Table 3.2.5**. The values predicted by

Equation 3.7 are also tabulated for comparison. The value of *Sp* (the slope of log-log plot of C_{sep} vs. μ) was calculated to be equal to -0.19. There is a large difference in the viscosities by the two equations. The value of *Sp* for SP-018 to be applied in Equation 3.9 was obtained by trial and error and was equal to -12.0. **Figure 3.2.3** is a plot using Equation 3.9 for hydrolyzed polyacrylamide polymer[67].

Table 3.2.5. SP-018 viscosity vs. salinity. Experimental and model (SP-018 conc. 0.25%)

Salinity (wt.%)	Eff. salinity, C_{sep} (meq/ml)	Lab. Visc. (cp)	Eqn 3.7 visc. (cp)	Eqn 3.9 visc. (cp)
0	0	140.6	-	130.6
2.5	0.43	7.5	365.9	21.4
5.0	0.85	5.6	320.9	11.7
7.6	1.29	5.6	296.2	7.9
9.8	1.70	5.6	282.1	6.2

Figure 3.2.2 Model to predict salinity effect for SP-018[60].

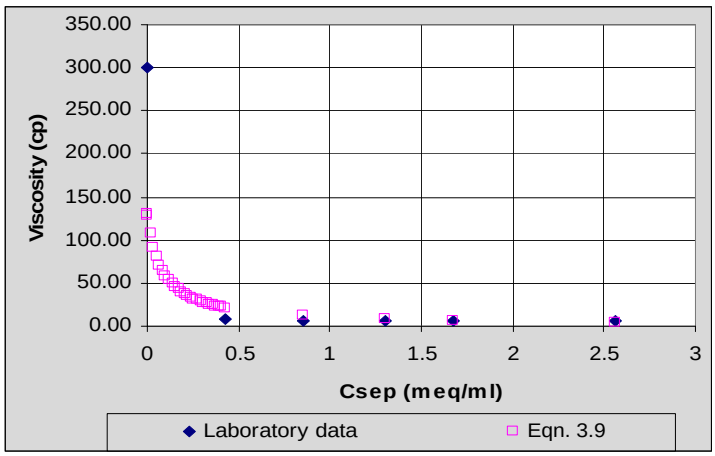

Figure 3.2.3 Model to predict salinity effect for polyacrylamide[67]

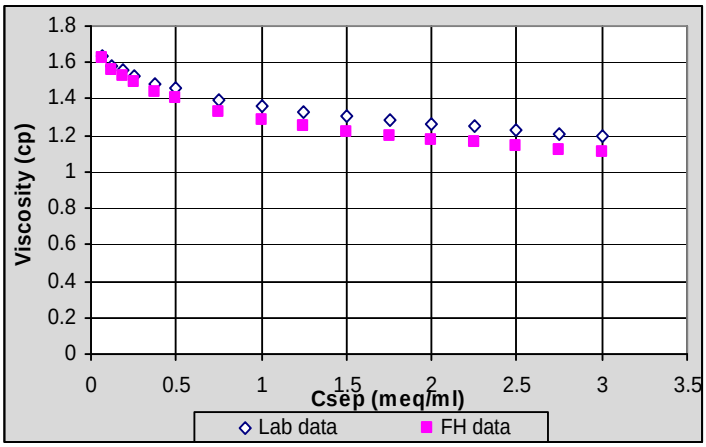

3.2.5.3. **Viscosity vs. Shear rate**. The Meter and Bird equation[64] was used to model the viscosity reduction due to shearing of the SP-018. The Meter and Bird equation[64] has also been applied to polyacrylamide polymer[61] and Xanthan gum[63]. In **Figure 3.2.4**, experimental values and values predicted by Equation 3.8 for SP-018 viscosities are shown at different shear rates. The value of P_α, that describes the abruptness of the change in viscosity was obtained by trial and error and is equal to 1.9 and $\gamma_{\frac{1}{2}}$ for SP-018, taken from the plot in **Figure 3.2.4** is equal to 19 sec^{-1}. The viscosity of the solution at infinite shear is equal to 1.0 cp or the viscosity of plain water. The dashed line is drawn through the determined values to highlight the shear thinning region. The power law exponent '*n*' is calculated using the Carreau method as described by Green and Willhite[68] from the shear thinning region of the plot. The value for n is 0.5.

Figure 3.2.4 Shear rate vs. Effective polymer solution viscosity.

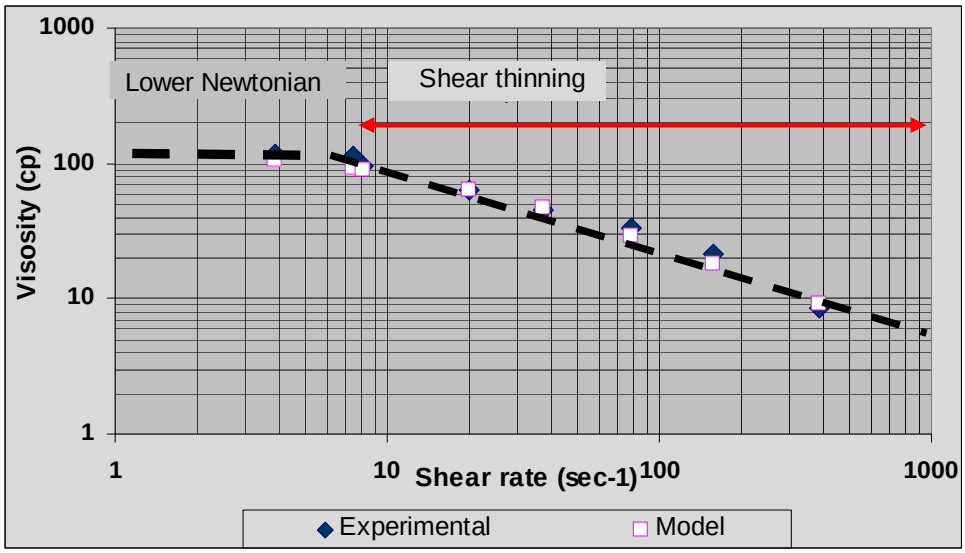

3.2.6 Conclusions.

1. The Flory-Huggins equation can be used to accurately predict SP-018 solution viscosities. The equation co-efficients were obtained by fitting Pfiffner et al.[60] data.
2. A model was proposed and tested to predict SP-018 polymer solution viscosities as a function of salinity. The model can also be used to predict polyacrylamide and xanthan gum viscosities.
3. The shear parameters for SP-018 polymer were estimated. The bio-polymer is a shear thinning polymer and the Meters and Bird viscosity model was adequate to predict polymer viscosity.
4. The relationships described can be used for polyacrylamide and xanthan gum with appropriate parameters and constants.

3.3 Core flood experiments.

3.3.1. Introduction. Previously, unconsolidated sand packs at waterflood residual oil saturation were treated with a solution of JF-2 bio-surfactant, 2,3-butanediol and partially

hydrolyzed polyacrylamide polymer resulting in recoveries close to 80% of the residual oil[5]. The flowrates in those experiments were higher than normal field rates and conditions favorable for the surfactant such as high permeability, vertical orientation of packs and relatively large surfactant preflush and postflush treatments were present in the pack. Since the ability of the JF-2 bio-surfactant to mobilize oil in actual reservoir type rock under reservoir type flowrates can be best demonstrated by using actual cores, Berea sandstone cores were selected for their uniform properties.

3.3.2. Theory. JF-2 bio-surfactant flooding experiments in unconsolidated sand packs showed that the addition of a polymer to the bio-surfactant improved the mobility ratio between the oil and surfactant and prevented the fingering of surfactant through the mobilized oil bank[69,70]. The water soluble alcohol, 2,3-butanediol, acted as a co-surfactant that improved the bio-surfactant's tolerance to salinity by increasing the bio-surfactant's optimal salinity[27]. Though questions remain about the effectiveness of adding alcohol to improve the bio-surfactant salinity tolerance[28], the fact that this alcohol is produced in nature by the JF-2 microbe under anaerobic conditions is seen as advantageous to the bio-surfactant.

Adsorption and polymer degradation, though important for tertiary recovery design were not studied in these experiments. Other features that were tested in the sand packs but not in the core floods were the use of a viscous preflush and graded polymer postflush.

3.3.3. Experiments.

This experimental study was divided into four experiments, numbered 1 to 4.

3.3.3.1. Experiment 1.

Procedure. Two six inch long and one-half inch in diameter Berea sandstone cores were oven dried at 60^{o} C for four days. The cores, numbered 1.1 and 1.2 were weighed, and their lengths and diameters measured. One core was treated at a time. Core 1.1 was placed in a Hassler core holder and 1500 psig of overburden pressure applied. A vacuum was applied to the core for twenty four hours to remove any air. The core was saturated with deaerated 5.0 % NaCl brine and then flooded with a 34^{0} API crude oil until the core reached residual water saturation. The oil saturated core was then flooded with 5.0% NaCl brine until it was near residual oil saturation and ready for surfactant treatment. Typically, brine flooding was stopped when only a trace of oil was being produced or 10.0 pore volumes (PVs) of brine had been injected through the core. Injection pressure at the core inlet was monitored to calculate end point effective permeabilities at the end of each stage of treatment. Core permeabilities and saturations were tabulated in **Table 3.3.3.1b**. A detailed step by step explanation of the flooding procedure is given in **Appendix A3** and a diagram of the experiment setup is given in **Appendix A4**.

The surfactant was a solution of JF-2 bio-surfactant, 1000 ppm partially hydrolyzed polyacrylamide polymer (PHPA) as the viscosifier and 10.0 millimoles 2,3-butanediol as co-surfactant alcohol. The surfactant composition has been described previously[70] and its preparation is described in **Appendix A1**. Two surfactant solutions, A and B, were prepared for the treatment of cores. Surfactant A had 11.0 ppm of *JF-2*

bio-surfactant and surfactant B had 41.0 ppm. Interfacial tension between crude oil and brine at the two bio-surfactant concentrations were measured (**Table 3.3.3.1a**).

Good experimental practice recommended that the surfactant samples with similar bio-surfactant concentrations be used for the experiments. But it took several days time to produce each sample in the laboratory. In order to save time, it was decided to use the produced bio-surfactant samples irrespective of their bio-surfactant concentration. The JF-2 bacterium produced different bio-surfactant concentrations in different samples.

Two pore volumes (PVs) of Surfactant A were injected into core 1.1 and 1.0 PV of Surfactant B into Core 1.2 at the rate of 3.14cc/hr. In Core 1.1, surfactant injection was stopped after the 2.0 PVs of surfactant was injected. In Core 1.2, the surfactant injection was followed by 3.0 PVs of 5.0% NaCl brine injected at the waterflood rate of 20.14 cc/hr. Core 1.2 received 1.0 PV of surfactant because it was thought that with a higher bio-surfactant concentration, 1.0 PV of Surfactant B would be sufficient to recover oil. The post surfactant brine injection was called postflush. Produced fluids from the core were collected in 10.0 cc sample flasks.

Observations. No oil was recovered from Core 1.1 but Core 1.2 yielded a 2.3 cc oil slug or 39.0 % of waterflood residual oil after 3.00 cc of postflush brine was injected. The production of an oil slug was characterized as a spike in oil production followed by a rapid decrease and disappearance of oil from the production stream. Just before the oil slug was produced, the injection pressure at the core inlet increased to nearly thirty times the waterflood injection pressure but then rapidly declined following oil production.

Discussion. Since no oil was recovered from Core 1.1 after 2.0 PVs of surfactant, it was thought that injecting postflush would not serve any purpose and the experiment was

stopped. The failure of the surfactant to recover oil from Core 1.1 even after 2.0 PVs of surfactant injection was caused by either insufficient bio-surfactant[21,28] or inefficient sweep by the surfactant due to viscous fingering. Viscous fingering was unlikely because the mobility ratio between the oil and surfactant was less than one and favorable. Surfactant adsorption is the primary cause for surfactant degradation in porous media. For JF-2 it could only be confirmed if studies are done to determine the adsorption losses. Capillary end effect was not an issue because the displacing aqueous phase flowed from the core without any abnormal injection pressure increase[71,72]. A third possibility was that the surfactant had mobilized some oil but the low surfactant flow rate may have resulted in the bypassing of this mobilized oil. It has been shown by Healy et al.[73] in laboratory studies that oil bypassing can occur at low surfactant flowrates if surfactant displacement is immiscible. Healy et al.[73] define low flowrates as less than 1.0 ft/ day. The frontal advance rate in core 1.1 was 1.0 ft/day. The experiment was classified an immiscible displacement process because the crude oil-brine IFT measured prior to the experiment was 2.5 dynes/cm. For miscible displacement the IFT has to be zero dynes/cm. Bypassing of oil at this flowrate in Core 1.1 was likely further aided by gravity segregation between the heavier surfactant and displaced oil[73].

Oil recovery from core 1.2 showed that bio-surfactant concentration as low as 41.0 ppm could recover almost 40.0 % of residual oil from a core with a low permeability of 27.0 md. The recovered oil was surfactant aided because no oil was being produced at the end of waterflooding. Oil production after only 3.00 cc of postflush injection showed that residual oil had been displaced within the core but was retained near the discharge end of the core during the surfactant flood. Injecting the brine postflush at ten times the

surfactant rate may have overcome the forces that retained this oil. The retention of oil near the core outlet can be also explained using the work of Healy et al.[73]. The displacement by surfactant B was immiscible because the oil-brine IFT was 1.2 dynes/cm and the velocity of surfactant was a relatively low 1.0 ft/day. The postflush injected at a higher frontal velocity likely displaced this oil from the core. The postflush effect meant that if a high rate postflush had been injected into Core 1.1, oil might have been recovered from it. Reported laboratory surfactant floods do not mention oil retention because laboratory displacement velocities generally varied between 5-80 ft/day, and bypassing may have been rarely observed[74]. The observations of Healy et al.[73] was the only report that mentioned oil retention. Gravity segregation and flow convergence caused by location of the core outlet point at the center of the core face may have caused retention.

The injection pressures observed during surfactant injection were most likely a combination of permeability reduction and oil retention near the outlet. Permeability reduction was by PHPA polymer retention[74,75,76] and oil retention near the outlet could have caused flow path blockage and the high injection pressures.

In conclusion, the combination of low surfactant flowrate and bio-surfactant adsorption may have prevented oil production before surfactant injection was completed. Higher surfactant rates to overcome oil bypassing are possible in the laboratory but high rates cause polymer shearing and viscosity reduction and frontal rates in the field rarely exceed 2.0 ft/day.

Table 3.3.3.1a. IFT measurements, Experiment 1.

Bio-surfactant concentration (ppm)	IFT (dynes/cm)
11.0	2.5
41.0	1.2

Table 3.3.3.1b. Experiment 1 results summary.

Core	K_{abs} (md)	PV (cc)	$S_{OR,Wf}$ (%)	Poro (Fr.)	Surf. Vol. (PV)	Recovery (%)	N_{cp} (WF)	N_{cp} (EOR)
1.1	35.0	23.9	20.9	0.14	2.0	0.0	1.9E-3	4.9E-3
1.2	26.5	39.0	15.1	0.14	1.0	39.0	1.5E-3	6.1E-3

Terminology

K_{Abs} = Absolute permeability of Berea sandstone core, md.

PV = Porevolume

$S_{OR, Wf}$ = Residual oil saturation at the end of waterflooding

IFT = Interfacial tension, dynes/cm

Ppm = parts per million

N_{cp} (WF) = Capillary number during waterflooding

N_{cp} (EOR) = Capillary number during polymer-surfactant flooding

3.3.3.2. Experiment 2.

Procedure. The effect of surfactant flowrate on oil recovery was studied in this experiment. Two cores, 2.1 and 2.2, each six inches long and one-half inches in diameter were waterflooded with 5.0% NaCl brine to residual oil saturation prior to surfactant injection. The surfactant contained 38.0 ppm of JF-2 bio-surfactant along with the polymer PHPA and co-surfactant alcohol. The IFT between the crude oil and brine in the presence of bio-surfactant was 1.65 dynes/cm. The two cores were injected with surfactant at different rates. Core 2.1 was injected with 1.0 PV of surfactant at 2.54 cc/hr followed by 1.0 PV of postflush at 5.14 cc/hr. Core 2.2 was injected with 1.0 PV of the same surfactant at 5.14 cc/hr followed by 1.0 PV of postflush at 10.0 cc/hr.

Observations. No oil was recovered from Core 2.1 during surfactant injection but the injection pressure at the core inlet increased to nearly thirty times the waterflood injection pressure. Following surfactant injection, the outlet end of the core was left open and 1.2 cc of oil drained out of the core, and the pressure decreased. When the pressure stopped decreasing, postflush brine was injected and another 1.1 cc of oil was produced after 3.0 cc of postflush injection. The total oil recovered was 47% of the residual oil (**Table 3.3.3.2b**). From Core 2.2, 1.0 cc of oil was recovered after 0.5 PV of surfactant injection and another 2.0 cc of oil was recovered after 4.0 cc of postflush. The total oil recovered was 45.0 % of residual oil. In both the cores, injection pressure at the core inlet increased at the start of postflush injection and rapidly declined following the oil slug production.

Discussion. The results showed that JF-2 bio-surfactant concentration as low as 38 ppm (0.0038 mg/L) recovered nearly 45% of residual oil from 30.0 md permeability cores (**Table 3.3.3.2a**).

Oil production within 4.0 cc of postflush injection from both the cores indicated that the bio-surfactant mobilized oil but this oil was retained near the core discharge. Comparison of the oil recovery profile from the cores showed the impact of surfactant flowrate. Injecting surfactant at a higher rate into Core 2.2 resulted in oil production after 0.5-0.6 PV of surfactant injection. Oil production during surfactant injection meant that the higher flowrate of 5.14 cc/hr (2.0 ft/day) partially overcame oil bypassing that may have occurred in Core 2.1 (2.54 cc/hr or 1.0 ft/day) and in Core 1.2 (3.14 cc/hr or 1.2 ft/day) and prevented oil production during the same period. Calculations also indicate that mobilized oil should normally breakthrough after 0.5-0.6 PV of surfactant injection.

The relationship between oil production and flow rate implies that if a higher flowrate or a higher bio-surfactant concentration is used then mobilized oil breakthrough will occur earlier because more residual oil is mobilized. Additionally, the oil fraction at breakthrough will also increase. This is also reported by Healy et al.[73] who showed that the fraction of oil recovered at breakthrough increased with flow rate.

Doubling the surfactant flowrate from 2.54 to 5.14 cc/hr had no impact on the total oil recovery. This was because the change in velocity was very small. If the change in velocity was large, like ten times, the increase in oil recovery would have been significant[76].

The observed dependence on flowrate is important from a field application point of view because the goal of a surfactant flood is to recover oil without consuming much surfactant and as quickly as possible. More oil could be produced at breakthrough before a 1.0 PV of bio-surfactant is used if a higher bio-surfactant flooding rate is used.

Flow blockage by the retained oil near the outlet combined with permeability reduction by polymer retention could explain the abnormal pressure rise in Core 2.1. The lack of duplicate core floods raised questions about the quality of results and their analyses. But the uniformity in the testing procedure and consistency of core data such as permeabilities, porosities, flooding rates and the brine and oil saturations provides confidence in the quality of results. Core replication was done in the remaining two experiments.

Table 3.3.3.2a. Experiment 2 results summary

Core	K_{abs} (md)	PV (cc)	$S_{OR,Wf}$ (%)	Poro (Fr.)	Surf vol. (PV)	Recovery (%)	N_{cp} (WF)	N_{cp} (EOR)
2.1	31.3	18.9	20.9	0.10	1.0	47.0	4.8E-4	5.1E-3
2.2	31.0	27.0	24.8	0.16	1.0	45.0	6.3E-4	6.8E-3

3.3.3.3. Experiment 3

Procedure. The impact of bio-surfactant concentration on oil recovery was studied in this experiment. Four Berea sandstone cores, each six inches long and one-half inches in diameter and numbered 3.1 to 3.4 were waterflooded with 5.0 % NaCl brine to residual oil saturation. Each core was treated with 1.0 PV of surfactant because experiment 2 results showed that 1.0 PV was sufficient to recover oil provided a high enough surfactant flowrate was used. Two surfactant solutions, A and B were prepared. Surfactant A had a bio-surfactant concentration of 21.0 ppm and Surfactant B had 10.5 ppm. Surfactant B was made from surfactant A by diluting it with nutrient media to a bio-surfactant concentration of 10.5 ppm. The IFT between crude oil and brine at the two bio-surfactant concentrations was measured (**Table 3.3.3.3a**). Cores 3.1 and 3.2 were injected with Surfactant A. Surfactant A was injected into Core 3.1 at 5.1 cc/hr and into Core 3.2 at 6.4 cc/hr. Surfactant B was injected into Cores 3.3 and 3.4 at 6.4 cc/hr. Following the surfactant injection, all four cores were flushed with 1.0 PV of brine at the waterflood rate of 30.9 cc/hr.

Observations. After 0.5 PV of surfactant was injected into Core 3.1, 1.0 cc of mobilized oil was produced. An additional 1.7 cc of oil was produced after 2.0 cc of postflush injection. The total recovery was 27.0 % of waterflood residual oil. From Core 3.2, 0.6 cc of oil was produced after 0.5 PV of surfactant injection and another 2.4 cc of oil after 3.0 cc of postflush injection. Residual oil recovery was 28.0 %. For both the cores oil production occurred as a slug and was accompanied by an increase in injection pressure until oil production. After the oil was produced the injection pressure declined.

Residual oil recoveries were 13.0 % and 16.0 % from Cores 3.3 and 3.4 respectively. From both the cores, small volumes of oil were produced after 0.5-0.6 PV of surfactant injection. The majority of total recovered oil was produced after the beginning of postflush injection. The injection pressure and oil production profiles during postflush injection were similar to those of Cores 3.1 and 3.2. The results are tabulated in **Table 3.3.3.3b**.

Discussion. It was observed that oil recoveries from Cores 3.3 and 3.4 were about 0.5 times the recoveries from Cores 3.1 and 3.2 when the bio-surfactant concentration was halved from 21.0 to 10.5 ppm. Oil recoveries were also significantly lower than the recoveries in Experiments 1 and 2 where the bio-surfactant concentrations were 41.0 and 38.0 ppm respectively. This relationship can be verified by further experiments. Another significantly important result was that nearly 25.0 % of residual oil was recovered with only 21.0 ppm (0.0021 gm/l) of bio-surfactant.

Surfactant flowrate was increased from 5.1 cc/hr in Core 3.1 to 6.4 cc/hr in Core 3.2 to determine if a higher flowrate increased oil recovery. The small increase in flowrate (20.0 %) was not sufficient to increase oil recovery at equal bio-surfactant concentrations. This was similar to the result of Experiment 2 where doubling the surfactant rate did not improve oil recovery.

Comparing the oil production profile to the production profiles of the previous experiments, it was also observed that injecting surfactant at a higher rate relative to flowrates in Experiments 1 and 2 resulted in oil breakthrough at close to the expected 0.5-0.6 PV of surfactant injection. This supports the idea that bypassing of some of the oil at low surfactant rates resulted in oil production during postflush injection. The higher

postflush flowrate provided enough force to move the trapped oil near the core's discharge end.

Results from Experiments 1, 2 and 3 showed that small changes in surfactant flowrate did not impact the total oil recovery but affected the timing of oil recovery. This is supported by the studies that relate capillary number to residual oil saturation which show that a small increase in flowrate is unlikely to have a large impact on residual oil saturations[77]. Interfacial tension reduction by increasing the bio-surfactant concentration had a greater effect on oil saturation reduction. From a field application point of view, this is advantageous because increasing bio-surfactant concentration is easier than increasing flowrates in the field. Investigators have reported that if IFT is reduced close to zero dynes/cm, flowrates would cease to have any impact on oil recovery[73,76].

Surfactant flowrates were not increased to large values in order to have realistic field front advance rates. Surfactant advance rates at 5.1 or 6.4 cc/hr translated to front advance rates between 2.0-2.8 ft/day while studies[73] show that field frontal advance rates generally are between 0.5-2.0 ft/day.

Table 3.3.3.3a. IFT measurements. Experiment 3.

Bio-surfactant concentration (ppm)	**IFT (Dynes/cm)**
21.0	1.42
10.5	2.04

Table 3.3.3.3b. Experiment 3 results summary

Core	**K_{abs} (md)**	**PV (cc)**	**$S_{OR,Wf}$ (%)**	**Poro. (Fr.)**	**Recovery (%)**	**N_{cp} (WF)**	**N_{cp} (EOR)**
3.1	34.8	25.0	40.8	0.15	26.5	1.8E-4	1.0E-2
3.2	22.8	30.0	36.0	0.19	27.8	1.4E-4	1.0E-2
3.3	-	26.5	51.4	0.16	13.4	1.6E-4	8.3E-3
3.4	29.7	26.5	39.6	0.17	16.2	1.6E-4	8.2E-3

3.3.3.4. Experiment 4.

Procedure. In the previous experiment, oil recovery appeared to be directly proportional to the JF-2 bio-surfactant concentration. The relationship was inconclusive since only two data points were available. To verify this relationship, six Berea sandstone cores, six inches long and one-half inches in diameter were treated with surfactant containing decreasing JF-2 bio-surfactant concentrations. The cores were numbered 4.1 to 4.6. One numbered Core 4.7 was injected with 2.0 PVs of surfactant to investigate if a larger volume of bio-surfactant could recover oil without using postflush. And finally, one numbered Core 4.8 was flooded with a solution of the co-surfactant, 2,3-butanediol and 1000.0 ppm PHPA polymer to quantify the role of polymer and co-surfactant in oil recovery by JF-2 surfactant. All the cores were at waterflood residual oil saturation before the surfactant or chemical treatment.

Three surfactant solutions, A, B and C were prepared. Surfactant A contained 11.0 ppm of JF-2 bio-surfactant; Surfactant B was diluted to 5.5 ppm and Surfactant C to 2.8 ppm of bio-surfactant. The measured interfacial tension between crude oil and brine at the different bio-surfactant concentrations are shown in **Table 3.3.3.4a**. Cores 4.1 and 4.2 were each injected with 1.0 PV of Surfactant A, Cores 4.3 and 4.4 with 1.0 PV of Surfactant B and Cores 4.5 and 4.6 with Surfactant C. Surfactant was injected into cores 4.1, 4.2 and 4.3 at 5.1 cc/hr and into Cores 4.4, 4.5 and 4.6 at 6.4 cc/hr. The rate was increased to reduce oil bypassing that prevented oil production during surfactant injection in Cores 4.1, 4.2 and 4.3. All the cores had 1.0 PV of postflush brine injected at the waterflood rate of 20.5 cc/hr.

Two pore volumes of Surfactant A was injected into Core 4.7 at 5.1 cc/hr followed by postflush brine and Core 4.8 was injected with 1.0 PV of polymer solution at 6.4 cc/hr followed by postflush brine.

Observations. No oil was recovered from Cores 4.1 and 4.2 during surfactant injection but 1.7 cc and 1.8 cc of oil were recovered from the two cores after 2.0 cc and 6.0 cc of postflush respectively. No oil was recovered from Core 4.3 during surfactant injection but 1.0 cc of oil was produced after 4.0 cc of postflush. From Core 4.4, 0.6 cc of oil was produced after 0.6 PV surfactant was injected into the core and another 0.5 cc of oil after 5.00 cc of postflush. Oil recoveries from Cores 4.1, 4.2, 4.3 and 4.4 were 14.0%, 16.0%, 9.0% and 10.0% respectively (**Table 3.3.3.4b**). No oil was recovered from Cores 4.5 and 4.6 during surfactant flooding but 1.3 cc and 1.7 cc of oil were produced after 4.0 and 5.0 cc of postflush. Oil recovery from both cores was close to 10.0 %.

From Core 4.7, 0.8 cc of oil was first produced after 1.6 PVs of surfactant injection. Another 1.5 cc of oil was produced after 4.0 cc of postflush. Residual oil recovery was 20.0 %. From Core 4.8, about 0.15 cc of oil was produced after 0.6 PV of polymer solution was injected and another 1.0 cc of oil was produced soon after the start of postflush. The total recovery was 10.0 % of residual oil. The oil production during postflush injection for all the cores had the slug production profile. The injection pressure rose significantly over the surfactant injection pressure and then rapidly declined following oil production.

Discussion. The residual oil recoveries did not verify the relationship observed between the bio-surfactant concentration and oil recovery from the previous experiment. Increasing the surfactant flowrate to 6.4 cc/hr in Core 4.4 caused a fraction of oil to be

produced after 0.5-0.6 PV of surfactant injection. But, the total oil recovery did not significantly change from Core 4.3. This again showed that a small change in flowrate did not affect oil recoveries when bio-surfactant concentrations were equal or similar. Oil production after 0.5-0.6 PV of surfactant injection when the cores were injected at 6.4 cc/hr again supported the idea that a higher rate can produce a greater fraction of oil at breakthrough.

Oil recovery from Cores 4.1 to 4.6 were between 9.0 % and 16.0 % of residual oil and appeared to be nearly similar to each other which suggested that recovery was independent of bio-surfactant concentration. If the similar oil recoveries from Cores 3.3 and 3.4 in Experiment 3 are added to Cores 4.1 to 4.6, a common feature among them is that they were treated with nearly equal quantities of bio-surfactant. If the oil recovery from Core 4.8 that was treated with 1.0 PV of plain polymer-alcohol solution and had a recovery of 10.0 % residual oil is also added to this list, it can be said that IFT reduction does affect oil recovery when bio-surfactant concentration is less than 11.0-15.0 ppm. This is because the 10.0 % of oil recovered from Core 4.8 was by improved displacement efficiency. Since all the cores with 11.0 ppm or less of bio-surfactant had oil recoveries close to 10%, it suggests that a minimum of 10.0-15.0 ppm of JF-2 bio-surfactant is required to recover residual oil by lowering the IFT. If this 10.0 % is subtracted from the oil recoveries from all the cores that received 1.0 PV of surfactant, the bio-surfactant contribution to oil recovery can be quantified. **Table 3.3.3.4c** shows the tabulated results after subtracting the 10.0 % of the polymer recovered oil. The results are plotted in **Figure 3.3.3.4a**.

Oil recovery from Core 4.7 showed that some oil can be recovered by only surfactant if a large enough (2.0 PVs) volume of surfactant is injected through the core at high enough velocity. Postflush at a higher rate would not be necessary for oil production. It was concluded that if Core 1.1 in Experiment 1 had been injected with surfactant at the same rate as Core 4.7 in this experiment, a similar oil recovery would have been observed since both surfactants had equal bio-surfactant concentrations.

Table 3.3.3.4a. IFT measurements, Experiment 4.

Bio-surfactant concentration (ppm)	IFT (Dynes/cm)
11.0	0.9
5.5	3.0
2.8	4.2

Table 3.3.3.4b. Experiment 4 results summary.

Core	K_{abs} md)	PV (cc)	$S_{OR,Wf}$ (%)	Poro. (Fr.)	Surf. Vol. (PV)	Recovery (%)	N_{cp} (WF)	N_{cp} (EOR)
4.1	108.0	31.5	39.0	0.18	1.0	13.8	9.4E-5	9.2E-3
4.2	72.0	32.0	35.3	0.18	1.0	15.9	9.5E-5	9.1E-3
4.3	72.2	32.0	35.6	0.18	1.0	8.8	9.5E-5	3.0E-3
4.4	68.7	30.0	40.0	0.17	1.0	9.6	1.0E-4	4.0E-3
4.5	60.9	31.8	39.6	0.18	1.0	10.3	9.5E-4	3.4E-3
4.6	122.9	32.5	39.4	0.18	1.0	13.3	9.4E-5	3.4E-3
4.7	103.0	31.0	36.8	0.18	2.0	20.2	9.7E-5	9.0E-3
4.8	240.0	33.0	36.1	0.19	1.0	9.7	9.2E-5	3.8E-4

Table 3.3.3.4c. Recovery after removing polymer effect.

Bio-surfactant concentration (ppm)	Recovery (Fraction)	Recovery – 0.1 (polymer) (Fraction)
41.0	0.39	0.29
38.0	0.48	0.38
38.0	0.45	0.35
21.0	0.27	0.17
21.0	0.28	0.18
10.5	0.13	0.03
10.5	0.16	0.06
11.0	0.14	0.04
11.0	0.16	0.06
5.5	0.09	0.0
5.5	0.1	0.0
2.8	0.1	0.0
2.8	0.13	0.03

Figure 3.3.3.4a. JF-2 bio-surfactant concentration and oil recovery.

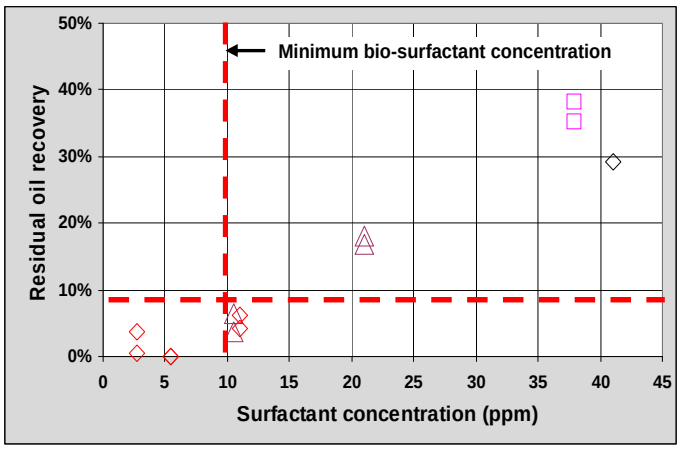

3.3.4. Summary. Results from Experiments 2, 3 and 4 showed that the surfactant injection rate affected the timing of oil production from the cores but not the cumulative oil recovery. Interfacial tension reduction had a greater impact on cumulative oil recovery than flow rate. This could be explained by the impact of changes in IFT and surfactant flowrate on the capillary number[77]. The reduction in IFT was usually bigger than the flowrate changes. Though both variables combine to give the capillary number, the impact of each on oil production showed which variable more easily changed the capillary number to lower the oil saturation.

The final objective of these experiments was to design a field-scale bio-surfactant aided microbial enhanced oil recovery flood. Oil production timing will be important since injecting a complete pore volume of surfactant will be uneconomic. It is not known if oil bypassing occurs in the field at typical advance rates of 0.5-1.5 ft/day. But it will be advantageous if a greater reduction in IFT through higher bio-surfactant concentration can overcome rate dependency and replace the effect of higher flowrates by IFT reduction[77].

Previous work suggests that surfactant and polymer degradation can be reduced by a viscous preflush ahead of the surfactant to displace high salinity resident brine[70,78]. But bio-surfactant generation within oil reservoirs can help reduce adsorption of bio-surfactant because transportation of bio-surfactant through the porous media is minimized. Nutrients and bacteria can be injected with normal waterflooding operation and reach parts of a reservoir that a viscous surfactant might not. Flowrate dependency can be reduced if sufficient bio-surfactant is generated. Lastly, there may be a relation between JF-2 bio-surfactant concentration and oil recovery (**Figure 3.3.3.4a**). But further studies are needed to confirm it. The relationship will be specific to the porous media.

3.3.5. Conclusions.

1. Concentrations of *Bacillus mojavensis* strain JF-2 bio-surfactant less than 41.0 ppm (0.0041 g/L) recovered up to 45.0 % of residual oil from low permeability Berea sandstone cores.
2. The oil recovered during surfactant injection is a function of surfactant flow rate but overall oil recovery is stronger function of bio-surfactant concentration and the resulting reduction of crude oil- brine IFT.
3. An approximately linear relationship was observed between the fraction of residual oil recovered and JF-2 bio-surfactant concentration.
4. The viscosifying polymer and co-surfactant alcohol recovered 10.0 % of residual oil through improved conformance.
5. A minimum concentration of JF-2 bio-surfactant between 10-15 ppm is required to recover residual oil by interfacial tension reduction when one pore volume of

surfactant is used to treat the cores.

6. A combination of resistance to flow by mobilized oil retention near the core outlet and permeability reduction by polymer retention was the most likely reason for high injection pressures observed during surfactant and post surfactant brine injection.

3.4 Summary and Conclusions. This chapter presented experimental studies and data analysis to use in a MEOR simulator for simulating JF-2 bio-surfactant based oil recovery. The IFT experiments led to the development of relationships between JF-2 bio-surfactant concentration and IFT and between IFT and brine salinity. The biopolymer studies characterized the SP-018 bio-polymer behavior for use in the MEOR simulator and the coreflood experiments showed that JF-2 bio-surfactant can recover residual oil from consolidated cores. The core experiments also served as physical models for numerical simulation. The conclusions from the experiments and data analysis are summarized:

1. A new mathematical model was developed to calculate IFT between oil and water as a function of JF-2 bio-surfactant concentration.
2. A linear relationship was used to calculate the change in IFT with increasing salinity.
3. The bio-polymer SP-018 was characterized using previous laboratory data. The effect of polymer concentration, salinity and shearing on viscosity were modeled using established mathematical Equations.
4. A new mathematical model was developed to calculate the change in fluid viscosity with salinity. The new model accurately predicted SP-018 and polyacrylamide viscosity at very low salinities.
5. Berea core flood experiments with JF-2 bio-surfactant showed that low JF-2 bio-

surfactant concentrations (0.021-0.041 mg/scc) could recover significant fractions of residual oil from consolidated Berea sandstone cores but a minimum of 10.0 to15.0 ppm (0.001-0.015 mg/scc) of bio-surfactant was required for IFT reduction to occur .

6. Oil recovery was observed to be proportional to JF-2 bio-surfactant concentration but that could not be verified with available data.

CHAPTER IV

MATHEMATICAL MODELS AND NUMERICAL FORMULATION

In this chapter the mathematical and numerical formulations used in the MEOR numerical simulator are described. The mathematical formulations are described first followed by the numerical formulations of the models.

4.1 Mathematical models.

The description of the mathematical models starts with the listing of the formulae used in the black oil solver to calculate the pressure and phase saturations. This is followed by the component transport model that uses the convection diffusion equation to calculate the concentrations of fourteen components. The oil recovery mechanisms and the modifications made to the existing model: aqueous phase polymer solution viscosity and salinity effects are presented next. Finally, the oil recovery and permeability reduction models coupled to the component transport model are discussed.

A multiphase black oil multi-component MEOR numerical model[6] was modified to add the effects of salinity, alcohol, polymer shearing and permeability reduction by polymer retention during a microbial treatment process. The features included in the modified MEOR simulator are:

1. New relationship between bio-surfactant concentration and IFT.

2. Addition of sodium chloride and calcium as components for aqueous phase salinity and hardness.
3. Increased oil-water IFT and surfactant adsorption due to salinity.
4. Effect of brine salinity and hardness on polymer viscosity and adsorption.
5. Polymer solution viscosity reduction due to shearing.
6. Reduction of permeability due to polymer retention.
7. Use of transport number instead of capillary number for residual oil mobilization.

4.1.1. Black oil model formulation

Multiphase pressures and saturations for the MEOR model were calculated with a black oil model that employed the IMPES formulation and LSOR solver[6,79]. Three phases; oil (o), water (w) and gas (g) were considered. Mass transfer between the water and oil phases and water or oil vaporization into the gas phase were neglected. The basic mass balance and continuity equations are[80]:

$$\frac{\partial}{\partial t}\left(\phi\frac{S_l}{B_l}\right) = \nabla.\left[\left(\frac{\vec{u}_l}{B_l}\right)\right] - Q_l \qquad \text{for } l = \text{o, w} \tag{4.1}$$

$$\frac{\partial}{\partial t}\left[\phi\left(\frac{S_g}{B_g}+\frac{R_{so}S_o}{B_o}+\frac{R_{sw}S_w}{B_w}\right)\right] = \nabla.\left(\frac{\vec{u}_g}{B_g}+\frac{R_{so}\vec{u}_o}{B_o}+\frac{R_{sw}\vec{u}_w}{B_w}\right) - \left(Q_g + R_{so}Q_o + R_{sw}Q_w\right)$$

for gas (4.2)

where, Q_o, Q_w and Q_g are volumetric flowrates per unit volume for pseudo oil, gas and water components:

$$Q_l = \frac{\tilde{m}_l}{\rho_l B_l} \qquad l = \text{o, w, g} \tag{4.3}$$

and $\tilde{m}_l$ is the mass flux of the oil, gas and water components per unit volume per unit time. The Darcy flux for the oil, water and gas phases is given by:

$$\vec{u} = -\frac{\overrightarrow{\overrightarrow{K}} K_{rl}}{\mu_l} \nabla (P_l - \rho_l \frac{g}{g_c} h) \tag{4.4}$$

where, $\overrightarrow{\overrightarrow{K}}$ is the diagonal permeability tensor, K_{rl}, μ_l, ρ_l and P_l are the relative permeability, phase viscosity and density and the phase pressure respectively. 'g' and 'g_c' are the gravitational constant and the conversion constant, and 'h' is the positive distance below a reference plane. The densities for oil, water and gas phases are related to the formation volume factor and gas solubility by:

$$\rho_l = \frac{1}{B_l}\left(\rho_{l,sc} + R_{s,l}\rho_{g,sc}\right) \qquad \text{for } l = \text{oil and water} \tag{4.5}$$

$$\rho_g = \frac{\rho_{g,sc}}{B_g} \tag{4.6}$$

The term '*sc*' in the subscripts stands for standard conditions. The oil, water and gas pressures, P_o, P_w and P_g, are related to each other by the capillary pressure:

$$P_{cow} = P_o - P_w \tag{4.7}$$

$$P_{cog} = P_g - P_o \tag{4.8}$$

The above equations were combined using IMPES to write a single governing equation in terms of the unknown oil phase pressure[6]:

$$\phi C_t \frac{\partial P}{\partial t} = \sum_{l=o,w,g} \beta_l \left[\nabla.(\psi_l \nabla P) + GC_l - \frac{q_l}{V_b} \right] \tag{4.9}$$

where, C_t is the total compressibility, β_l is the formation volume factor for phase *l*, ψ_l is the transmissibility for phase *l*, GC_l is the term comprising of gravity and capillary pressure for phase *l*, q_l is the volumetric injection or production rate for phase *l*.

$$C_t = \frac{1}{\phi}\frac{\partial \phi}{\partial P} + \sum_{l=o,w}\left(-\frac{1}{B_l}\frac{\partial B_l}{\partial P} + \frac{B_g}{B_l}\frac{\partial R_{sl}}{\partial P}\right)S_l + -\frac{1}{B_g}\frac{\partial B_g}{\partial P}S_g \tag{4.10}$$

$$\beta_l = B_l - R_{sl}B_g \qquad \text{for } l = \text{o,w} \tag{4.11}$$

$$\beta_g = B_g \tag{4.12}$$

$$\psi_l = \overrightarrow{\overrightarrow{K}}\frac{K_{rl}}{B_l \mu_l} \qquad \text{for } l = \text{o,w} \tag{4.13}$$

$$\psi_g = \overrightarrow{\overrightarrow{K}}\frac{K_{rg}}{B_g \mu_g} + R_{so}\psi_o + R_{sw}\psi_w \tag{4.14}$$

$$GC_o = -\nabla.\left[\psi_o \nabla\left(\rho_o \frac{g}{g_c} z\right)\right] \tag{4.15}$$

$$GC_w = -\nabla.\left[\psi_w \nabla\left(\rho_w \frac{g}{g_c} z + P_{cow}\right)\right] \tag{4.16}$$

$$GC_g = -\nabla.\left[\psi_g \nabla\left(\rho_g \frac{g}{g_c} z - P_{cog}\right)\right] + R_{so}GC_o + R_{sw}GC_w \tag{4.17}$$

$q_l = Q_l V_b$ for *l* = oil and water (4.18)

$q_g = Q_g V_b + R_{so}q_o + R_{sw}q_w$ (4.19)

The phase saturations are evaluated after solving for the phase pressures with the following equations:

$$\frac{\partial}{\partial t}\left(\phi \frac{S_l}{B_l}\right) = \nabla.(\psi_l \nabla P) + GC_l - \frac{q_l}{V_b} \qquad \text{for } l = \text{o, w} \tag{4.20}$$

$S_g = 1 - S_o - S_w$ (4.21)

4.1.2 Component transport formulation

The convection diffusion equation with adsorption and component generation describing the movement of the fourteen component MEOR model through the system is explained here. The transport of the following components is modeled: nutrients, metabolic by-products, microorganisms and sodium chloride and calcium ions. The sodium chloride and calcium ions have been added to the components that were included in the earlier MEOR model. Component transport occurs under the influence of viscous, gravity, capillary and dispersion forces. It is assumed that all the components are only transported through the water phase. A general material balance for a component 'k' is[6]:

$$\frac{\partial}{\partial t}\left(\frac{\phi S_w}{B_w}C_k + \phi C_{ks}\right) = -\nabla.\left(\frac{\vec{u}_t}{B_w}C_k\right) + \nabla.\left(\frac{\phi S_w}{B_w}\overrightarrow{\overrightarrow{D}}_k \nabla(C_k)\right) - Q_w C_k + \frac{\phi S_w}{B_w}R_k \qquad (4.22)$$

where, C_k and C_{ks} are the flowing and sorbed mass concentrations at surface conditions for component 'k', ϕ is the rock porosity, S_w, B_w and Q_w are saturation, formation volume factor and the volumetric injection/production rate for the water phase, V_b is the bulk volume of the medium, $\vec{u}_t$ is the total flow velocity and is defined as the sum of the Darcy and chemotactic velocities for only bacteria and the Darcy velocity for all the other components, the physical dispersion tensor for the component 'k' in the water phase is represented by $\overrightarrow{\overrightarrow{D}}_k$ and the biological bacterial growth, product formation or nutrient consumption rates by R_k.

The two terms on the left side of equation 4.22 represent the accumulation of component 'k' in the aqueous phase and the adsorption of component 'k' in the pore space. The four terms on the right hand side of the equation are convection, dispersion, external injection/production and the metabolic reaction of component 'k'. The

component ‘k’ can be bacteria (b), metabolic products (p), or substrates/nutrients (s). The velocity $\vec{u}_t$ in the convection term of the equation 4.23 is defined as[81]:

$$\vec{u}_t = \vec{u}_w + K_c \nabla(\ln C_s) \qquad \text{for bacteria} \tag{4.23}$$

$$\vec{u}_t = \vec{u}_w \qquad \text{for metabolic products, substrates/nutrients and ionic components} \tag{4.24}$$

where, $\vec{u}_w$ represents the Darcy velocity (flux) for the water phase, K_c is the chemotactic coefficient and C_s is the substrate or nutrient concentration. Chemotactic movement is defined as the directed movement of a cell toward an attractant (generally a nutrient). Microorganisms can sense a nutrient-rich environment and move in that direction. Darcy flow occurs due to pressure gradient while chemotactic migration of bacteria is assumed to be proportional to an exponential change in substrate concentration[81]. Chemotactic flow of bacteria is much smaller than convective flow. Hence, it is significant only near static conditions.

The elements of the dispersion tensor include both molecular diffusion and mechanical dispersion. For an isotropic medium, these elements are given as[82]:

$$D_{kw,ij} = \frac{D_k}{\tau} + \frac{(\alpha_{lw} - \alpha_{tw})}{\phi S_w} \frac{u_{wi} u_{wj}}{\left|\overrightarrow{u_w}\right|} + \frac{\delta_{ij} \alpha_{tw} \left|\overrightarrow{u_w}\right|}{\phi S_w} \tag{4.25}$$

$\delta_{ij} = 0$ when $i \neq j$

where, D_k is the molecular diffusion coefficient for component ‘k’ in the aqueous phase, α_{lw} and α_{tw} are the longitudinal and transverse dispersivities and u_{wi} (i = X, Y or Z) is the Darcy velocity component in the X-, Y- and Z directions, $D_{kw,ij}$ (i = X,Y or Z, j =X, Y or Z) is the dispersion coefficient in the ‘j’ direction when flow is in the ‘i’ direction and τ

is the tortuosity of the porous medium. The resultant aqueous phase Darcy velocity or the norm of the Darcy velocity is:

$$\left|\overrightarrow{u_w}\right| = \sqrt{u_{wx}^2 + u_{wy}^2 + u_{wz}^2} \tag{4.26}$$

The physical dispersion phenomenon is characterized by a full dispersion tensor[82]:

$$\overrightarrow{\overrightarrow{D}} = \begin{bmatrix} D_{kw,xx} & D_{kw,xy} & D_{kw,xz} \\ D_{kw,yx} & D_{kw,yy} & D_{kw,yz} \\ D_{kw,zx} & D_{kw,zy} & D_{kw,zz} \end{bmatrix} \tag{4.27}$$

If the X axis is aligned with the direction of average velocity, the dispersion co-efficients that represent the cross terms, $D_{kw,xy}$, $D_{kw,yx}$, $D_{kw,xz}$, $D_{kw,zx}$, $D_{kw,yz}$, $D_{kw,zy}$ become zero and the dispersion tensor is :

$$\overrightarrow{\overrightarrow{D}} = \begin{bmatrix} D_{kw,xx} & 0 & 0 \\ 0 & D_{kw,yy} & 0 \\ 0 & 0 & D_{kw,zz} \end{bmatrix} \tag{4.28}$$

4.1.3 Bacterial growth, metabolic byproduct generation and nutrient consumption rate formulation

Bacterial growth can occur in either a single-substrate or a double-substrate medium. Growth can be inhibited by alcohol, a metabolic product. A Monod type of specific growth rate with modifications of double-substrate limitation and growth inhibition by end product can be expressed as[6,83]:

$$\mu_b = \mu_{bm}\left(\frac{C_{s1}}{K_{b/s1}+C_{s1}}\right)\left(\frac{C_{s2}}{K_{b/s2}+C_{s2}}\right)\left(\frac{K_i}{K_i+C_i}\right) \tag{4.29}$$

where, μ_{bm} is maximum specific growth rate; C_{s1} and C_{s2} are concentrations for substrates 1 and 2, $K_{b/sl}$ and $K_{b/s2}$ are saturation constants for substrates 1 and 2. The specific growth rate of the bacteria is equal to half its maximum value at these saturation constants; K_i is the inhibition constant and C_i is the inhibitor concentration. If growth inhibition does not occur and growth is controlled by one substrate then Equation 4.29 reduces to a regular Monod model where the biomass multiplication rate by the planktonic (R_{bf}) and sessile (R_{bs}) phases of bacteria is computed by[6,83]:

$$\mu_b = \mu_{bm}\left(\frac{C_{s1}}{K_{b/s1}+C_{s1}}\right)\left(C_b + \sigma\rho_{b,sc}\right) \tag{4.30}$$

where, C_b is the concentration of the flowing bacteria, σ is the pore volume fraction occupied by bacteria sorbed on the pore surfaces, $\rho_{b,sc}$ is the biomass density at surface conditions and is constant.

It is assumed that metabolic production occurs in both the planktonic and sessile phases of bacteria. An empirical equation is used to calculate product production rate[6,83]:

$$R_p = \mu_{pm}\frac{C_s - C_{sc}}{K_{p/s}+C_s-C_{sc}}\left(C_b+\sigma\rho_b\right) \qquad \text{for } C_s > C_{sc} \tag{4.31}$$

where, μ_{pm} is maximum specific production rate; $K_{p/s}$ is the saturation constant for production of product 'p' by consumption of nutrient/substrate 's'; C_{sc} is the critical substrate concentration for metabolism. The metabolic products that are modeled are nitrogen, carbon dioxide, acid, alcohol, bio-surfactant and bio-polymer.

Microbial growth, metabolic production and maintenance energy is provided by nutrients/substrates consumption[6,83]:

$$R_s = -\frac{R_{bf} + R_{bs}}{Y_{b/s}} - \left(\sum_p \frac{R_p}{Y_{p/s}}\right) - m_s\left(C_b + \sigma\rho_{bsc}\right) \tag{4.32}$$

where, R_s, R_{bs}, R_{bf} and R_p are rates for substrate consumption, sessile and flowing bacterial growth and metabolic production formation respectively, $Y_{b/s}$ and $Y_{p/s}$ are yield coefficients for biomass and product and m_s is the maintenance energy coefficient provided by consuming substrate or nutrient.

4.1.4 Polymer viscosity model formulation.

Polymer addition to the water in secondary and tertiary oil recovery waterfloods is done to lower the mobility of the water phase and improve its displacement efficiency. In micellar polymer floods, a viscous solution injection behind the surfactant helps displace retained surfactant and improve the displacement efficiency of the surfactant[37,69,84]. The polymer can be bio-polymers produced by bacteria, or polysaccharides such as xanthan gum or synthetic polymers like hydrolyzed polyacrylamide mixed in water or brine.

The increase in water viscosity when polymers are dissolved in water and the relationship between polymer concentration and the solution's apparent viscosity depends on the polymer. Polymer viscosity is determined by the Flory-Huggins equation[61,62,63]:

$$\mu_{w,p} = \mu_w\left(1 + (Ap_1 C_7 + Ap_2 C_7{}^2 + Ap_3 C_7{}^3)\right) \tag{4.33}$$

where, μ_w and $\mu_{w,p}$ are the water phase viscosities before and after polymer addition, Ap_1, Ap_2, Ap_3 are viscosity parameters and C_7 is the polymer concentration. Equation 4.34 has been used to predict xanthan gum and polyacrylamide solution viscosities[61,63]. It was shown in Chapter 2 that Equation 4.33 can be also used to predict solution viscosity when the bio-polymer SP-018 is dissolved in water[60].

A major problem that adversely affects the polymer in field floods is polymer degradation and the subsequent reduction in viscosity and loss of mobility control. Degradation is generally microbial in nature for bio-polymers and chemical for synthetic polymers. Primarily, chemical degradation is caused by salinity and hardness in reservoir brines. Salinity is caused by sodium chloride and hardness is generally caused by calcium and magnesium ions. Salinity and hardness have a strong adverse effect on polymer viscosity, especially if the polymer is a polyacrylamide[62]. The ions coat the polymer chains in aqueous solution creating a double layer of charge. This results in reduced repulsion between polymer molecules and a loss in polymer viscosity[69,85,86]. Studies have shown that calcium ions have a stronger effect on polymer molecules than sodium chloride[87]. Based on the work by Camilleri et al.[40] and Saad[63], to account for the presence of sodium chloride and calcium ions in water, Equation 4.33 is modified to:

$$\mu_{w,p} = \mu_w \left(1 + (Ap_1 C_7 + Ap_2 C_7^{\,2} + Ap_3 C_7^{\,3}) \left(\frac{1.0}{1.0 - S_p C_{Sep}} \right) \right) \tag{4.34}$$

where, C_{sep} is the effective salinity for polymer and S_p is the slope of the log-log plot of polymer viscosity and effective brine salinity and is a constant. Generally, *Sp* is small and positive for Xanthan gum and Xanflood and large and negative for polyacrylamide and bio-polymers. The modification to Equation 4.34 from the original equation proposed by Camilleri et al.[40] and Saad[63] was explained in Chapter 3. The salinity adjusted viscosity predicted by Equation 4.34 is shown in **Figure 3.2.2** and **3.2.3**.

Effective brine salinity for polymer is given by[40,63,86]:

$$C_{Sep} = C_{Chlorideions} + \left((Bp - 1) C_{Calciumions} \right) \tag{4.35}$$

where, $C_{Chloride\ ions}$ and $C_{Calcium\ ions}$ are the sodium chloride and calcium ionic concentrations (meq/ml) and *Bp* is a parameter controlling the contribution of the calcium ions towards the loss in polymer viscosity. Though reservoir brine also contains many other chemical species, only sodium chloride and calcium were considered in the formulation because studies have consistently shown that these two ions have the greatest impact on polymer solution viscosity.

Following the calculation of the polymer solution viscosity salinity effects, the solution viscosity is adjusted for shearing. A polymer solution is sheared when it flows through heterogeneous porous media. If the polymer is shear thinning, then the polymer solution's viscosity reduces leading to loss of displacing fluid mobility. Polyacrlamides, xanthan gum and the bio-polymer SP-018 are all shear thinning polymers. Shearing can be severe if flow velocity is high and the rock is highly heterogeneous[37]. A typical region in the reservoir with high shear is near a wellbore where fluid flow converges or diverges. The velocity decreases away from the wellbore and low flow rates are present in most of the reservoir. If shearing is within the elastic limit of the polymer, the solution can regain its viscosity in the low velocity region. Viscosity reduction by shearing is modeled by the Meter and Bird equation[33,36,64]:

$$\mu_{\dot{\gamma}} = \mu_{\infty} + \frac{\mu_0 - \mu_{\infty}}{\left(\frac{\dot{\gamma}}{\gamma_{\frac{1}{2}}}\right)^{P_{\alpha}-1}} \tag{4.36}$$

where, $\mu_{\dot{\gamma}}$ and μ_0 are the polymer solution viscosity before and after shear correction, μ_{∞} is the viscosity of the solution at infinite shear rate and is generally taken to

be that of water, $\dot{\gamma}$ is the shear rate of flowing polymer solution, $\gamma_{\frac{1}{2}}$ is the shear rate of the flowing polymer solution when its viscosity is half the viscosity at zero shear rate and P_α is a dimensionless shear rate parameter that defines the abruptness of change in viscosity with increasing shear rate. The shear rate of the polymer solution flowing through a porous media is calculated by[36, 63, 88,89]:

$$\dot{\gamma} = \left(\frac{3n}{4n-1}\right)^{\frac{n}{n-1}} 4\frac{|u_t|}{\sqrt{8KK_{rl}\phi S_l}} \tag{4.37}$$

where, n is the dimensionless fluid exponent, u_t the water phase velocity, K and ϕ are the absolute permeability and porosity of the medium and K_{rl} and S_l are the relative water permeability and saturation. The water saturation term is included because shearing increases when oil is also present in the core. Equations 4.36 and 4.37 were verified for the bio-polymer SP-018 as discussed in Chapter 3.

4.1.5 Adsorption models

4.1.5.1 Microbial adsorption.

Adsorption of microorganisms in pore space is the result of the net mass exchange between retention and detachment[6,90]:

$$\frac{\partial C_{bs}}{\partial t} = K_r \left|\vec{u}_w\right| C_b(1-\sigma) - K_d(\sigma\rho_{bs})\left|\vec{\nabla}\Phi_w\right| \tag{4.38}$$

where, K_r and K_d are retention and detachment rates for microorganisms, respectively; $\vec{u}_w$ is water-phase Darcy velocity; C_b is the concentration of flowing bacteria; σ is pore-space fraction occupied by bacteria deposited on the pore surface; ρ_b is biomass density; and $\mathbf{\Phi}_w$ is the water-phase potential. The cell retention rate is proportional to the biomass

entering a given area, that is '$\left|\vec{u}_w\right|C_b$' and to the plugging capacity of the porous media, '1-σ'. The cell detachment rate is a function of the retained biomass, '$\sigma\rho_b$' and the shear force between the flowing and stationary forces '$\left|\nabla\Phi_w\right|$'.

Adsorption of nutrients and metabolic products are modeled by the Langmuir adsorption isotherm. The Langmuir isotherm assumes instantaneous equilibrium compared with the rate of convection and dispersion[6,21,91]:

$$C_{ks} = \frac{a_k C_k}{1 + b_k C_k} \tag{4.39}$$

where, C_{ks} is the adsorbed mass of component 'k' per unit volume, a_k and b_k are Langmuir isotherm constants and C_k is the mass concentration of the component 'k' in aqueous suspension.

4.1.5.2 Polymer and surfactant adsorption

Modifications are introduced to the polymer and bio-surfactant adsorption isotherms to account for the increased adsorption due to brine salinity. Brine salinity increases the adsorption of surfactant and polymer[26,27,28]. Laboratory and field studies have shown a relationship between brine salinity and polymer and surfactant adsorption[36]. The Langmuir isotherm parameters were modified to account for the adverse role of salt in the aqueous phase. For the polymer, the term 'a_k' is modified to[40]:

$$a_k = a_{k1} + a_{k2} C_{sep} \tag{4.40}$$

and for bio-surfactant:

$$a_k = a_{k1} + a_{k2} C_{Se} \tag{4.41}$$

where, a_{k1} and a_{k2} are adsorption constants and C_{sep} and C_{se} are effective salinities for the polymer and bio-surfactant respectively.

The calculation of C_{sep}, the effective salinity for polymers is given by Equation 4.35. But for surfactants, the effective salinity, C_{se} is not only a function of the sodium chloride and calcium ion concentrations, but also the co-surfactant alcohol concentrations. Co-surfactant alcohols are added to surfactants to improve oil recovery. Water soluble alcohols increase the surfactant's optimal salinity and improves the surfactant's salinity tolerance[27,63,92].

The effective salinity for the surfactant, C_{sep} including the effect of the co-surfactant alcohol is given by[40,63]:

$$C_{Se} = \frac{C_{11}}{\left(1-\beta_{12} f^{s}{}_{12}\right)\left(1-\beta_5 f_5^s\right)} \tag{4.42}$$

where, β_{12}, and β_5 (<0) are slope parameters for calcium and alcohol dilution effects[40], f_{12}^s and f_5^s are the fraction of calcium ions and alcohol associated with the bio-surfactant and C_{11} is the concentration of chloride ions in the aqueous solution (meq/ml).

$$f_5^s = \frac{\frac{C_5}{\rho_5}}{\frac{C_5}{\rho_5}+\frac{C_6}{\rho_6}} \tag{4.43}$$

$$f_{12}^s = \frac{C_{12}}{C_{11}+C_{12}} \tag{4.44}$$

where, C_5, C_6, are the mass concentrations of alcohol and the surfactant, C_{11} and C_{12} are the equivalent concentrations of sodium chloride and calcium ions in the aqueous solution and ρ_5 and ρ_6 are the densities of the alcohol and bio-surfactant at standard conditions.

4.1.6 Permeability reduction model

4.1.6.1 Microbial retention

Biomass accumulation on pore surfaces forms a stationary biofilm (sessile bacteria) which can increase in mass by consumption of nutrients[90]:

$$\frac{\partial \sigma \rho_{bs}}{\partial t} = R_d - R_r + R_{bs} = K_r \left|\vec{u}_w\right| C_b (1-\sigma) - K_d (\sigma \rho_{bs}) \left|\vec{\nabla} \Phi_w\right| + R_{bs} \tag{4.45}$$

Permeability modification is assumed to be caused by both pore-surface retention and pore-throat plugging by bacterial cells. The permeability reduction factor is defined as[41,42,43]:

$$\frac{K}{K_o} = f\left(\frac{\phi}{\phi_0}\right)^3 \tag{4.46}$$

where, K_0 and ϕ_o are initial permeability and porosity, respectively; K and ϕ are the instantaneous permeability and porosity; f is defined as flow efficiency factor which accounts for pore-throat plugging phenomena.

4.1.6.2 Polymer retention

Permeability reduction is caused by polymer retention. Polymer molecules get stuck in the constrictions within the porous media. Polymer retention is greater for polyacrylamides compared to polysaccharides[69]. The loss of permeability is measured in terms of residual resistance factor or *RRF*. This term is modeled by[36,63,88]:

$$RRF = 1 + \frac{(R_{k,\max} - 1) b_{rk} C_7}{1 + b_{rk} C_7} \tag{4.47}$$

where, $R_{k,max}$ is the resistance factor that is a function of polymer concentration C_7 and salinity, porosity and permeability of the system and b_{rk} is a permeability reduction parameter. $R_{k,max}$ is given by[36]:

$$R_{k,\max} = \left(1 - \frac{c_{rk}\left(\frac{A_{p1}}{1 - S_p C_{sep}} \right)^{1/3}}{\left(\frac{\sqrt{K_x K_y}}{\phi} \right)^{1/2}} \right)^{-4} \tag{4.48}$$

where, c_{rk} is a permeability reduction parameter.

Permeability reduction through retention is a function of salinity and the porous medium properties and is considered permanent. Some laboratory studies have shown that this reduction may not persist after a large number of pore volumes of fluid throughput. Prolonged fluid injection may eventually reduce the permeability reduction[89].

4.1.7 Oil recovery model

4.1.7.1 Interfacial tension reduction

In this section, mathematical equations that describe the mechanisms for enhanced oil recovery by microbial activity are given. These include interfacial tension reduction, capillary desaturation, relative permeability alteration and mobility control by polymer or bio-polymer.

The interfacial tension model used is based on a exponential correlation between interfacial tension (IFT) and the bio-surfactant concentration[56]:

$$\log(\sigma_{ow}) = \log(\sigma_{\min}) + \left[\log\left(\frac{\sigma_{\max}}{\sigma_{\min}} \right) \right] \left(\frac{C_{sf,\max} - C_{sf}}{C_{sf,\max} - C_{sf,\min}} \right)^{ES} \tag{4.49}$$

where, σ_{ow}, σ_{min} and σ_{max} are the instantaneous, minimum and maximum interfacial tensions between the oleic and aqueous phases, C_{sf}, $C_{sf,max}$ and $C_{sf,max}$ are the instantaneous, maximum and minimum bio-surfactant concentrations and ES is an exponent parameter. However, it was shown in the experimental IFT measurement

section of Chapter 3 that the relationship between IFT and JF-2 bio-surfactant concentration is more suitably described when Equation 4.49 is piecewise applied for different bio-surfactant concentration ranges.

The IFT between oil and water also depends on the aqueous phase salinity. In fact, brine salinity is the most important reservoir property that can adversely affect IFT. Various studies have conclusively shown that increasing brine salinity results in the increase in oil-water IFT [7,25-27]. A distinct increase in IFT was observed with increasing salinities for the JF-2 bio-surfactant is the focus of this work. Based on the results from Chapter 3, the following relationship corrects the IFT for the reservoir brine.

$$\sigma_{ow} = \sigma_{ow} + Par1\left(\Delta C_{11}\right) \tag{4.50}$$

where, *Par1* is equal to the slope of the plot between change in IFT and the change in brine salinity with respect to the base salinity of 5.0 % NaCl. The value of *Par1* is calculated in Chapter 3. C_{11} is the concentration of sodium chloride in the aqueous phase. The second term on the right side of Equation 4.50 calculates the increase in IFT with increasing brine salinity.

4.1.7.2 Capillary desaturation.

With decreasing interfacial tension, the trapping number increases. Residual phase saturations are modeled as a function of the trapping number:

$$S_{lr} = S_{lr}^{h} + \left(S_{lr}^{w} - S_{lr}^{h}\right)T_{l1}\left[\log\left(N_{tl}\right) + T_{l2}\right] \qquad S_{lr}^{h} \le S_{lr} \le S_{lr}^{w} \tag{4.51}$$

where, subscript l refers to the oil or water phase, S_{lr}^{w} and S_{lr}^{h} are residual saturations for phase l at low and high trapping numbers, respectively. N_{tl} is the trapping number for phase l, T_{l1} and T_{l2} are parameters related to the capillary desaturation curve. T_{l1} and T_{l2} are calculated by[45,63]:

$$T_{l1} = \left[\log\left[\frac{N_{tl}^{w}}{N_{tl}^{h}} \right] \right]^{-1} \tag{4.52}$$

$$T_{l2} = -\log\left(N_{tl}^{h}\right) \tag{4.53}$$

The trapping number is the sum of the capillary number that is the ratio of viscous forces to capillary forces and the gravity number which is the ratio of buoyancy to capillary forces[46,95]. The trapping number for a phase in a three dimensional system is given by[47]:

$$N_{tl} = \frac{1}{\sigma_{ow}} \left\{ \left[K_{xx} \left(-\frac{\partial \Phi_l}{\partial x} \right) \right]^2 + \left[K_{yy} \left(-\frac{\partial \Phi_l}{\partial y} \right) \right]^2 + \left[K_{zz} \left(-\frac{\partial \Phi_l}{\partial z} \right) - K_{zz} \Delta\rho \frac{g}{g_c} \right]^2 \right\}^{\frac{1}{2}} \tag{4.54}$$

where, K_{xx}, K_{yy} and K_{zz} are the absolute permeabilties of the porous medium in the X, Y and Z directions, Φ_l is the phase (aqueous) potential, $\Delta\rho$ is the difference in density of the displaced and displacing phases (oil and water) and σ_{ow}, the oil-water interfacial tension is determined by Equation 4.50.

4.1.7.3 Capillary pressure

A linear model was used to incorporate the oil-water capillary pressure dependence P_{cow} on oil-water interfacial tension σ_{ow} [56]:

$$P_{cow} = P_{cow}^{w} \left(\frac{\sigma_{ow} - \sigma_{\min}}{\sigma_{\max} - \sigma_{\min}} \right) \tag{4.55}$$

where, P_{cow}^{w} is the oil water capillary pressure at the low capillary number.

4.1.7.4 Relative permeability modification

The computed residual phase saturations are then used to determine the relative permeability for phase l[44,56]:

$$K_{rl}(S_l) = K_{rl}^{w}(S_l) + \frac{S_{lr}^{w} - S_{lr}}{S_{lr}^{w} - S_{lr}^{h}}\left[K_{rl}^{h}(S_l) - K_{rl}^{w}(S_l)\right] \quad (4.56)$$

where, subscript *w* and *h* refer to conditions at low and high trapping numbers respectively. Phase relative permeabilities at high capillary numbers are given by straight line models[44]:

$$K_{rl}^{h} = S_l \qquad \text{for } l = \text{oil or water} \quad (4.57)$$

4.1.7.5 Gases

The contribution of the produced gases, nitrogen and carbon dioxide, to enhanced oil recovery is through the black oil model. The gases increase the gas phase pressure causing the displacement of oil from the porous medium. The production rates for nitrogen and carbon dioxide are given by:

$$q_{g.k} = \frac{R_k V_{pw}}{\rho_{k,sc} B_w} \quad (4.58)$$

where, $q_{g.k}$ is the volumetric production rates at surface conditions for component 'k'. Here 'k' is either carbon dioxide or nitrogen. R_k is the mass generation for the gas component, V_{pw} is the pore volume occupied by the aqueous phase and $\rho_{k,sc}$ is the density of the gas at standard conditions.

4.2 Numerical formulation and finite difference equations.

4.2.1 Pressure equation

The difference equation that defines the material balance in terms of grid block pressures is[6,79]:

$$\left(\frac{V_p^n C_t^n}{\Delta t}\right)_{xyz}\left(P^{n+1}-P^n\right)_{xyz}=\left(B_o-R_{so}B_g\right)_{xyz}^n\left(\Delta A_o^n\Delta P^{n+1}+GCOT-Q_o\right)_{xyz}+$$
$$\left(B_w-R_{sw}B_g\right)_{xyz}^n\left(\Delta A_w^n\Delta P^{n+1}+GCWT-Q_w\right)_{xyz}+$$
$$\left(B_g\right)_{xyz}^n\left(\Delta A_g^n\Delta P^{n+1}+\Delta R_{so}^n\Delta A_o^n\Delta P^{n+1}+\Delta R_{sw}^n\Delta A_w^n\Delta P^{n+1}\right)_{xyz}+$$
$$\left(GCGT-Q_g\right)_{xyz} \tag{4.59}$$

where the term A represents the phase transmissibility across a face of a grid block in each direction of the grid block; west, east, north, south, top and bottom directions:

$$\Delta A\Delta P = A_{x-\frac{1}{2}}\left(\Delta P_{x-1}-\Delta P_x\right)+A_{x+\frac{1}{2}}\left(\Delta P_{x+1}-\Delta P_x\right)+A_{y-\frac{1}{2}}\left(\Delta P_{y-1}-\Delta P_y\right)+A_{y+\frac{1}{2}}\left(\Delta P_{y+1}-\Delta P_y\right)+$$
$$A_{z-\frac{1}{2}}\left(\Delta P_{z-1}-\Delta P_z\right)+A_{z+\frac{1}{2}}\left(\Delta P_{z+1}-\Delta P_z\right) \tag{4.60}$$

and

$$\Delta P_{xyz} = P_{xyz}{}^{n+1}-P_{xyz}{}^{n} \tag{4.61}$$

The solution is calculated in terms of ΔP_{xyz} because that increases the numerical precision of the equation.

The terms GCOT, GCWT and GCGT are terms that represent the gravity and capillary pressure. They are defined as:

$$GCOT = -\Delta A_o^n\Delta\left(\rho_o h\right)^n \tag{4.62}$$

$$GCWT = -\Delta A_w^n\Delta\left(\rho_w h+P_{cow}\right)^n \tag{4.63}$$

$$GCGT = -\Delta A_g^n\Delta\left(\rho_w h-P_{cog}\right)^n-R_{so}^n\Delta A_o^n\Delta\left(\rho_o h\right)^n-R_{sw}^n\Delta A_w^n\Delta\left(\rho_w h+P_{cow}\right)^n \tag{4.64}$$

The gravity and capillary pressure terms in the X direction are expressed as:

$$\Delta_x A_l^n \Delta_x (\rho_l h)^n = A_{l,x-1}^n \left(\frac{\rho_{l,x-1}^n + \rho_{l,x}^n}{2} \right) (h_{x-1} - h_x) + A_{l,x+1}^n \left(\frac{\rho_{l,x+1}^n + \rho_{l,x}^n}{2} \right) (h_{x+1} - h_x) \quad (4.65)$$

$$\Delta_x A_l^n \Delta_x (P_{cll'})^n = A_{l,x-1}^n \left[(P_{cll'})_{x-1}^n - (P_{cll'})_x^n \right] + A_{l,x+1}^n \left[(P_{cll'})_{x+1}^n - (P_{cll'})_x^n \right] \quad (4.66)$$

where, l, $l' = o, w, g$ and $l \neq l'$. Similarly, the gravity and capillary terms can be expanded in

the Y and Z directions.

The final finite difference equation is written in terms of P^{n+1} using all the above terms and expanding them in the Y and Z direction is:

$$AT_z P_{z-1}^{n+1} + AN_y P_{y-1}^{n+1} + AW_x P_{x-1}^{n+1} + AE_{xyz} P_{xyz-1}^{n+1} + AE_x P_{x+1}^{n+1} + AS_y P_{y+1}^{n+1} + AB_z P_{z+1}^{n+1} = B_{xyz} \quad (4.67)$$

However, if the equation is written for the immediate timestep change in pressure at each grid block, $\Delta P_{x,y,z}$, greater numerical precision can be achieved. The finite difference formulation is then written as:

$$AT_z \Delta P_{z-1}^{n+1} + AN_y \Delta P_{y-1}^{n+1} + AW_x \Delta P_{x-1}^{n+1} + AE_{xyz} \Delta P_{xyz-1}^{n+1} + AE_x \Delta P_{x+1}^{n+1} + AS_y \Delta P_{y+1}^{n+1} + AB_z \Delta P_{z+1}^{n+1} = \hat{B}_{xyz} \quad (4.68)$$

where,

$$\hat{B}_{xyz} = B_{xyz} - \left(AT_z P_{z-1}^n + AN_y P_{y-1}^n + AW_x P_{x-1}^n + AE_{xyz} P_{xyz}^n + AE_x P_{x+1}^n + AS_y P_{y+1}^n + AB_z P_{z+1}^n \right) \quad (4.69)$$

And,

$$A(E,W)_x = \left[B_o + 0.5 B_g \left(R_{so,x\pm1} - R_{so} \right) \right]^n A_{o,x\pm\frac{1}{2}} + \left[B_w + 0.5 B_g \left(R_{sw,x\pm1} - R_{sw} \right) \right]^n A_{w,x\pm\frac{1}{2}} + B_g^n A^n_{g,x\pm\frac{1}{2}} \quad (4.70)$$

$$A(S,N)_y) = \left[B_o + 0.5B_g\left(R_{so,y\pm1} - R_{so}\right)\right]^n A_{o,y\pm\frac{1}{2}} + \left[B_w + 0.5B_g\left(R_{sw,y\pm1} - R_{sw}\right)\right]^n A_{w,y\pm\frac{1}{2}} + B_g^n A^n_{g,y\pm\frac{1}{2}} \tag{4.71}$$

$$A(T,B)_z) = \left[B_o + 0.5B_g\left(R_{so,z\pm1} - R_{so}\right)\right]^n A_{o,z\pm\frac{1}{2}} + \left[B_w + 0.5B_g\left(R_{sw,z\pm1} - R_{sw}\right)\right]^n A_{w,z\pm\frac{1}{2}} + B_g^n A^n_{g,z\pm\frac{1}{2}} \tag{4.72}$$

$$E_{xyz} = -\left[AT_z + AN_y + AW_x + AE_x + AS_y + AB_z + \left(\frac{V_p^n C_t^n P^n}{\Delta t}\right)_{xyz}\right] \tag{4.73}$$

$$B_{xyz} = -\left[QOWG + \left(\frac{V_p^n C_t^n P^n}{\Delta t}\right)_{xyz}\right] \tag{4.74}$$

$$QOWG = \left(B_o - B_g R_{so}\right)^n_{xyz}\left(GCOT - Q_o\right)_{xyz} + \left(B_w - B_g R_{sw}\right)^n_{xyz}\left(GCWT - Q_w\right)_{xyz} + \left(B_g\right)^n_{xyz}\left(GCGT - Q_g\right)_{xyz} \tag{4.75}$$

Phase transmissibilities across grid blocks are defined as:

$$A_{l,i\pm\frac{1}{2}} = \left(\frac{2(KA)_i(KA)_{i\pm1}}{(\Delta i)_i(KA)_{i\pm1} + (\Delta i)_{i\pm1}(KA)_i}\right)\left(\frac{K_{rl}}{\mu_l B_l}\right)_{upstream} \qquad i = x, y, z \text{ and } l = o, w, g \tag{4.76}$$

where, K is the absolute directional permeability, A is the cross-sectional area, Δi is the grid block length in the 'i' direction and K_{rl} is the phase 'l' relative permeability. The pressure and saturation dependent functions in the mobility term are evaluated by the upstream weighting method[79].

The new pressures are determined implicitly by first calculating the change in pressure and adding it to the old pressure. Then the phase saturations are explicitly calculated using the following discrete equations:

$$S^{n+1}_{l,xyz} = \left(\frac{B_l}{V_p}\right)^{n+1}_{xyz}\left[\left(V_p\frac{S_l}{B_l}\right)^n + \Delta t\left(\Delta A_l \Delta P^{n+1} + GCOT - q_l\right)\right]_{xyz} \qquad l = o, w \tag{4.77}$$

$$S_{g,xyz}^{n+1} = 1 - S_{o,xyz}^{n+1} - S_{w,xyz}^{n+1} \quad (4.78)$$

4.2.2. Grid system

A block centered grid system was selected for the finite difference formulation. The X and Y directions are the areal co-ordinates and the positive Z direction is normal to the bedding plane in the downward direction. The blocks are numbered in natural order. The blocks are first numbered within a row, then row by row and then plane by plane. There are NX blocks in each row, NY blocks in each column and NZ blocks (layers) in each vertical column. So there are a total of NX x NY x NZ blocks in the entire system. Figure 4.1 and 4.2 show the grid system for a 3 x 3 x 3 grid system and the resultant co-efficient matrix[6]. The main diagonal in the matrix is the co-efficient E_{xyz}. The other co-efficients in each row represent the blocks on the east, west, north, south, top and bottom directions. The co-efficient matrix changes with block ordering. Direct and iterative methods can be used to solve the co-efficent matrix. Since the matrix is sparse, iterative methods are preferred because the amount of data stored is less compared to direct methods. The co-efficients are calculated using the finite difference formulation shown in the earlier section. The right hand of the matrix system is not shown.

Figure 4.1 Grid block numbering for a 3 x 3 x 3 system.

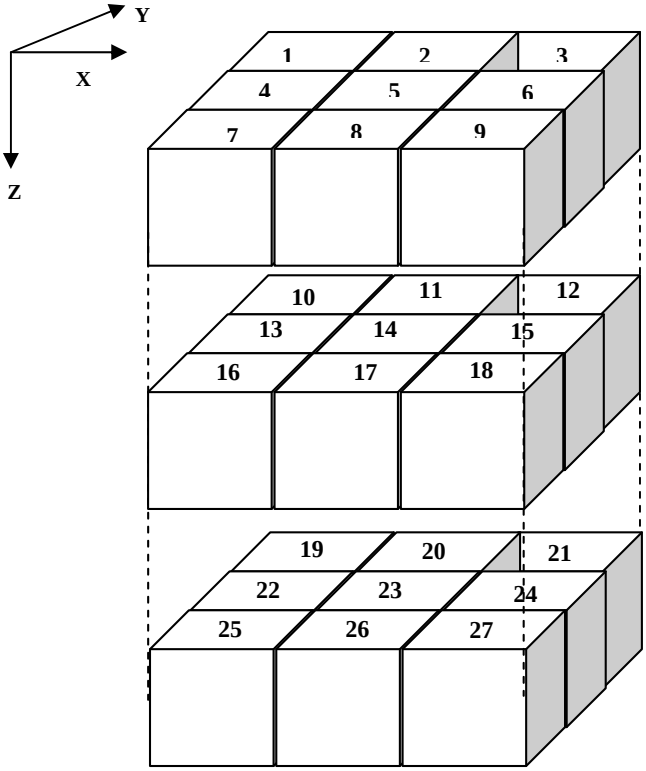

Figure 4.2 Coefficient matrix for the row-wise numbering system[79]

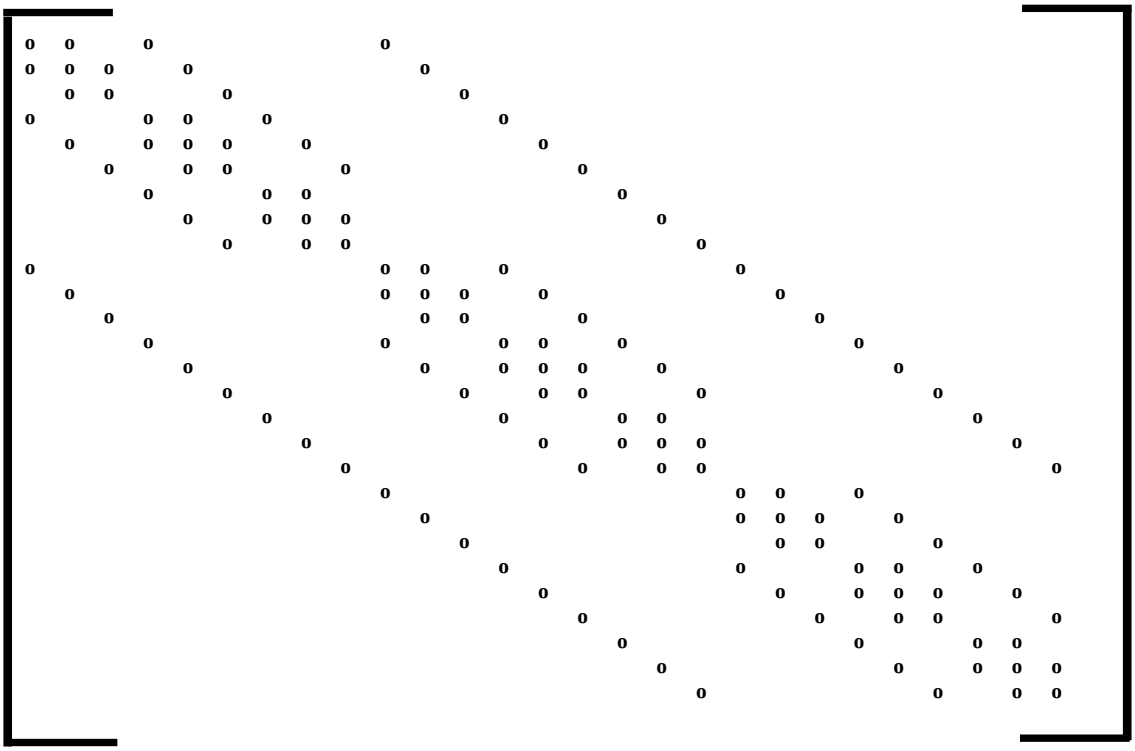

4.2.3. Component transport equations

The mass transport equations for the metabolic products, nutrients and salt ions is

$$\frac{\partial}{\partial t}\left(\frac{\phi S_w}{B_w}C_k + \phi C_{ks}\right) = -\nabla.\left(\frac{\vec{u}_t}{B_w}C_k\right) + \nabla.\left(\frac{\phi S_w}{B_w}\overrightarrow{\overrightarrow{D}}_k \nabla(C_k)\right) - Q_w C_k + \frac{\phi S_w}{B_w}R_k \tag{4.79}$$

Langmuir isotherms model the adsorption of the various components. If changes in porosity, phase saturations and formation volume factors are assumed to be small compared to changes in concentrations then Equation 4.79 can be written as:

$$\frac{\partial C_k}{\partial t} = \frac{1}{D_s}\left[-\nabla.\left(\frac{\vec{u}_w}{B_w}C_k\right) + \nabla.\left(\frac{\phi S_w}{B_w}\overrightarrow{\overrightarrow{D}}_k \nabla(C_k)\right) - \frac{q_w}{V_b}C_k + \frac{\phi S_w}{B_w}R_k\right] \tag{4.80}$$

where,

$$D_s = \frac{\phi S_w}{B_w} + \frac{\phi a_k}{(1+b_k C_k)^2} \tag{4.81}$$

At a grid block level, if Equation 4.80 is discretized spatially, then

$$\left(\frac{\partial C_k}{\partial t}\right)_{xyz} = \left[\frac{1}{D_s}\left[-\nabla.\left(\frac{\vec{u}_w}{B_w}C_k\right) + \nabla.\left(\frac{\phi S_w}{B_w}\overrightarrow{\overrightarrow{D}}_k \nabla(C_k)\right) - \frac{q_w}{V_b}C_k + \frac{\phi S_w}{B_w}R_k\right]\right]_{xyz} \tag{4.82}$$

The convection term in Equation 4.82 can be discretized in the X, Y or Z direction by:

$$\left[\nabla.\left(\frac{\vec{u}_w}{B_w}C_k\right)\right]_{xyz} = \sum_{i=x,y,z}\frac{1}{\Delta i_i}\left[\left(\frac{u_{wi}}{B_w}\right)_{i+\frac{1}{2}} C_{k,i+\frac{1}{2}} - \left(\frac{u_{wi}}{B_w}\right)_{i-\frac{1}{2}} C_{k,i-\frac{1}{2}}\right] \quad i = x, y, z \tag{4.83}$$

The convection concentrations of component ‘k’ at the grid block boundaries are calculated using Leonard’s third order upstream formula that is employed for variable grid block sizes[63]:

For the case where the water phase potential in block ‘*i*-1’ is greater than the water phase potential in block ‘*i*’,

$\Phi_{w,i-1} > \Phi_{w,i}$,

$$C_{k,i-\frac{1}{2}} = C_{k,i-1} + A_{i-1}\left(C_{k,i-1} - C_{k,i-2}\right) + 2B_{i-1}\left(C_{k,i} - C_{k,i-1}\right) \qquad i = x, y \text{ or } z \qquad (4.84)$$

and,

$$C_{k,i+\frac{1}{2}} = C_{k,i} + A_{i}\left(C_{k,i} - C_{k,i-1}\right) + 2B_{i}\left(C_{k,i+1} - C_{k,i}\right) \qquad i = x, y \text{ or } z \qquad (4.85)$$

For the case where the water phase potential in the downstream block is greater than the potential in the upstream block,

$\Phi_{w,i-1} < \Phi_{w,i}$,

$$C_{k,i-\frac{1}{2}} = C_{k,i} + 2A_{i}\left(C_{k,i-1} - C_{k,i}\right) + B_{i}\left(C_{k,i} - C_{k,i+1}\right) \qquad i = x, y \text{ or } z \qquad (4.86)$$

and,

$$C_{k,i+\frac{1}{2}} = C_{k,i+1} + 2A_{i+1}\left(C_{k,i} - C_{k,i+1}\right) + B_{i+1}\left(C_{k,i+1} - C_{k,i+2}\right) \qquad i = x, y \text{ or } z \qquad (4.87)$$

A_i and B_i are defined as[6],

$$A_i = \frac{\Delta i_i}{3\left(\Delta i_i + \Delta i_{i-1}\right)} \quad , \qquad B_i = \frac{\Delta i_i}{3\left(\Delta i_{i+1} + \Delta i_i\right)} \qquad i = x, y \text{ or } z \qquad (4.88)$$

When the grid block is a boundary block or adjacent to the boundary block and one of the nodes in the formula lies outside the reservoir boundary, single point upstream calculation is done to calculate the upstream concentration.

The dispersion term is expressed as tensor and is written as[6]:

$$\nabla.\left(\frac{\phi S_w}{B_w}\vec{\vec{D}}_k \nabla\left(C_k\right)\right)_{xyz} = \sum_{i=x,y,z}\sum_{j=x,y,z}\frac{\partial}{\partial i}\left[\frac{\phi S_w}{B_w}\left(D_{kw,ij}\frac{\partial C_k}{\partial j}\right)\right] \qquad (4.89)$$

Using centered finite difference to discretize Equation 4.89, the dispersion term in the X direction is[6]:

$$\frac{\partial}{\partial X}\sum_{j=x,y,z}\left[\frac{\phi S_w}{B_w}\left(D_{kw,xj}\frac{\partial C_k}{\partial j}\right)\right]=$$

$$\frac{1}{\Delta X}\{\left(\left(\frac{\phi S_w D_{kw,xx}}{B_w}\right)_{x+\frac{1}{2}}\frac{\left(C_{k,x+1}-C_{k,x}\right)_{x+\frac{1}{2}}}{\Delta x_{x+\frac{1}{2}}}-\left(\frac{\phi S_w D_{kw,xx}}{B_w}\right)_{x-\frac{1}{2}}\frac{\left(C_{k,x-1}-C_{k,x}\right)_{x-\frac{1}{2}}}{\Delta x_{x-\frac{1}{2}}}\right)+$$

$$\left(\left(\frac{\phi S_w D_{kw,xy}}{B_w}\right)_{x+\frac{1}{2}}\frac{\left(C_{k,y+1}-C_{k,y}\right)_{x+\frac{1}{2}}}{\Delta y_{y+\frac{1}{2}}+\Delta y_{y-\frac{1}{2}}}-\left(\frac{\phi S_w D_{kw,xy}}{B_w}\right)_{x-\frac{1}{2}}\frac{\left(C_{k,y-1}-C_{k,y}\right)_{x-\frac{1}{2}}}{\Delta y_{y+\frac{1}{2}}+\Delta y_{y-\frac{1}{2}}}\right)+$$

$$\left(\left(\frac{\phi S_w D_{kw,xz}}{B_w}\right)_{x+\frac{1}{2}}\frac{\left(C_{k,z+1}-C_{k,z}\right)_{x+\frac{1}{2}}}{\Delta z_{z+\frac{1}{2}}+\Delta z_{z-\frac{1}{2}}}-\left(\frac{\phi S_w D_{kw,xz}}{B_w}\right)_{x-\frac{1}{2}}\frac{\left(C_{k,z-1}-C_{k,z}\right)_{x-\frac{1}{2}}}{\Delta z_{z+\frac{1}{2}}+\Delta z_{z-\frac{1}{2}}}\right)\} \tag{4.90}$$

where,

$$\Delta x_{x\pm\frac{1}{2}}=\frac{\Delta x_x+\Delta x_{x\pm1}}{2} \tag{4.91}$$

$$\Delta y_{y\pm\frac{1}{2}}=\frac{\Delta y_y+\Delta y_{y\pm1}}{2} \tag{4.92}$$

$$\Delta z_{z\pm\frac{1}{2}}=\frac{\Delta z_x+\Delta z_{x\pm1}}{2} \tag{4.93}$$

The component concentrations at block boundaries are calculated by the upstream method[6]:

For

$$\Phi_{w,i\pm1}>\Phi_{w,i},\qquad \left(C_{k,j\pm1}\right)_{i\pm\frac{1}{2}}=\left(C_{k,j\pm1}\right)_{i\pm1}\qquad \text{For } i,j=x,y,z \text{ and } i\neq j \tag{4.94}$$

$$\Phi_{w,i\pm1}<\Phi_{w,i},\qquad \left(C_{k,j\pm1}\right)_{i\pm\frac{1}{2}}=\left(C_{k,j\pm1}\right)_{i}\qquad \text{For } i,j=x,y,z \text{ and } i\neq j \tag{4.95}$$

The physical term in the co-efficients in Equation 4.91 is calculated by[6,82]:

$$\left(\frac{\phi S_w D_{kw,ij}}{B_w}\right)_{i\pm\frac{1}{2}} = \frac{D_k}{\tau}\left(\frac{\phi S_w}{B_w}\right)_{i\pm\frac{1}{2}} + \frac{(\alpha_{lw}-\alpha_{tw})}{B_{w,i\pm\frac{1}{2}}}\frac{\left(u_{ij}^2\right)_{i\pm\frac{1}{2}}}{\left|\vec{u}_w\right|_{i\pm\frac{1}{2}}} + \delta_{ij}\frac{\alpha_{tw}\left|\vec{u}_w\right|_{i\pm\frac{1}{2}}}{B_{w,i\pm\frac{1}{2}}} \quad \text{For } i, j = x, y, z$$

(4.96)

where,

$$\left|\vec{u}_w\right|_{i\pm\frac{1}{2}} = \sqrt{\sum_{i=x,y,z}\left(u_{wi}\right)^2_{i\pm\frac{1}{2}}} \qquad \text{For } i = x, y, z \tag{4.97}$$

Average first order upstream velocity weighting is used to calculate the Darcy velocity.

The bacterial transport equation is written as[6]:

$$\frac{\partial C_l}{\partial t} = \frac{1}{D_s}\left[-\nabla.\left(\frac{\vec{u}_w}{B_w}C_1\right) - K_c\nabla\left(C_1\nabla\ln C_8\right) + \nabla.\left(\frac{\phi S_w}{B_w}\overrightarrow{\overrightarrow{D}}_{1w}\nabla C_1\right) - \frac{Q_w}{V_b}C_1 + \frac{\phi S_w}{B_w}R_1 + \phi\left(R_d - R_r\right)\right]$$

(4.98)

where,

$$D_s = \frac{\phi S_w}{B_w} \tag{4.99}$$

The treatment of bacterium, nutrients, products and salt ions is the same for the purpose of discretizing the equations. Since bacterial movement also includes chemotactic movement aided by nutrient concentration gradients, that term is included only in the bacterial equation:

$$K_c\nabla\left(C_1\nabla\ln C_8\right) = K_c\left[\sum_{i=x,y,z}\frac{\partial}{\partial i}\left(\frac{1}{C_8}\frac{\partial C_8}{\partial i}C_1\right)\right] \tag{4.100}$$

and

$$\frac{\partial}{\partial i}\left(\frac{1}{C_8}\frac{\partial C_8}{\partial i}C_1\right)_{xyz} = \frac{1}{\Delta i}\left[\frac{4\left(C_{8,i+1}-C_{8,i}\right)\left(C_1\right)_{i+\frac{1}{2}}}{\left(C_{8,i}-C_{8,i+1}\right)\left(\Delta i_i-\Delta i_{i+1}\right)}-\frac{-4\left(C_{8,i-1}-C_{8,i}\right)\left(C_1\right)_{i-\frac{1}{2}}}{\left(C_{8,i}-C_{8,i-1}\right)\left(\Delta i_i-\Delta i_{i-1}\right)}\right]$$

for $i = x, y, z$ (4.101)

Leonard's third order upstream weighting formula was used to calculate the apparent concentration of bacteria at the block boundaries[6]:

If $C_{8,i-1} > C_{8,i}$

$$C_{1,i-\frac{1}{2}} = C_{1,i-1} + A_{i-1}\left(C_{1,i-1}-C_{1,i-2}\right)+2B_{i-1}\left(C_{1,i}-C_{1,i-1}\right) \qquad \text{For } i = x, y, z \qquad (4.102)$$

If $C_{8,i-1} < C_{8,i}$

$$C_{1,i-\frac{1}{2}} = C_{1,i} + 2A_i\left(C_{1,i-1}-C_{1,i}\right)+B_i\left(C_{1,i}-C_{1,i+1}\right) \qquad \text{For } i = x, y, z \qquad (4.103)$$

The terms A_i and B_i are calculated as shown in Equation 4.88.

4.2.4. Computation process

The numerical computation is a sequence of steps. First the grid block pressure is calculated implicitly using the IMPES formulation. The LSOR algorithm is used to solve for the pressure values. Phase saturations are explicitly calculated from the pressure calculations. Darcy fluxes across the grid block boundaries are then calculated. The fluxes are used to explicitly calculate the dispersion concentrations. The solution of component concentrations is by the 'Method of Lines'[6]. This is an integration process that uses a Runge-Kutta[6] fifth order process to calculate the new concentrations of the components.

4.2.6 Updating the variable values

After each pressure and saturation calculation, block pressure and saturations, both primary variables are updated:

$$P_{xyz}^{n+1} = P_{xyz}^{n} + \Delta P_{xyz}$$

$$S_{l,xyz}^{n+1} = S_{l,xyz}\,\text{calculated} \tag{4.113}$$

The next step requires calculating aqueous velocity at each face of a block. Velocity is a secondary variable that depends on block pressure and relative water permeability.

$$u_{w,i\pm\frac{1}{2}} = \frac{A_{w,i\pm\frac{1}{2}}}{A_{i\pm\frac{1}{2}}}\left[\left(P + \rho_w \frac{g}{g_c} + P_{cow}\right)_i - \left(P_{i\pm1} + \rho_w \frac{g}{g_c} + P_{cow}\right)_{i\pm1}\right] \tag{4.114}$$

Component concentrations, also primary variables, are calculated at time 'n+1' by the 'Method of Lines' method and updated to the new value:

$$C_{k,xyz}^{n+1} = C_{k,xyz}^{n} + \Delta C_{k,xyz} \tag{4.115}$$

where $\Delta C_{k,xyz}$ is the change in component concentration calculated over the time step.

If the relative change in pressure, saturation or component concentrations are less than or equal to the maximum limits, the time step is increased. Before calculating the pressure and saturation at the next time level, the relative permeability is corrected for the trapping number in the grid block. The trapping number is calculated using interfacial tension which in turn is calculated using the updated bio-surfactant concentration.

4.2.5. Time step selection

The selection of time step is an automatic process incorporated into the calculations to avoid instability and reduce computing time. The pressure, phase saturations and component concentrations are first calculated for a time step applied to the entire grid. Following the computation of the new values of the primary dependent variables, P^{n+1}, S^{n+1} and C^{n+1}, the relative change in value of the variables is calculated,

$$\left(\Delta P\right)_m = \frac{\left|P_m^{n+1} - P_m^{n}\right|}{P_m^{n+1}} \tag{4.104}$$

$$\left(\Delta S_l\right)_m = \frac{\left|\left(S_l\right)_m^{n+1} - \left(S_l\right)_m^n\right|}{\left(S_l\right)_m^{n+1}} \tag{4.105}$$

$$\left(\Delta C_k\right)_m = \frac{\left|\left(C_k\right)_m^{n+1} - \left(C_k\right)_m^n\right|}{\left(C_k\right)_m^{n+1}} \tag{4.106}$$

where, 'm' is the grid block number.

The maximum relative change is then estimated as[6]:

$$\left(\Delta P\right)_{\max} = \max\left[\left(\Delta P\right)_m\right] \tag{4.107}$$

$$\left(\Delta(S)\right)_{\max} = \max\left\{\max\left[\left(\Delta\left(S_l\right)\right)_m\right]\right\} \tag{4.108}$$

$$\left(\Delta(C)\right)_{\max} = \max\left\{\max\left[\left(\Delta\left(C_k\right)\right)_m\right]\right\} \tag{4.109}$$

and these maximum relative changes are checked against a specified upper limit for these changes, $\left(\Delta P\right)_{\lim}$, $\left(\Delta(S)\right)_{\lim}$, $\left(\Delta(C)\right)_{\lim}$.

If the relative changes are less than the specified upper limits, then the time step for the next calculation is increased by a factor F_{inc}:

$$\Delta t^{n+1} = F_{inc}\, \Delta t^n \tag{4.110}$$

And if the changes exceed the specified upper limits then the time step is reduced by a factor F_{dec} and the calculations are repeated with the adjusted time step:

$$\Delta t^{n+1} = F_{dec}\, \Delta t^n \tag{4.111}$$

The new step should not exceed a certain value or decrease below a certain value, hence limits are specified for the maximum and minimum timestep sizes:

$$\Delta t_{min} \leq \Delta t^{n+1} \leq \Delta t_{max} \tag{4.112}$$

4.3. Summary

Mathematical models and finite difference equation in the modified MEOR simulator were listed. In the next chapter, numerical simulations using the simulator are described.

CHAPTER V

NUMERICAL SIMULATION

Numerical simulations using the MEOR simulator are discussed in this chapter. Simulator output was compared with analytical solutions to verify the simulator's accuracy in the first section of this chapter. Next, the modifications to the MEOR simulator were tested. Modifications were made because the existing MEOR program[6] did not include the flow of micellar/polymer solutions or the salinity effects on polymer and bio-surfactant behavior. It was important to have a simulator that combined MEOR mechanisms with polymer flow and salinity effects to design and test bio-surfactant based MEOR processes. Six JF-2/PHPA surfactant core floods described in Chapter 3 were simulated in the third section.

5.1 Verification with analytical solutions. The MEOR simulator results for a 1-D waterflood and 1-D tracer injection were compared to analytical solutions.

5.1.1 Comparison of MEOR simulator predicted 1D-core waterflood result with the analytical Buckley-Leverett solution. The simulated water saturation profile after a 0.5 PV of waterflood was compared to the Buckley-Leverett analytical solution. Capillary pressure and gravity forces were neglected in the solution. Input data for the simulation are listed in **Table B1.1** in **Appendix B**. The two solutions were plotted and compared in

Figure 5.2.1. The MEOR simulator result agreed well with the analytical solution. The analytical solution for the 1-D waterflood is[96]:

$$x = \frac{QL}{A\phi}\left(\frac{df}{dS_w}\right)_{Sw} t \tag{5.1}$$

where,

x = Distance (ft) (5.2)

t = Time (days) (5.3)

Figure 5.1.1. Analytical and MEOR simulator solution for a 1-D waterflood.

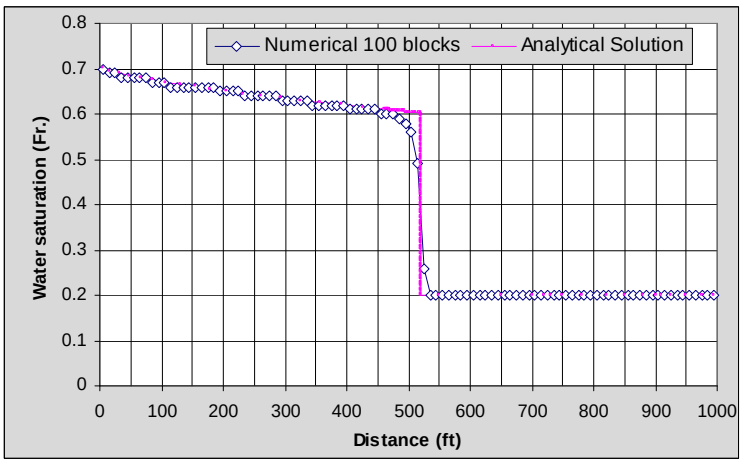

5.1.2 Comparison of a 1D tracer injection results and the analytical solution.

The simulator predicted injected tracer concentration profile for a 100 block model was compared with the analytical solution of a 1-D tracer injection. Input data are listed in **Table B1.2** in **Appendix B**. The numerical and analytical solutions are compared in **Figure 5.1.2**. The MEOR simulator solution agreed well with the analytical solution. The analytical solution for the one dimensional convection-dispersion equation is[97,98]:

$$\frac{C}{C_i} = \frac{1}{2} erfc\left(\frac{|x_D - t_D|}{2\sqrt{\frac{t_D}{N_{Pe}}}} \right) \quad \text{if } x_D - t_D \le 0 \tag{5.4}$$

$$\frac{C}{C_i} = 1 - \frac{1}{2} erfc\left(\frac{|x_D - t_D|}{2\sqrt{\frac{t_D}{N_{Pe}}}} \right) \quad \text{if } x_D - t_D > 0 \tag{5.5}$$

where,

C_i is the concentration of injected tracer and

Peclet number, $N_{Pe} = \frac{\Delta x}{\alpha_L}$ (5.6)

Dimensionless distance, $x_D = \frac{x}{L}$ (5.7)

Dimensionless time, $t_D = \int_0^t \frac{Q dt}{Vp}$ (5.8)

$$erfc(x) = 1 - erf(x) = 1 - \frac{2}{} \int_0^x e^{-x^2} dx \tag{5.9}$$

Figure 5.1.2. Comparison of MEOR simulator output and analytical solution.

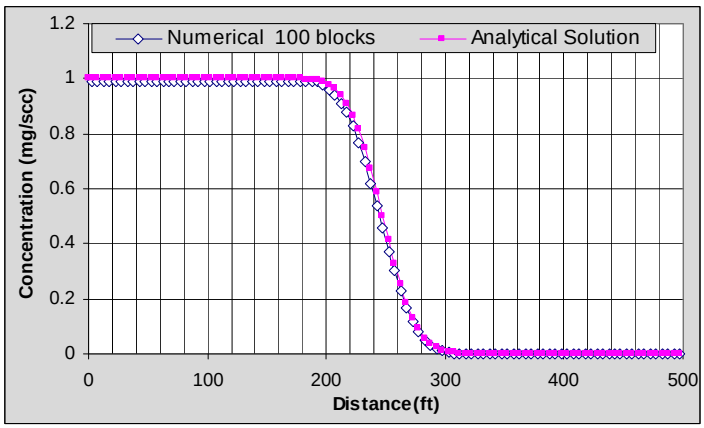

5.2 Simulator applications. Simulation studies to test and validate the MEOR simulator modifications are reported. The simulator was modified to add the ability to simulate the flow of bio-surfactant/polymer solutions through porous media and include the effect of brine salinity on oil recovery. The modifications were:

a) The effect of improved surfactant mobility control by polymer addition to JF-2 bio-surfactant solution.
b) The effect of sodium chloride in reservoir brine on plain JF-2 bio-surfactant.
c) The effect of sodium chloride in reservoir brine on JF-2/polymer solution.
d) The effect of calcium ions in reservoir brine on JF-2/polymer solution.

Simulation results were also used to investigate the relationship between oil recovery and JF-2 bio-surfactant concentration by injecting a core model with a surfactant solution with increasing JF-2 bio-surfactant concentrations and 2.0 PVs of surfactant. Oil production and cumulative oil recovery plots were used to compare the effects of different conditions on surfactant flooding performance.

Core properties were taken from a Berea sandstone core used in a laboratory waterflooding experiment. The bio-polymer SP-018 was used to simulate JF-2-polymer flooding experiments because MEOR applications will utilize microbial byproducts instead of the synthetic polymers. Bio-polymer SP-018 data was described in Chapter 3.

Grid block selection for core model: The optimum number of grid blocks needed to simulate JF-2 surfactant/bio-polymer core floods was determined by simulating micellar/polymer injection in a core model with increasing number of blocks. Selection of proper longitudinal and transverse dispersivity values was important because dispersion was a critical mechanism in chemical floods. The longitudinal dispersivity (α_L)

value was selected so that the Peclet number, N_{Pe} was equal to 1.5. The transverse dispersivity (α_T) was equal to 0.0033α_L. These values follow recommendations made by Zheng and Bennet[99]. The small Peclet number meant that dispersion would be large, as expected in core flooding experiments[100]. The plots shown in **Figure 5.2.1** are the relative change in oil recovery and the oil recovery plotted as a function of number of grid blocks. A 100 grid block model was chosen to simulate the core floods because the change in recovery was very small between 90 and 100 grid blocks.

Figure 5.2.1 Optimum number of grid blocks

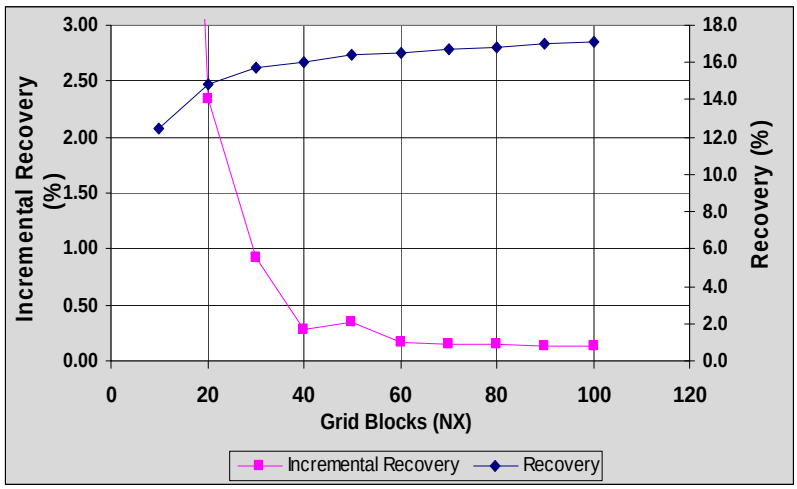

5.2.1 JF-2 bio-surfactant and SP-018 biopolymer solution treatment. Sand packs had shown that increasing the bio-surfactant solution viscosity with polymer improved oil recovery[5]. The benefit of increasing bio-surfactant viscosity was investigated with numerical simulation. A Berea core model at residual oil saturation was treated with a 1.0 PV of JF-2/SP-018 solution, plain JF-2 bio-surfactant and plain SP-018 bio-polymer solution.

5.2.1.1. JF-2 and SP-018 surfactant. A JF-2 bio-surfactant/ SP-018 solution with 11.0 ppm of bio-surfactant and 1000.0 ppm of SP-018 was injected through the core model.

Input data are in **Table B2.1**, **Appendix B**. The viscous JF-2 surfactant recovered 1.6 cc or 15.0 % of residual oil. The mobilized oil was produced after 0.5 PV of surfactant was injected as shown by the rise in oil production in **Figure 5.2.2**. The cumulative oil recovery is plotted in **Figure 5.2.3**.

5.2.1.2 Plain JF-2 bio-surfactant. The benefit of adding polymer to reduce surfactant mobility and improve oil recovery was investigated. 1.0 PV of plain 11.0 ppm JF-2 surfactant solution was injected into the core model. Input data are listed in **Table B2.2** in **Appendix B**. The oil production profile and total oil recoveries by the viscous and non-viscous surfactants are compared in **Figures 5.2.2** and **5.2.3**. The lack of polymer in the surfactant led to the absence of oil bank formation and the sudden rise in oil production was not observed in the non-viscous surfactant's case. A small increase in production near the end of surfactant flooding was some mobilized oil reaching the outlet. Comparison of cumulative oil recovery in **Figure 5.2.3** showed total oil recovery was 3.0 % compared to 15.0 % with the viscous surfactant.

5.2.1.3 Plain SP-018 bio-polymer. 1.0 PV of 1000.0 ppm SP-018 solution without any JF-2 bio-surfactant was injected through the core to quantify the bio-polymer's contribution to oil recovery by JF-2/SP-018 flooding. Input data are listed in **Table B2.3**, **Appendix B**. The oil production profile when compared to the profiles from cases **5.2.1.1** and **5.2.1.2** in **Figure 5.2.1.2** showed that the plain bio-polymer solution formed an oil bank but the amount of mobilized oil was less than when both bio-polymer and bio-surfactant were combined. The total recovery was about 9.0 % of residual oil. The cumulative oil recovery profiles are compared in **Figure 5.2.3**. The highest recovery when JF-2/SP-018 solution was injected into the core showed the benefit of combining

polymer with the JF-2 bio-surfactant. This is also shown by the sizes of the zones swept free of residual oil in the core model in **Figures 5.2.4 a, b** and **c**. The left side of the model is the injector side and the blue colored area is the swept zone. The swept zone was largest in **Figure 5.2.4a** where JF-2 and SP-018 were used together, became smaller in **5.2.4b** when plain SP-018 solution was injected and was the smallest in **5.2.4c** when only JF-2 bio-surfactant was used. The results also suggested that the polymer had a more significant impact on oil recovery than bio-surfactant because of low bio-surfactant concentration.

Figure 5.2.2. Oil production profile for cases 5.2.2 to 5.2.4

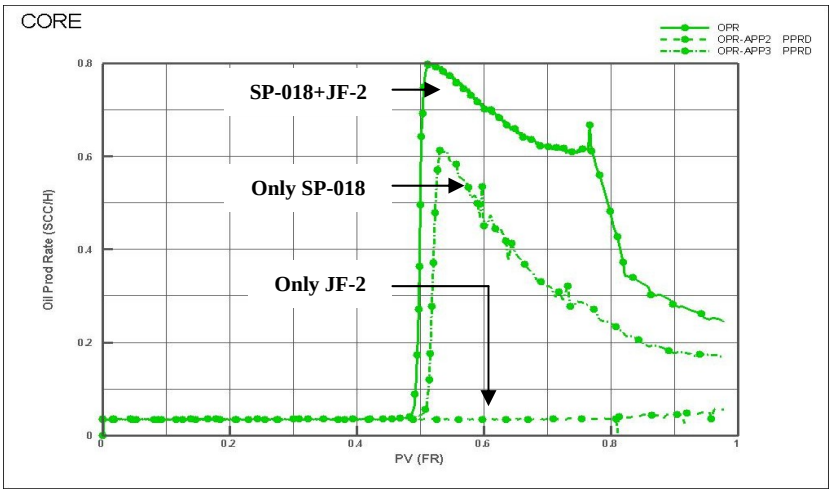

Figure 5.2.3. Cumulative oil production profile for cases 5.2.1.1 to 5.2.1.3

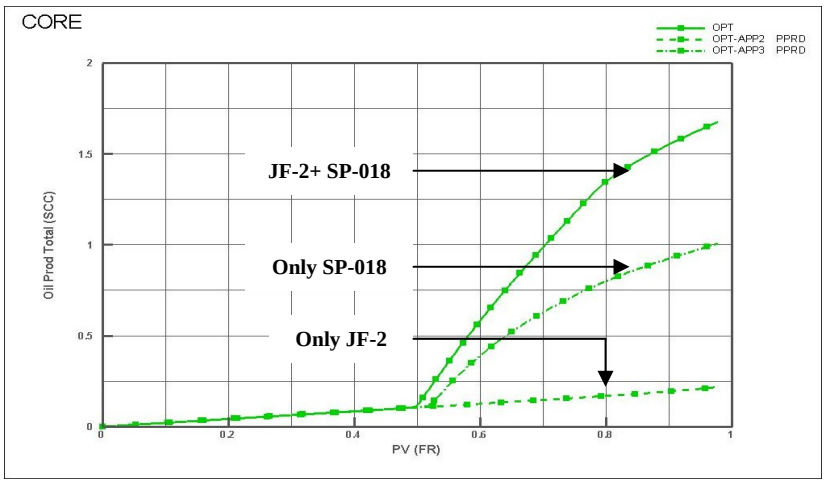

Figure 5.2.4. Oil saturation distribution for cases 5.2.2 to 5.2.4

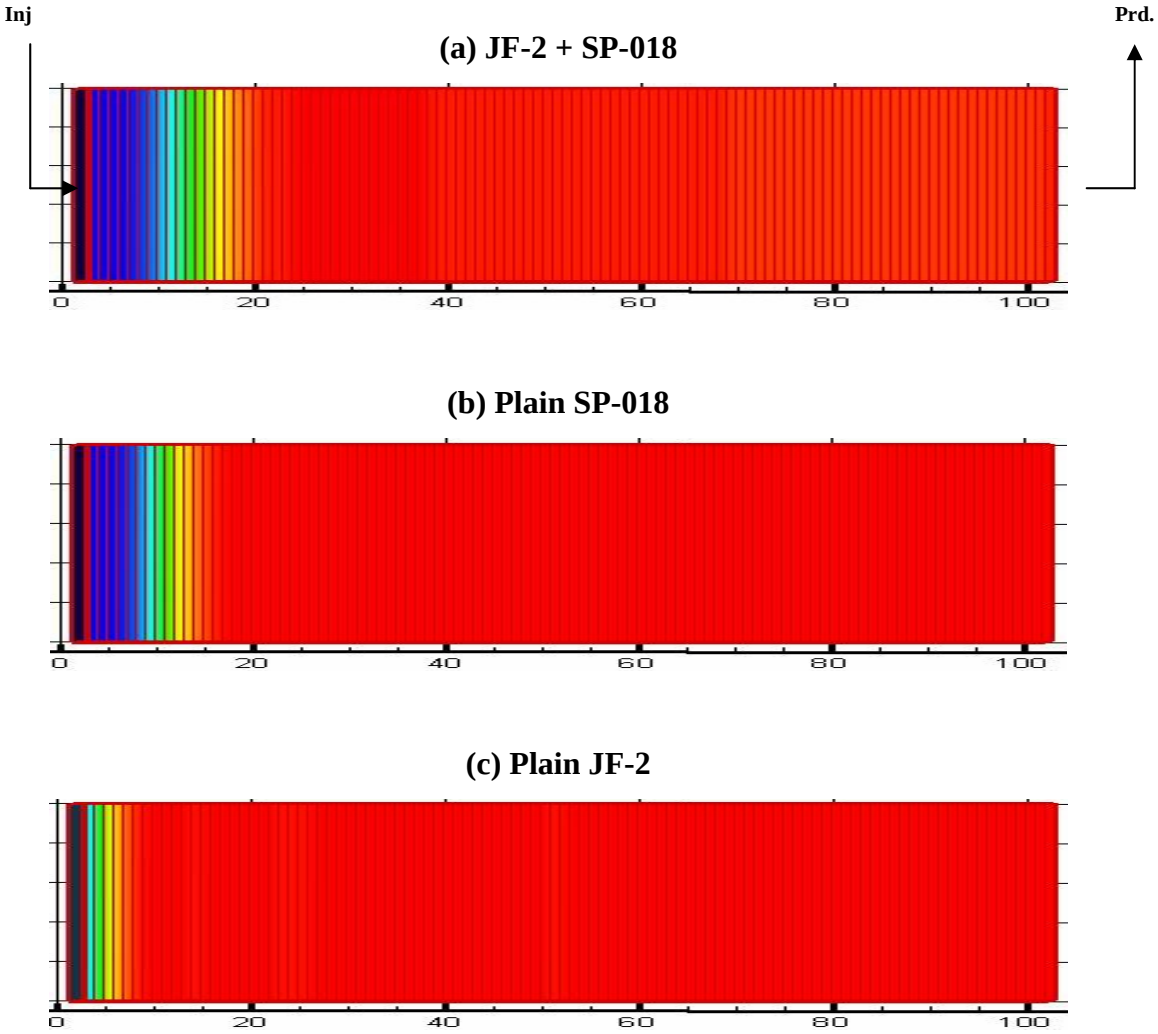

5.2.4 Bio-surfactant concentration and oil recovery. JF-2/SP-018 solutions with increasing bio-surfactant concentrations – 11.0, 21.0, 31.0 and 41.0 ppm were injected into a core to investigate the relationship between bio-surfactant concentration and oil recovery. Input data are listed **Table B2.4**, **Appendix B**. Oil production and cumulative oil at the four concentrations are plotted in **Figures 5.2.5** and **5.2.6**. A higher bio-surfactant concentration mobilized more oil and achieved a higher recovery. Oil production started earlier for the 21.0, 31.0 and 41.0 ppm solutions than the 11.0 ppm

solution. The oscillation in the production profiles at 21.0, 31.0 and 41.0 ppm were caused by changes in oil water ratio. Small variations in oil saturation during oil bank production caused fluctuations in the oil and water rates and manifested as oscillations on the oil rates and water cut profiles. This could not be removed even with small time steps.

Figure 5.2.7 shows the slope of oil recovery factor (RF) and bio-surfactant concentration ($C_{Bio\text{-}surf.}$) curve, $dRF/dC_{Bio\text{-}surf.}$ (the relative change oil recovery) decreasing with increasing bio-surfactant concentration. This trend is explained by the capillary desaturation curve profile for porous media (residual oil saturation, S_{OR} - capillary number, N_{CP})[101]. S_{OR} asymptotically tends to zero with increasing capillary number after decreasing rapidly initially. If $1\text{-}S_{OR}$ or RF for a porous media is plotted against N_{CP}, a plot similar to **Figure 5.2.7** is produced. N_{CP} can be replaced by bio-surfactant concentration because its value increases with bio-surfactant concentration. The asymptotic behavior indicated that beyond certain S_{OR} or recovery factor, increase in N_{CP} by lowering IFT was insufficient to mobilize additional oil. Similarly, additional oil recovery with bio-surfactant will continue to diminish until it becomes constant at very high $C_{Bio\text{-}surf}$. Simulations showed oil recovery was proportional to concentrations until $C_{Bio\text{-}surf.}$ was less than 21.0 ppm, but the relative improvement in recovery would reduce at higher concentrations. The results also showed that the impact of bio-surfactant on oil recovery was more significant compared to the polymer with increasing JF-2 concentrations. This was because the change in capillary number by IFT reduction was greater than the change by the increase in surfactant viscosity.

Figure 5.2.5. Oil production rate at 11.0, 21.0, 31.0 and 41.0 ppm of bio-surfactant

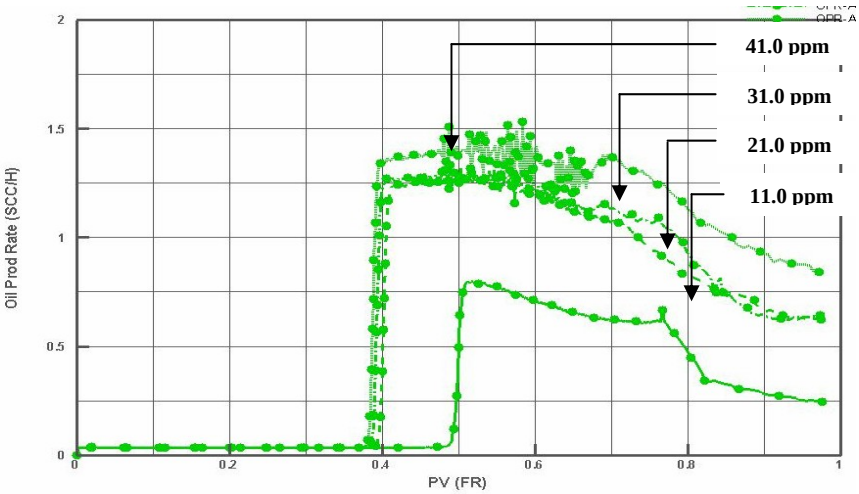

Figure 5.2.6. Cumulative oil recovery at 11.0, 21.0, 31.0 and 41.0 ppm of bio-surfactant

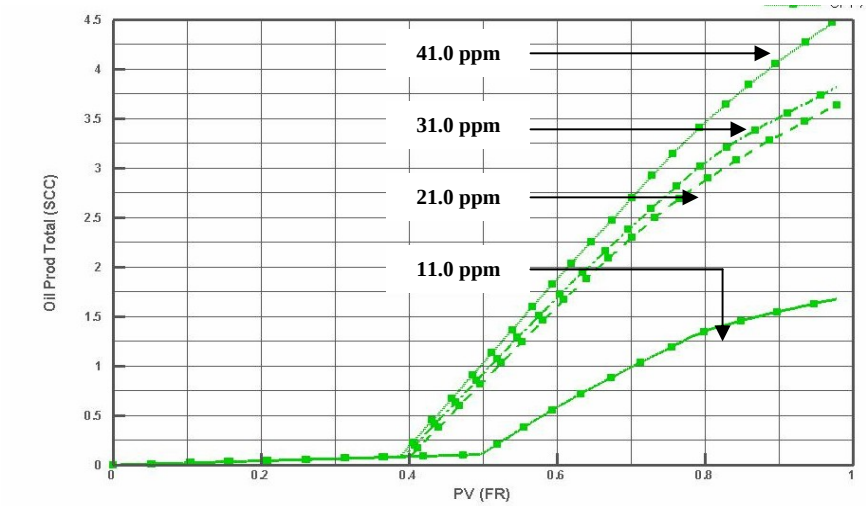

Figure 5.2.7. Plot of Oil fraction recovered vs. Bio-surfactant concentration.

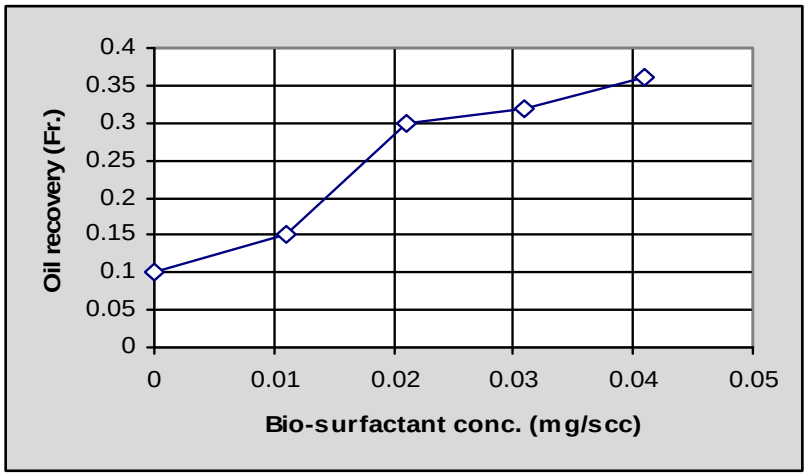

5.2.5 Effect of sodium chloride (NaCl) on adsorption and viscosity. This set of simulations explored the effect of NaCl concentration on surfactant and polymer adsorption and surfactant viscosity for a core treated with JF-2/SP-018 solution. The NaCl concentrations in the reservoir brine were 2.0 %, 3.0 % and 5.0 % respectively. Input data are in **B2.5**, **Appendix B**. Oil production and cumulative oil recovery for the three cases are plotted in **Figures 5.2.8** and **5.2.9**. Nearly 6.4 cc of oil was recovered when surfactant salinity was 2.0 %, 5.0 cc when the salinity was 3.0 % and only 3.5 cc when the salinity was 5.0 %. The salt reduced the surfactant viscosity leading to lower oil mobilization and delayed oil breakthrough as shown in **Figure 5.2.8**. The salt also increased polymer and bio-surfactant adsorption. A combination of these resulted in the final oil recovery decreasing with higher salt concentrations. The total oil recovery is compared in **Figure 5.2.9**.

Figure 5.2.8. Oil production under increasing NaCl in the JF-2/SP-018 solution

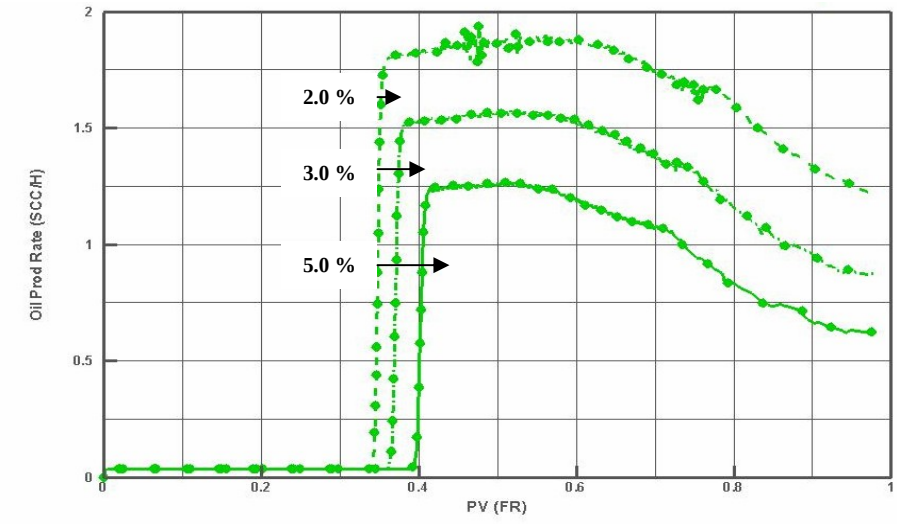

Figure 5.2.9. Cumulative oil recovery with increasing NaCl in the JF-2/SP-018 solution

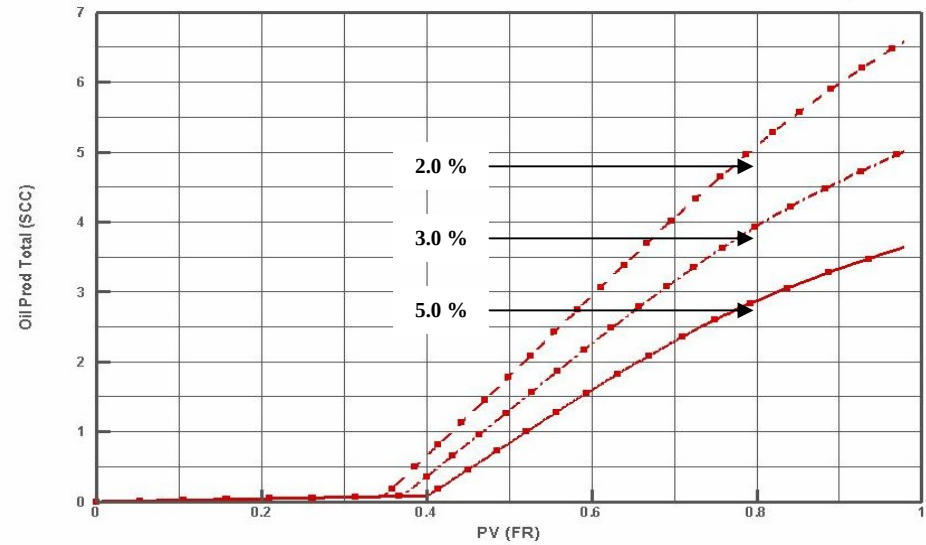

5.2.5 Effect of sodium chloride (NaCl) on IFT. This series of simulations investigated the impact of NaCl on IFT. Plain surfactant solution was used in this experiment.The concentration of NaCl in the injected surfactant was 3.0 %, 5.0 % and 10.0 %. Oil recoveries at NaCl concentrations above and below 5.0 % NaCl were compared with the

5.0 % NaCl case. The base case of 5.0% NaCl was selected from the IFT vs. NaCl concentration model described in chapter 3. Input data are listed in **B2.5**, **Appendix B**. Cumulative recovery for the three cases is compared in **Figures 5.2.10**. The mobilized oil bank breakthrough at 10.0 % NaCl was delayed compared to 5.0 % and 3.0 % NaCl. The volume of mobilized oil and the total oil recovery decreased with increasing salinities. At 10.0 % salt, IFT was higher than at 5.0 % NaCl, which was higher than the IFT at 3.0 % NaCl. A higher IFT combined with increased adsorption and lower surfactant viscosity led to a decline in oil recovery as NaCl concentration increased. The results suggested that the impact of higher salinity was greater than a lower salinity (compared to 5.0 % NaCl). At 5.0 % NaCl, the recovery was about 15.0 % (1.2 cc) of residual oil. But oil recovery at 10.0 % NaCl had decreased significantly to 4.0 % (0.3 cc). On the other hand, oil recovery at 3.0 % NaCl had only slightly increased to 17.0 % (1.3cc) of recovered oil. Halving the salinity increased the recovered oil volume by just 2.0 % but doubling the salinity decreased recovery by 10.0 %.

Figure 5.2.10. Increasing NaCl in JF-2 surfactant effect on oil recovery

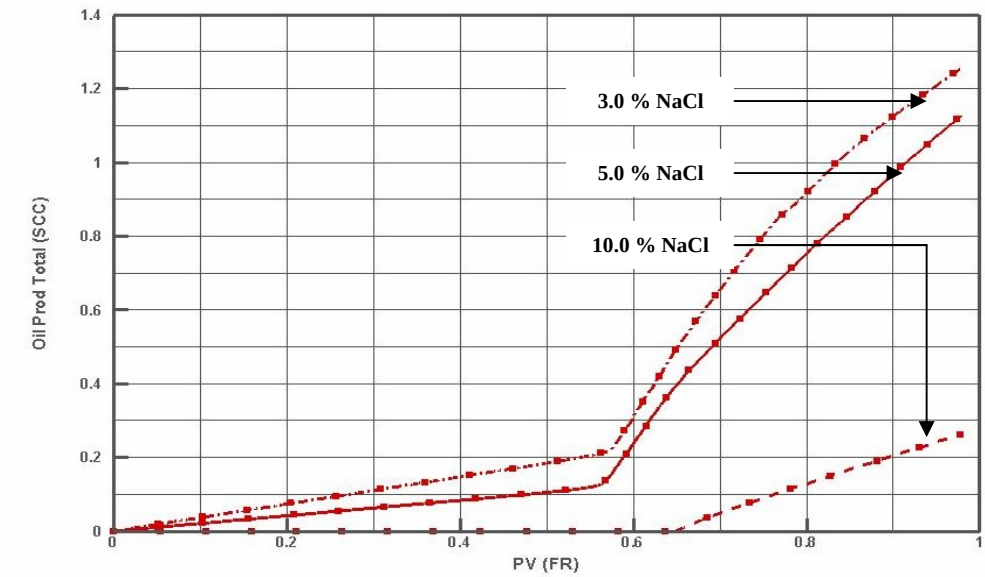

5.2.7 Effect of calcium (Ca^{2+}) on JF-2/SP-018 flooding. In this series of simulations, the effect of divalent Ca^{2+} ions on SP-018 bio-polymer (surfactant) viscosity and oil recovery was investigated by comparing the performance of a JF-2/SP-018 solution in a core flood with and without 2.0 % Ca^{2+} ions in the resident brine. Input data are in **B2.6**, **Appendix B**. The oil production and cumulative recovery plots for the two cases are compared in **Figures 5.2.12** and **5.2.13**. Greater shielding of polymer molecules by the Calcium ions compared to shielding by NaCl ions reduced the surfactant viscosity more than when just NaCl was present. The surfactant recovered less oil (8.0 % compared to 15.0 %) and the core experienced a delayed breakthrough of mobilized oil when calcium ions were present. The reaction to Ca^{2+} ions varies from polymer to polymer. It is known to be strong for polyacylamides[10] and was assumed to be strong for SP-018.

Figure 5.2.11. Oil production with and without Ca^{2+}.

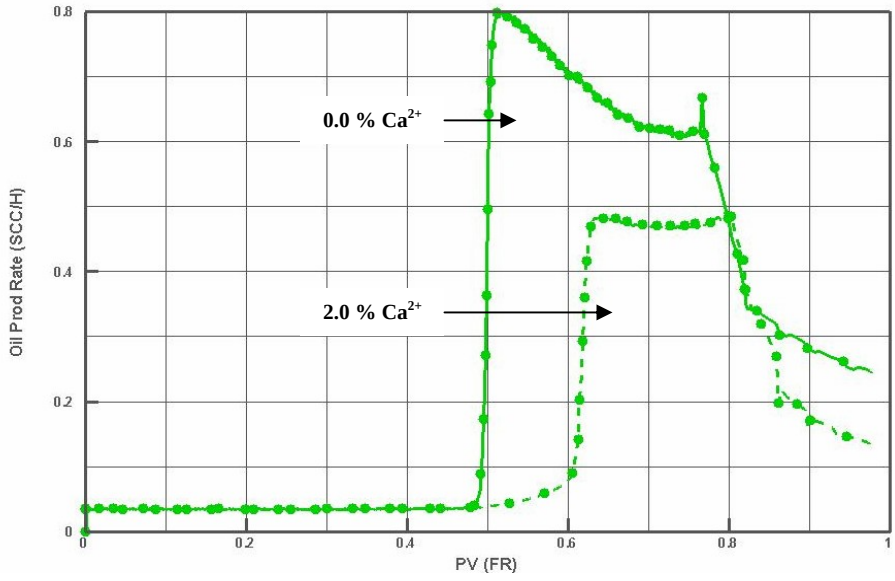

Figure 5.2.12. Cumulative oil recovery with and without Ca^{2+}

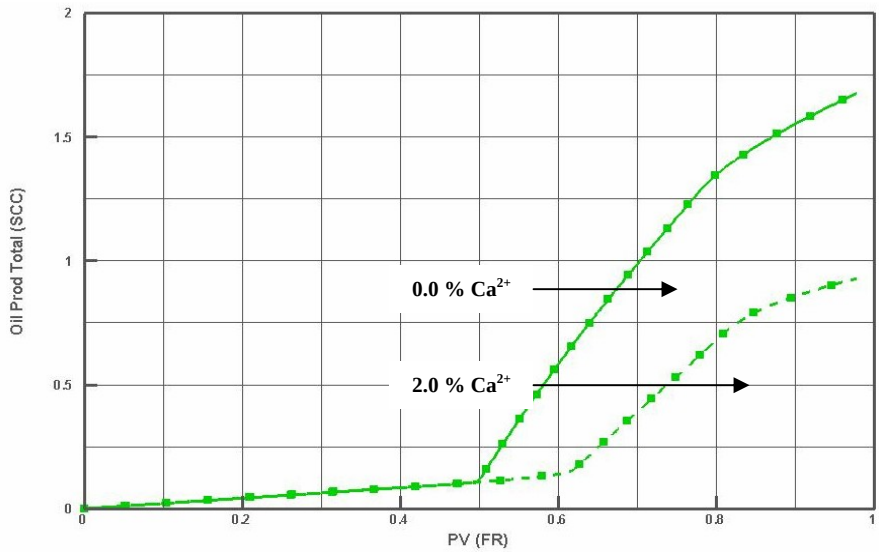

5.2.8 Two pore volumes (PVs) of JF-2/SP-018 solution. 2.0 PVs of 11.0 ppm JF-2/ SP-018 solution were injected in a simulated Berea core. The bio-polymer concentration was 1000.0 ppm. The simulation investigated oil recovery by an extended bio-surfactant treatment. Though injecting 2.0 PVs is probably not economic, the life of a MEOR treatment depends on when oil production peaks and when it is no longer economic. Extended treatment can be applied if simulations indicate a profitable increase in oil recovery. The cumulative oil recovery and oil production profile in **Figure 5.2.13** shows that of the 2.3 cc of oil recovered after 2.0 PVs of surfactant injection, 1.0 cc of oil was recovered during the second pore volume of surfactant injection. Oil recovery nearly doubled during the second pore volume of surfactant injection. This suggests that an extended treatment of a core with 11.0 ppm of bio- may result in a substantial increase in oil recovery.

Figure 5.2.13. Oil production and cumulative oil recovery after 2 PVs treatment

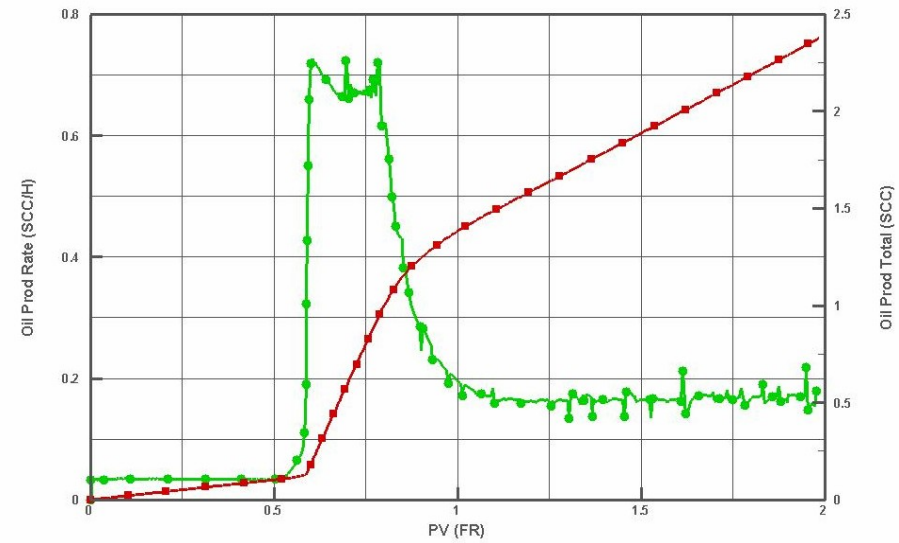

Summary: JF-2/SP-018 core flooding simulation results under different conditions have been shown. The results are tabulated in **Table 5.2.1**. The impacts of NaCl, Calcium and bio-surfactant concentration were demonstrated through the simulations. The model has shown its ability to simulate oil recovery by MEOR bio-surfactant flooding.

Table 5.2.1 Results of some numerical simulations and comparison of results.

Type of treatment	**Tertiary recovery (%)**
JF-2 and SP-018	15.0
JF-2	3.00
Plain SP-018	10.0
SP018 with NaCl	3.00
SP-018 without NaCl	15.0
SP-018 with Ca^{2+}ions	8.00
2.0 PV's of surfactant	28.0

5.3 Simulation of JF-2/PHPA core flood experiments. Six JF-2 bio-surfactant/partially hydrolyzed polyacrylamide (PHPA) surfactant core floods described in Chapter 3 were simulated. Simulated and experimental results were then compared.

Input variables selection. The selection of important general variables is explained below.

1. **Effective end point oil permeability** $k_{ro,\ cw}$ and **effective end point water permeability** $k_{rw,sor}$: Effective oil permeability and effective water permeability for each core was determined at connate water saturation after oil flooding and at residual oil saturation following waterflooding prior to JF-2/PHPA surfactant injection. Corey's relation was used to calculate intermediate relative permeability values. The water relative permeability exponent was 2.5 and the oil exponent was 1.5. The cores were assumed to be homogenous and isotropic, with uniform porosity, oil saturation and water saturation.
2. **PHPA (Pusher 520) adsorption constants**: The polyacrylamide polymer used to increase the surfactant's viscosity was Pusher 520. Adsorption parameters for Pusher 520 were taken from Berea core test literature[32]. Because the required salinities and core permeabilities were not listed in available literature, the closest possible values were used to select the parameters.
3. c_{rk}, b_{rk}: The two polymer retention parameters were equal to 0.015 and 1000.0 respectively. These values were taken from a Xanthan field flooding simulation study[63] because no data was available for PHPA core floods. Studies however show that at 5.0 % NaCl, retention of PHPA is low[36].
4. A_{p1}, A_{p2} and A_{p3}, Sp: Viscosity parameters for Pusher 520 polymer were taken from a study of its properties[32]. The co-efficients were calculated by fitting the Flory Huggins equation through the viscosity values for the polymer solution in fresh water. The values of the co-efficients are shown in the **Figure 5.3.1**. The salinity parameter

Sp was calculated by using the viscosity measurement of a 1500 ppm Pusher 520 polymer solution in 3.0% NaCl[32]. The value of *Sp* was equal to -7.5 ml/meq.

Figure 5.3.1. Plot of PHPA (Pusher 520) concentration vs. Viscosity

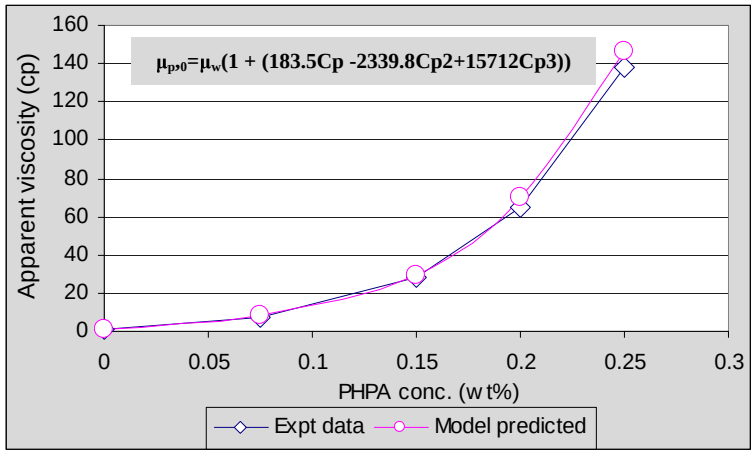

5. $\gamma_{\frac{1}{2}}$**,** P_a*, n*: The shear constant and viscosity parameter of Pusher 520 were calculated using viscosity vs. shear rate data measured in the laboratory[32]. The shear rate constant was equal to 25.0 sec^{-1} and the viscosity parameter was equal to 1.9. Solution viscosity is plotted against shear rate in **Figure 5.3.2**. Pusher 520 is a shear thinning polymer. Using Carreau's model[32], the power law fluid exponent was calculated equal to 0.6.

Figure 5.3.2. Plot of PHPA (Pusher 520) viscosity vs. Shear rate

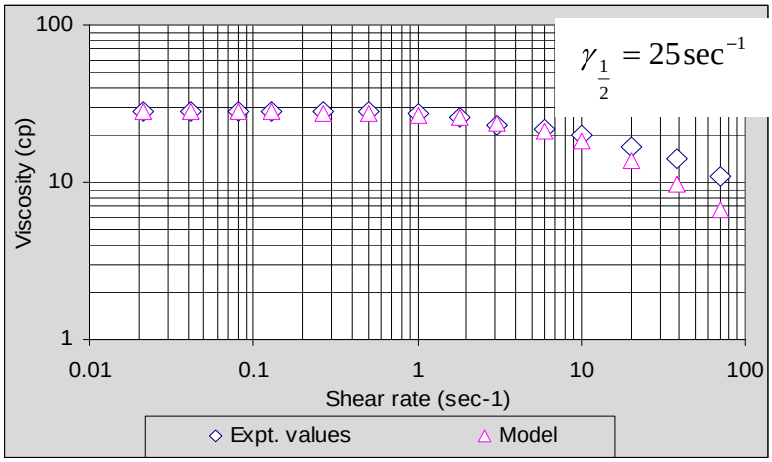

6. **JF-2 bio-surfactant adsorption parameters**: The JF-2 bio-surfactant adsorption parameters were made equal to the Pusher 520 adsorption parameters because no experiment was conducted to determine the bio-surfactant's adsorption co-efficients. The parameters to include salinity effects were taken from a Xanthan flood simulation study[63]. Based on core flooding experiments described in Chapter 3, the minimum bio-surfactant concentration was set equal to 11.0 ppm.
7. **Grid block longitudinal dispersivity α_L, tranverse dispersivity α_T** and **diffusion constant *D***: The value of α_L kept the Peclet number equal to 1.5 (< 2.0) as recommended by Zheng and Bennet[99]. Each grid block was 0.15 cm in length and the value of α_L was 0.1 cm. α_T was equal to 1/300th of the longitudinal value or 0.003 cm. Studies show that at these dispersivity values, dispersion in the core will be high. But high dispersion is consistent for short core experiments[101]. The diffusion co-efficient, ***D*** was equal to 0.044 cm^2/hr.

5.3.1 Core 1. The input data for the core flood are in **Table B3.2**, **Appendix B**. The core model was initially at residual oil saturation before surfactant injection. The total experimental oil recovery was 1.7 cc. It was produced as a 1.7 cc oil slug after 2.0 cc of

post-surfactant brine was injected into the core at six times the surfactant flood rate in the laboratory. Oil was not produced during surfactant injection because it was retained near the core outlet. The simulator predicted a total recovery equal to 1.9 cc with oil production starting after 0.5-0.6 PV of surfactant injection .Oil production would have started during surfactant injection with the total recovery unchanged if oil retention had not occurred. Oil retention and the abnormal oil slug production were not simulated because its causes were not known. The simulated cumulative oil recovery was compared to total oil recovered at the end of post surfactant brine injection. The core's effective water permeability was increased from 4.0 md to about 30.0 md to increase the mobility of the viscous bio-surfactant phase. This is discussed later. The simulated oil production, cumulative oil and water cut are plotted in **Figure 5.3.3**. The final oil recovery was the only available experimental data to compare simulated results.

Figure 5.3.3. Flow profile for the core 1 experiment.

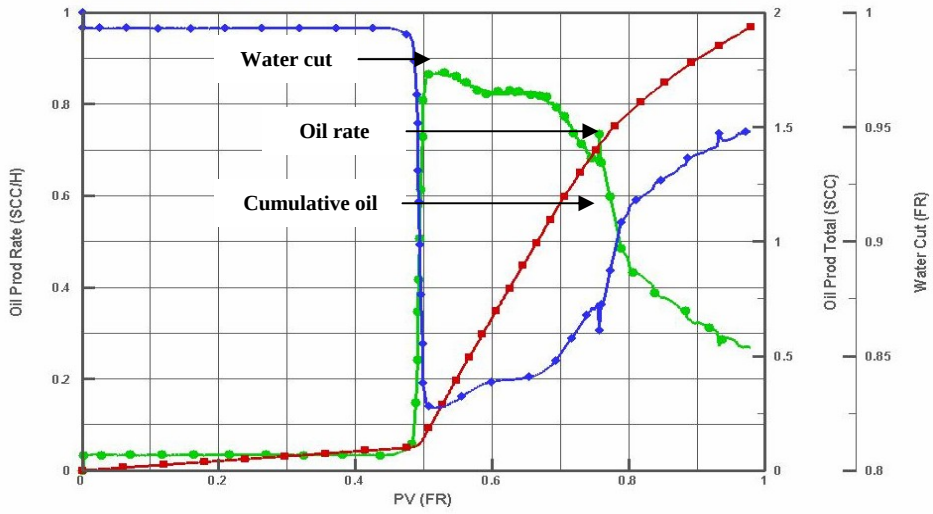

5.3.2 Core 2. Input data are listed in **Table B3.3**, **Appendix B**. The simulated total recovered oil was 1.8 cc and the experimental value was 1.7 cc. While the simulator

predicted oil production to start after 0.5 PV of surfactant injection, no oil was produced in the experiment until 3.0 cc's of post-surfactant brine was injected into the core due to oil retention near the core outlet. The effective water permeability was increased from 5.0 md to 24.0 md to increase the surfactant's mobility.

5.3.3 Core 3. Input data are listed in **Table B3.4**, **Appendix B**. The total volume of recovered oil in the experiment was 2.3 cc. The first 0.3 cc of oil was produced after 1.7 PVs of surfactant injection and the remaining 2.0 cc was produced when post-surfactant brine was injected into the core at four times the surfactant rate. The simulated recovered oil volume was equal to 3.1 cc. The effective water permeability was increased from 4.9 md to 30.0 md to increase the surfactant's mobility.

5.3.4 Core 4. Input data are listed in **Table B3.5**, **Appendix B**. The JF-2 bio-surfactant concentration was 21.0 ppm. The simulated oil recovery was equal to 2.2 cc of oil compared to the experimental value of 2.7 cc. The simulated oil breakthrough time after 13.5 cc of surfactant injection was close to the experimental value of 14.0 cc when a 1.0 cc oil slug was produced. The closeness in breakthrough volumes (time) meant that fractional fluid flow within the core in the experiment was similar to the fractional flow predicted by simulation. Since the comparison of the simulation to the experiment was constrained by the total oil recovery and breakthrough time, the simulation was reasonably accurate. But while the simulated oil production was uninterrupted following breakthrough, oil production in the experiment stopped after 1.0 cc of oil was produced following breakthrough. The remaining 1.7 cc was recovered during post surfactant brine injection. The effective water permeability was increased from 5.2 md to 16 md. The oil

production, cumulative recovery and water cut profiles are plotted in **Figure 5.3.4.** The experimental oil breakthrough point is marked as straight red line on the figure.

Figure 5.3.4. Flow profile for the core 4 experiment

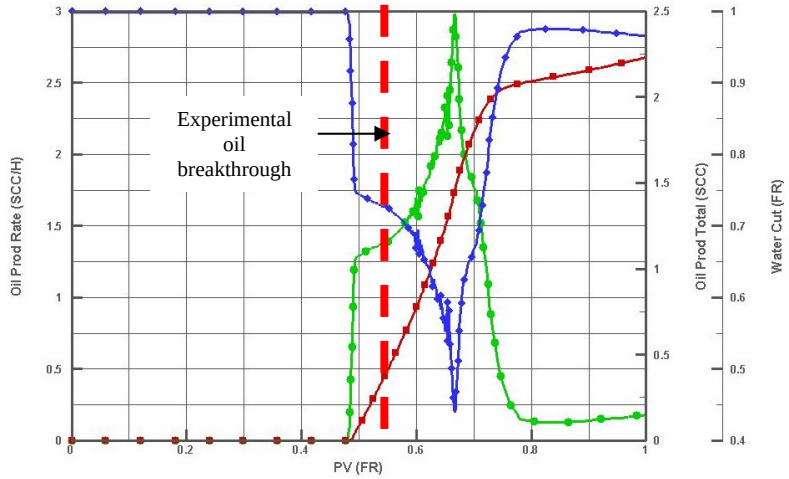

5.3.5 Core 5. Input data are listed in **Table B3.6**, **Appendix B**. The simulated total oil recovery was equal to 1.8 cc and the experimental recovery was equal to 2.3 cc. The effective water permeability was not increased in this simulation. The experimental result showed that all the oil was produced during post surfactant brine injection because of oil retention near the core outlet during surfactant injection. The simulation predicted oil production to start after 0.4 PV of surfactant injection.

5.3.6 Core 6. Input data are listed in **Table B3.7**, **Appendix B**. Oil recovery by plain PHPA solution was simulated to quantify the polymer's role in surfactant flood simulations. The simulated oil recovery was equal to 1.1 cc compared to the experimental value of 1.2 cc. Also, the simulated oil breakthrough after 0.5 PV of surfactant injection was close to the experimental value of 0.55 PV. While the simulated oil production remained uninterrupted following breakthrough, only 0.4 cc of oil was recovered in the experiment and the remaining 0.8 cc of oil was recovered during post-surfactant brine injection.

5.3.7 Banking of oil near the outlet end. Input data are listed in **Table B3.8**, **Appendix B**. This series of simulations investigated oil retention near the core outlet. This was done because retention had prevented timely oil production and caused higher than expected injection pressures. It was observed that if no oil (or some oil) was produced from a core treated with the surfactant at a specific flow rate, then some oil (or larger volume of oil) would be produced from a core with similar properties when it was treated with the same surfactant at a higher flow rate. In other words, oil retention reduced at a higher surfactant rate. A 100 x 1 x 4 blocks cross-sectional model of a Berea core shown in **Figure 5.3.5** was constructed to investigate retention. Four pore volumes of JF-2/PHPA surfactant was injected into the model at 5.14, 6.4 and 12.0 cc/hr. The oil production and cumulative recovery profiles at the three rates are plotted in **Figure 5.3.6**. The oil saturation profiles after surfactant injection at the three rates are shown in **Figures 5.3.7a, b** and **c**. The profiles show a darker region near the outlet where the oil saturation was high due to oil retention caused by gravity segregation. The region got smaller when the surfactant rate increased. On comparing the oil production in **Figure 5.3.6**, the oil fraction at oil breakthrough was higher at the higher rate. This helped explain the experimental observations and supported the study made by Healy et al.[73]. Healy et al.[73] reported a higher oil fraction at higher surfactant rates in cores. Numerical instability was observed in all three cases and it is been explained previously.

These simulations do not completely explain the reasons for oil retention at the outlet and the oil slug production when a high rate post flush injection was started. The likely reason is a combination of flow convergence and the inaccurate modeling of the source and sinks terms in the simulator. The simulator modeled the inlet and outlet ends

of the core as simple source/sink terms where flow is assumed to occur across the full face of the core. In reality, the core inlet and outlets were complex geometry near the centers of the core faces where flow divergence or convergence occurred. Fine gridding and a better description of the flow process near the injector and producer blocks could potentially simulate the problem but was not done using the MEOR simulator. The combination all these mechanisms may have retained the oil at the core outlet and resulted in oil slug production. Since the causes for oil retention were not fully modeled, the oil slug production could not be simulated and the surfactant injection pressures were not compared to the simulated values.

Figure 5.3.5. 100 x 1 x 4 grid model

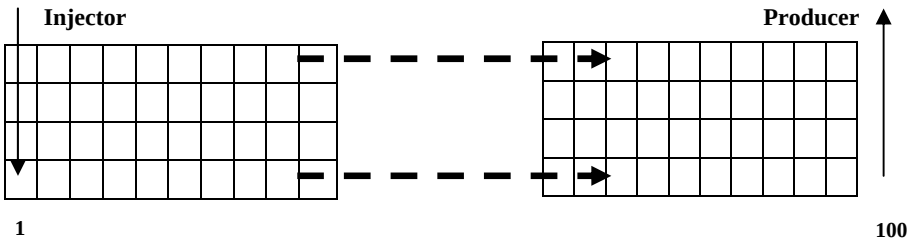

Figure 5.3.6. Oil production and cumulative recovery at different rates.

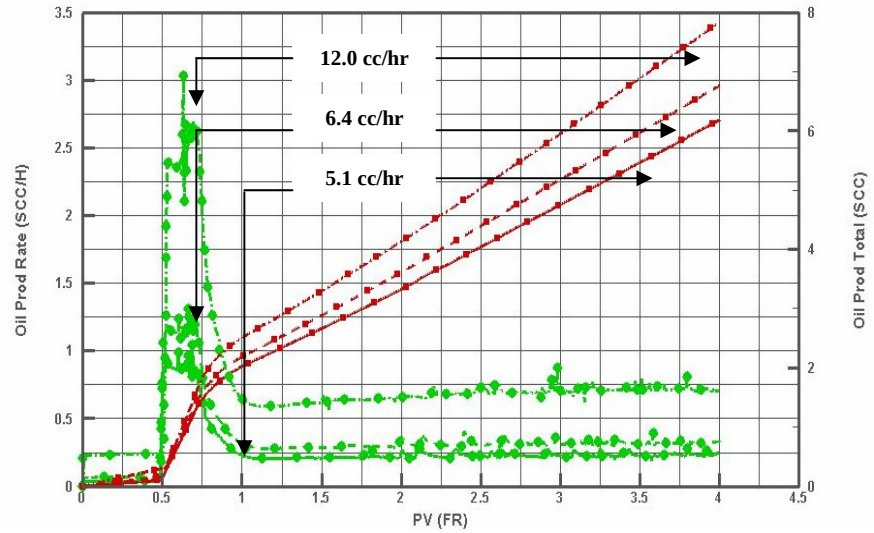

Figure 5.3.7. Cross-sectional view of oil saturation

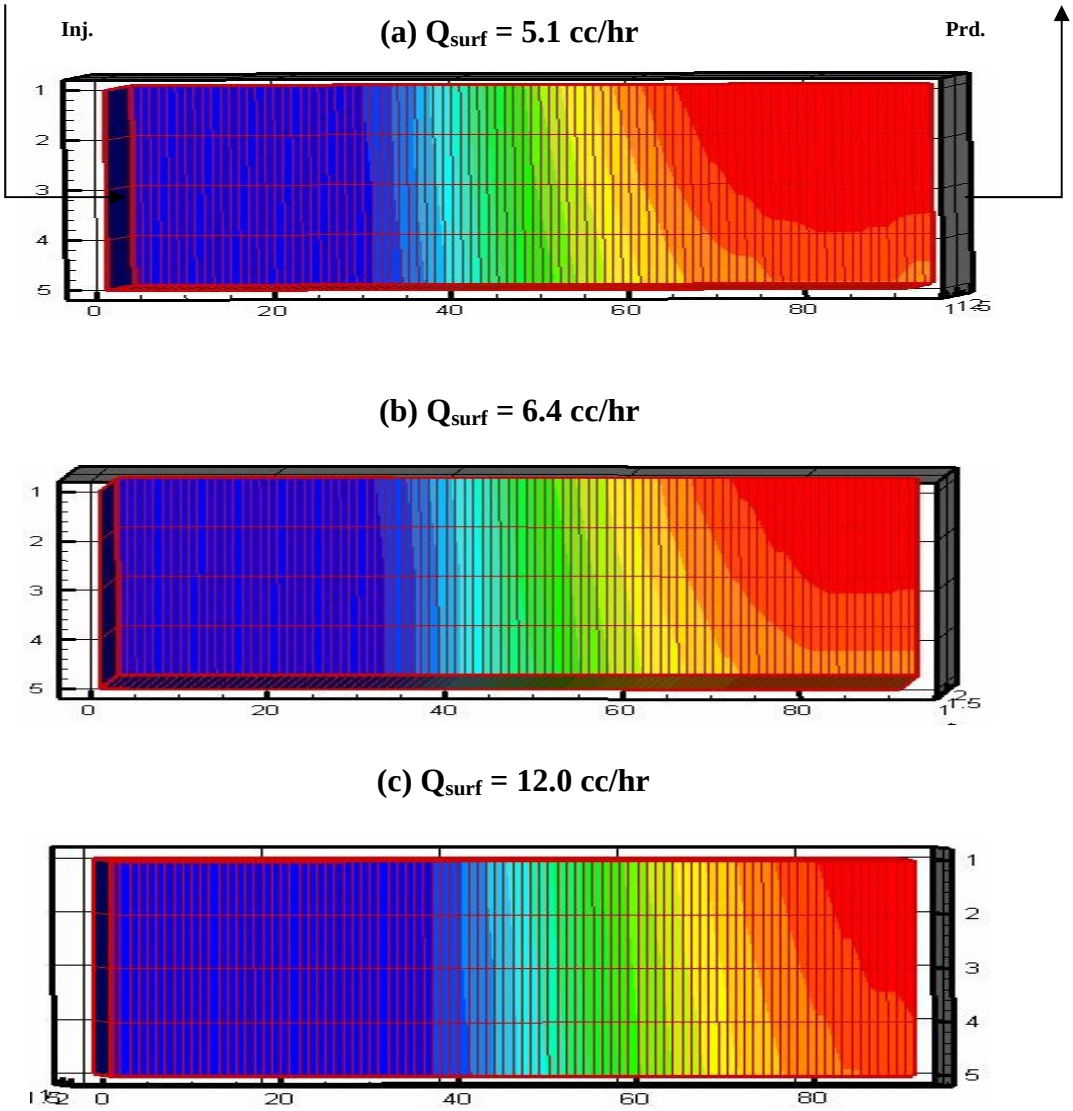

5.4 Results.

1. The MEOR simulator was able to show the benefit of mobility control in the surfactant by simulating and comparing oil recovery for a viscous surfactant, plain polymer solution and plain JF-2 bio-surfactant solution.
2. The MEOR simulator showed the impact of sodium chloride and calcium on polymer and bio-surfactant behavior and oil recovery. The simulations were done with SP-018 bio-polymer as the mobility control agent. Simulations were also done for

polyacrylamide polymer. The simulator predicted oil recovery along expected trends with different polymers, monovalent and divalent ions and bio-surfactant concentrations.

3. Core experiments were simulated and the simulated oil recoveries were compared to the experimental observations. The simulated oil recoveries were less than experimental values and the difference between the two increased with bio-surfactant concentration. The timing of oil breakthrough for two of the cores was close to the experimental values. This meant that fractional flow curves and relative mobilities of the surfactant and oil phases may have been close to the true values. The simulated and experimental results are tabulated in **Table 5.4.1** and plotted in **Figure 5.4.1**.

Table 5.4.1. Comparison of numerical simulation results with laboratory experiments.

Simulation #	Surf. Conc (mg/scc)	Simulated Recovery (Fr.)	Experimental Recovery (Fr.)
5.3.1	0.011	0.06	0.06
5.3.2	0.011	0.05	0.04
5.3.3	0.011	0.28	0.20
5.3.4	0.021	0.13	0.17
5.3.5	0.041	0.22	0.29
5.3.6	0.0	0.10	0.09

Figure 5.4.1 Bio-surfactant concentration vs. Simulated and experimental oil recovery.

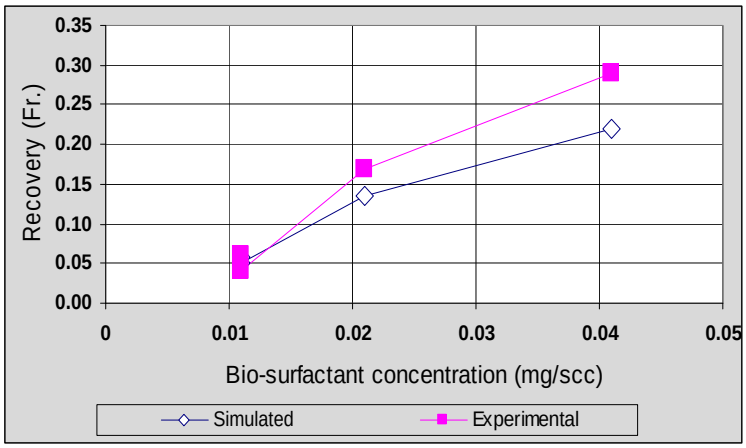

4. Cross-sectional model simulations were able to identify gravity segregation as a contributing reason for oil retention but oil slug production and oil retention near the core outlet could not be simulated. As a result, simulated injection pressures were not compared to the experimental injection pressures.
5. Simulated results showed that oil recovery was not proportional to bio-surfactant concentration as observed in the core flood experiments. The relative increase in oil recovery decreased with increasing bio-surfactant concentration because the bio-surfactant was unable to change capillary numbers enough to further lower oil saturation.
6. Polymer retention and permeability reduction were simulated. The impact of permeability reduction was observed through the higher inlet pressures. By observing the simulated injection pressures it was possible to show that the experimental injection pressures were a combination of permeability reduction and flow resistance caused by oil retention.

5.5 Discussion.

1. Appropriate variables for comparing simulations to core experiments are injection pressure and oil production. The experimental injection pressure was the result of a combination of permeability reduction and oil retention at the outlet. Oil production was also affected by oil retention in all six core experiments. No oil was produced during surfactant injection from four of the cores and a small fraction (0.3-0.2 fraction) of the total mobilized oil was produced during surfactant injection for the two remaining two. Most of the oil (0.7-1.0 fraction) was retained near the core outlet and produced as a slug at the start of a high rate brine injection following the

surfactant. Since the oil retention mechanism and the affected fluid injection pressures and oil production could not be simulated, the two time dependent variables were not selected for comparing the simulated and experimental results. Instead cumulative oil recovery was chosen for comparing the two results.

2. The simulation using cross-sectional models showed one reason for oil retention near the core outlet could be gravity segregation. Gravity caused oil to move towards the upper portion of the core. But the simulation did not completely explain why the mobilized oil would collect so close to the core outlet that a higher rate could displace it as a slug. It is likely that retention was a combination of gravity and flow constriction near the core outlet. Flow constriction was not modeled by the simulator which defines the core inlet and outlet as simple source and sink terms. The model assumed outlet across all layers rather than as small openings located at the center of the core face.
3. While simulating the JF-2 micellar/polymer experiments, it was observed that the low mobility of the viscous surfactant resulted in time steps close to zero to constrain saturation, pressure and concentration changes. This problem was overcome and the simulation speeded up by increasing the core's effective brine permeability. Though relative permeability curves are assumed to be unchanged for aqueous polymer flow, laboratory studies of polymer oil displacement have shown that polymers can change the end point value for brine without changing the oil end point[102]. One mechanism that can cause this is the creation of an emulsion between the polymer, surfactant, oil and water at the oil displacement interface. The emulsion may have altered the rock wettability from water wet to mixed wet. Increasing the brine end point permeability

may reflect these changes. The change in brine end point permeability is graphically shown in **Figure 5.3.9**.

Figure 5.5.1. Increase of the water/brine effective permeability

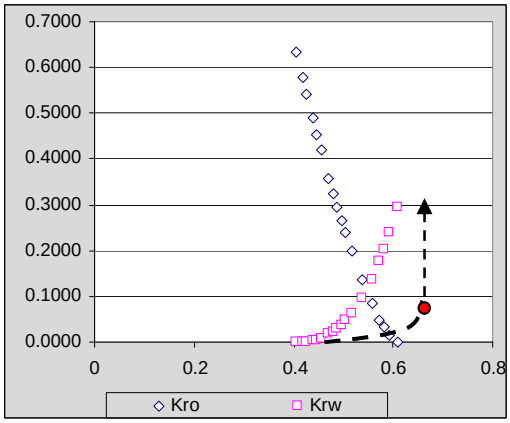

Mobility could also be altered by reducing surfactant viscosity but that made it difficult to simulate the benefit of reduced surfactant mobility, and was not considered. Once the surfactant flowed without the time step reducing to zero, the PHPA shear constant was adjusted within a range of 5 sec^{-1} to bring the simulated results as close as possible to the experimental value. This is an acceptable range especially at the high salinity of 5.0% NaCl[24].

4. The increasing difference between the experimental and simulated oil recovery as bio-surfactant concentration increased indicated that the simulated oil displacement was not as effective as it was in the cores. This could be caused by a difference in simulated and experimental surfactant mobility at the oil displacement interface within the cores. The formation of an emulsion whose properties were different from the surfactant could explain the difference in results. The emulsion's viscosity may have increased with bio-surfactant concentration and this could not be simulated by the simulator resulting in the difference in oil recoveries increasing with bio-

surfactant concentration. But this negated the increase in brine end point permeability done to overcome the small time steps. It is possible that a complex chemical interaction occurred at the oil displacement interface which could not be simulated leading to the difference between the simulated and experimental recoveries.

5. Besides sodium chloride and calcium, reservoir brine has many other chemical species that may affect polymer and bio-surfactant behavior. But only these two components were included because studies had mainly reported on monovalent and divalent ions since they had the largest impact on polymer and surfactant behavior.
6. Adsorption input data for the polymers and bio-surfactant were taken from literature. If not available, properties of similar chemicals were used[32]. Literature reports on adsorption data for polyacrylamides are available but not for JF-2 bio-surfactant. Further core experiments are needed to provide bio-surfactant adsorption data.

5.6 Conclusions.

1. The modified MEOR numerical simulator was used to successfully simulate the effect of mobility control on surfactant flooding, salinity effects on polymer and bio-surfactant behavior, polymer retention and polymer shearing. These features were tested by simulating core flood experiments.
2. JF-2 bio-surfactant core flood experiments with Berea sandstone cores were simulated. The simulated results were smaller than the experimental results but compared reasonably. The simulator could be used to help explain reasons for oil retention near the core outlet observed in the core flood experiments.

3. The simulator predicted increased oil recovery with bio-surfactant concentration. It showed that the relative increase in oil recovery decreased as bio-surfactant concentration increased beyond 21.0 ppm.
4. The simulations using the model captured the important phenomena within a core but did not simulate flow constrictions near the outlet or complex chemical interactions between the various phases and chemical species present during a core flood. These can explain the difference between the experimental and simulated results.

CHAPTER VI

A NEW MODEL FOR TERTIARY OIL RECOVERY

6.1 Introduction. A method to simulate residual oil mobilization in tertiary oil recovery as organic chemical contaminant removal from an aquifer is discussed. This method was motivated by the approach used by hydrologists and environmental engineers to simulate non-aqueous phase liquid (NAPL) contaminant removal from aquifers and soils. It is believed that simulating tertiary recovery as a contaminant transport problem in a single aqueous phase models the physics of the process more realistically and may be computationally simpler than conventional multiphase multi-component finite difference simulation. An advantage of this method is that it could be used to simulate component transport by streamlines resulting in better reservoir description and reduced computation time. The transport equation is the dispersion-convection equation with an additional adsorption term.

6.2 Theory. Studies have shown that in oil reservoirs, the non-wetting phase at residual saturation exist as isolated globules surrounded by wetting phase[103]. The morphology and distribution of oil globules or ganglia is dependent on pore geometry and rock wettability[103]. For example, studies by Stegemier[48] and Chatzis et al.[104] have reported that in water wet porous media, residual water gets pushed into the smallest pores and residual oil exists as isolated strands of ganglia or globules within the larger pores surrounded by water. Oil recovery under these conditions is achieved by overcoming the

capillary forces and pore geometry effects that trap the oil. In tertiary oil recovery, surfactants and polymers in water can be used to reduce the oil-water IFT and overcome the capillary forces[77].

Organic contaminants in aquifers and soils are also retained within the pores as isolated ganglia or globules by capillary and electrostatic forces[103]. The morphology and distribution of the non-aqueous contaminants is similar to that of residual oil in reservoirs. Since the trapping mechanisms and the morphology of organic contaminants and residual oil are the same, residual oil recovery will be similar to the removal of organic or non-aqueous phase liquids (NAPLs) pollutant from aquifers. Since most crude oils are lighter than water, tertiary oil recovery can be classified as the recovery of lighter NAPLs or LNAPLs from porous media.

Mathematical models and simulators treat chemical pollutant recovery as a transport problem for a chemical species in a single aqueous phase[50,52,53]. Residual oil recovery models could be similarly developed where the single phase is the reservoir brine mixed with a solvent or surfactant. In the following sections, the mathematical equations that model chemical species transport in a single phase through porous media are extended to micellar-polymer solution based residual oil recovery to develop a transport model for tertiary oil recovery.

6.3 Mathematical equations. The mass balance for a chemical species '*i*' in a multiphase system for a representative elemental volume (REV) is[51]:

$$\frac{\partial}{\partial t}\left(\phi\sum_{j=1}^{N_P}\rho_j S_j\omega_{ij}+(1-\phi)\rho_s\omega_{is}\right)+\nabla.\left(\sum_{j=1}^{N_P}\left(\rho_j\vec{u}_j\omega_{ij}-\phi\rho_j S_j\overrightarrow{\overrightarrow{D}}_{ij}.\overrightarrow{\overrightarrow{\nabla}}\omega_{ij}\right)\right)=\phi\sum_{j=1}^{N_P}S_j r_{ij}+(1-\phi)r_{is}+\sum_{j=1}^{N_P}\omega_{ij}\rho_j Q_j$$

, $i=1,.....N_C$

(6.1)

where, N_P is the number of phases, N_C is the number of components, S_j is the phase saturation, ϕ is the average porosity of the REV, $\overrightarrow{\overrightarrow{D}}_{ij}$ is the dispersion tensor, ρ_j is the density of the phase, ρ_s is the density of the solid phase, ω_{ij} is the mass fraction of the chemical species per unit pore volume and ω_{is} is the mass fraction of the species deposited on the solid rock. The right side of Equation 6.1 is the source term represented by r_{ij} , the sum of the homogenous chemical reaction rates of species '*i*' in phase '*j*', r_{is}, the sum of the homogenous chemical reaction rates on the solid and Q_j, the volumetric rate of phase '*j*' in or out of the representative volume. The first term on the left side of Equation 6.1 represents the rate of total accumulation of species '*i*' in the pore volume as a free phase and due to accumulation within the rock. The second term is the net flux of the species by advection and total dispersion. Total dispersion is a combination of diffusion and mechanical dispersion caused by heterogeneity. Diffusion dominates the dispersive mass transfer at low flow rates and mechanical dispersion controls mass transfer at high flow rates[105].

If the chemical species flow simultaneously in a single fluid phase regardless of composition changes, no physical source and sink terms are present, and no chemical reaction involving the species '*i*' is assumed to occur, the equation for any species '*i*' in a single phase becomes:

$$\frac{\partial}{\partial t}\left(\phi\rho\omega_i + (1-\phi)\rho_s\omega_{is}\right) + \nabla.\left(\left(\rho\vec{u}\omega_i - \phi\rho\overrightarrow{\overrightarrow{K}}_i.\overrightarrow{\nabla}\omega_i\right)\right) = 0 \quad (6.2)$$

It is important to realize that in this study, the residual oil is assumed to flow as disconnected globules within the aqueous phase. Equation 6.2 represents a case where oil is transported as discrete globules in the aqueous phase. But when oil saturations are high, like near producing wells, the oil globules can combine to flow as another phase. Under those circumstances the chemical species transport model will not applicable. The summation term over all the phases and the second subscript '*j*' are removed because a single phase is present. Equation 6.2, in terms of chemical concentration is:

$$\frac{\partial}{\partial t}\left(\phi C_i + (1-\phi)C_{is}\right) + \nabla.\left(\left(\vec{u}C_i - \phi\overrightarrow{\overrightarrow{K}}_i.\overrightarrow{\nabla}C_i\right)\right) = 0 \quad (6.3)$$

where,

$C_i = \rho\omega_i$ and, (6.4)

$C_{is} = \rho_s\omega_{is}$ (6.5)

$$\rho\overrightarrow{\nabla}\omega_i = \overrightarrow{\nabla}\rho\omega_i \quad (6.6)$$

The concentration of species '*i*' in the flowing phase is C_i and its concentration retained on the solid surface is C_{is}. In oil reservoirs where oil content is expressed as saturation, oil content can be expressed as concentration through its density.

Retention and mobilization of chemical species in porous media. The amount of LNAPL solute that is retained and the relationship between the retention (sorption) and mobilization (desorption) mechanisms determines how much of the LNAPL is recovered from the porous media. Oil retention and mobilization is similar to LNAPL contaminant

retention and removal. So the amount of oil that is recovered depends on the relationship between oil mobilization and retention.

Trapped residual oil mobilization and retention within a porous media channel is shown in **Figure 6.1**. The arrows indicate the flowing aqueous solution (containing surfactant and/or polymer). Oil is mobilized when the capillary trapping forces are overcome or reduced by displacing fluid- reservoir brine containing surfactants and/or polymers. When a mobilized oil drop flowing with the aqueous phase or solvent contacts trapped oil, the mobile oil can mobilize a part of the trapped oil to increase the free oil concentration, the mobile oil can get trapped in the pores along with the trapped oil to reduce the oil concentration, or the mobile oil can flow past the trapped oil at constant oil concentration.

Figure 6.1. Flow of oil drops by the displacing liquid inside a pore channel

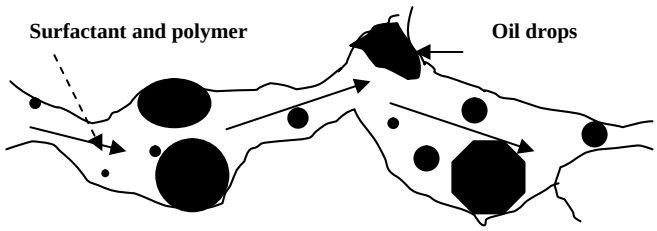

Equation 6.3 can be used for residual oil recovery if the concentration of the retained oil or the residual oil within the representative element, C_{is} is expressed in terms of the parameters controlling oil mobilization and retention. In the following discussion, the oil is at residual concentration and an aqueous phase containing surfactant flows through the reservoir. All the equations derived earlier are still valid because the aqueous solution has the same properties as the resident water and its density is unchanged. C_{is} can be then written as:

C_{is} = ***f*** (oil mobilization, oil retention) (6.7)

Oil mobilization. Oil mobilization depends on the ability of the aqueous solution to displace the residual oil. Studies of porous media have shown that the following parameters to control oil mobilization [46,77,101]:

1. Velocity of the displacing aqueous solution, u
2. Viscosity of the displacing aqueous solution, μ
3. Interfacial tension between the displacing aqueous solution and oil, σ
4. Density difference between the displacing solution and oil, $(\rho_w - \rho_o)$
5. The amount of the residual oil in the representative element, ϕC_i

The velocity, u, and viscosity, μ, of the aqueous solution represent the viscous forces that can displace and transport residual oil. Oil mobilization increases when the fluid velocity or viscosity increases. Interfacial tension, σ, between the oil and aqueous solution lowers the capillary trapping forces within the element. Oil mobilization increases with decreasing σ. Interfacial tension is considered an oil mobilizing parameter instead of a retention parameter because it is a function of surfactant concentration in the aqueous solution[77,101]. Buoyancy forces, proportional to the difference between the aqueous phase and residual oil densities tends to increase oil mobilization[46]. The amount of mobile oil in the element, ϕC_i determines the oil mobility or ease of mobilizing additional oil within an element. The relationship between mobile and retained oil is similar to adsorption isotherms that relate adsorbed mass to the flowing mass of a chemical in porous media. More oil will be mobilized when the oil concentration is high and less oil will be mobilized if oil concentration is low. The oil mobilizing parameters are then written as:

$$f(\text{oil mobilization}) = f\left(u, \mu, (\rho_1 - \rho_2), \frac{1}{\sigma}, \phi C_o\right) \quad (6.8)$$

Oil retention. Oil retention may be more complicated than oil mobilization. Retention within an element depends on pore geometry, wettability and the amount of oil in the element[48,104,103]. The parameters that affect oil retention in porous media are:

1. Pore size distribution, geometry and aspect ratio, F (ϕ).
2. Wettability of porous media, θ.
3. Interfacial surface area between oil and rock surface, a_{ios}, a_{iow}.
4. Amount of mobile oil in the element, ϕC_i.

One study that examined residual oil under water wet conditions related the oil trapping mechanism to pore aspect ratio (ratio of pore body diameter to pore throat diameter)[103]. The study showed that oil retention occurred by water bypassing the oil when the aspect ratio was small and oil drop snap-off was the dominant mechanism when the aspect ratio was large. Pore geometry and aspect ratio effects in an element can be represented by average properties of the element, F (ϕ). These could then be related to oil saturation. Use of average properties can make the modeling simpler because pore scale information is rarely available. The interfacial surface area between the oil and aqueous phase and oil and rock surface, a_{ios}, a_{iow}, are useful to describe oil concentrations at the oil-water and oil-rock interface. These have been used by hydrologists to determine residual organic contaminant saturation in porous media and could serve the same function in enhanced oil recovery[106]. Interfacial area can be determined in the laboratory[107]. Rock wettability is a measure of the electrostatic attraction between the solid rock surface and pore fluids. It is expressed as the contact angle between the wetting fluid and the rock surface, θ and

can be measured in the laboratory. Most reservoirs are generally mixed wet and wettability varies with location. An average wettability can be used for the porous medium. When porous media is water wet, the effort required to displace oil is less than when the media is oil wet. The impact of the amount of oil in an element, ϕC_i, on oil retention has been discussed earlier.

The parameters that could control oil retention are written as:

$$\boldsymbol{f}\text{(oil retention)} = \boldsymbol{f}\left(\mathrm{F}(\phi), \theta, a_{iow}, a_{ios}, \phi C_o\right) \tag{6.9}$$

In addition to the discussed parameters, studies in contaminant literature and residual oil recovery indicate that oil mobilization and entrapment are affected by saturation history [103,108]. Capillary desaturation curves between residual oil saturation and capillary number are shown to be different for the oil mobilization and retention. Capillary desaturation curves combine the aqueous solution's velocity and viscosity, rock wettability and interfacial tension into a non-dimensional entity called the capillary number. Buoyancy forces are combined with the capillary number to give another non-dimensional entity called the transport number[47]. The transport number–oil saturation relation does not consider pore geometry effects or interfacial surface area.

The important parameters that may affect oil retention and mobilization have been discussed. In order to express the retained oil concentration in terms of the mobile oil concentration and the above parameters, the parameters are combined to:

$$\boldsymbol{C_{is}} = \boldsymbol{f}\left(\frac{u\mu}{\sigma.\cos\theta}, \frac{(\rho_1 - \rho_2)g}{\sigma.\cos\theta}, \mathrm{F}(\phi), a_{iow}, a_{ios}, \phi C_i\right) \tag{6.10}$$

where,

$\frac{u\mu}{\sigma.\cos\theta}$ = $N_{CP,}$ is the capillary number of the ratio between the displacing viscous forces and capillary forces

$\frac{(\rho_1 - \rho_2)g}{\sigma.\cos\theta}$ = N_B, is the Bond number which is the ratio of buoyancy forces to the capillary forces.

and $N_T = N_{CP} + N_B$ where N_T is the transport number.

In conventional simulation methods, pore geometry and wettability effects are captured by the relative permeability curves. But in the approach presented here, the relative permeability curves are not considered because of single phase flow. Relative permeability curves are based on a continuously connected phase. That is not the case here because oil is transported as another dispersed species in the aqueous phase. This species transport model for residual oil recovery could be a simpler than the multiphase finite difference model because only a single phase exists and residual oil is a contaminant that is washed from within the rock and transported within that phase. Studies are needed to understand the significance of some of the parameters and how to measure and represent them. For example, pore geometry for a porous media could be represented as a statistical average value that represents pore geometry. Adsorption isotherms may simplify residual oil transport modeling because all the factors could be combined into two parameters leaving only the residual and mobile oil concentrations as the variables but because concentrations of contaminants are very low relative to residual oil concentrations, the accuracy of isotherms at large concentrations needs to be established. Further research may show that some parameters will not be needed and new ones are needed.

6.4 Numerical simulation. Mass transport by the convection-dispersion problem occurs by two different mechanisms. Transport by advection occurs along the direction of flow and transport by dispersion occurs in different directions. Numerical simulation has to solve both the hyperbolic advection part and the parabolic dispersion part of the equation. Numerical methods to solve this problem can be categorized between Eulerian, Lagrangian and mixed Eulerian-Lagrangian techniques.

Eulerian models. In Eulerian methods, the entire model is divided into grid blocks and the contaminant concentration is calculated at each block after every timestep. The solution method could be direct solver algorithms, method of lines integration or iterative solutions[109]. Numerical oscillation and numerical dispersion are two major problems associated with finite difference methods. These two problems happen when dispersion is quite small or the transport is advection dominated. Fine gridding and upstream weighting overcome oscillation but increase computation times and numerical dispersion. To reduce numerical dispersion, the Courant number, which places a limit on the maximum distance contaminant can travel in a single timestep, should not exceed one[110]. The stability criterions change when retention and desorption are included[110]. Some finite difference contaminant transport modeling numerical codes are UTCOMP developed at the University of Texas[88] and the MT3D developed by Zheng[110]. Similar constraints also apply to finite element modeling.

Lagrangian method. Lagrangian methods are not constrained by the Courant number requirement and are free of numerical dispersion. They are effective at solving advection dominated transport problems. Streamline simulation and particle tracking are two Lagrangian techniques used to solve the transport problem. Streamline simulation has

been used to simulate contaminant transport with dispersion[55] and without dispersion[12]. Particle sorption can be modeled by dividing the fluid velocity by a retention parameter. Lagrangian methods where dispersion was not included have reduced computation times significantly compared to finite difference methods with acceptable accuracy[12]. If dispersion is intensive and is included then the modeling process can become computationally intensive and negate the reduced computation time benefit. Some numerical codes that have implemented the Lagrangian model for contaminant transport modeling are 3DSL[54], RANDOMWALK[110] (an early two dimensional code), RAN3D[110] which is an extension of RANDOMWALK in three dimensions and FRONTSIM (a Schlumberger commercial streamline simulator).

Mixed Eulerian and Lagrangian methods. Since the Eulerian method models dispersion better and the Lagrangian method models the advection part better, the mixed approach was designed to combine the two methods. In these methods, the advection part is solved using a Lagrangian technique and the dispersion part using an Eulerian technique. Further details about this are explained by Zheng and Bennet[110]. Zheng and Bennet[110] report that the Method of Characteristics (MOC) code successfully combines the two methods.

6.5 Summary. The application of contaminant transport application in environmental science suggests that a contaminant transport approach could be applied to residual oil recovery. This would be a numerically and conceptually simpler approach than finite difference simulation A significant benefit of this approach to oil recovery modeling could be its use of streamline simulation methods. The reduction in computational effort

and time can be significant without loss in accuracy. No study is reported that compares computation times for contaminant transport by finite difference methods.

6.6 Conclusions.

1. A functional form of a tertiary oil recovery model that treats residual oil as a chemical species in a single aqueous phase has been proposed.
2. The likely parameters that affect oil retention and oil mobilization have been identified.

CHAPTER VII

CONCLUSIONS AND RECOMMENDATIONS

7.1 Conclusions

1. Berea sandstone core flood experiments successfully demonstrated that 10.0-41.0 ppm (0.001-0.04 mg/scc) of JF-2 bio-surfactant mixed with a mobility control agent, can recover 10-30% of waterflood residual oil under field flow rates and pressures.
2. The capabilities of a microbial enhanced oil recovery numerical simulator were extended to simulate bio-surfactant/polymer solution flooding through cores and account for the effect of sodium chloride, calcium ions, polymer shearing, polymer retention and polymer and surfactant adsorption on bio-surfactant/polymer based oil recovery.
3. The modified simulator simulated six JF-2/PHPA surfactant core flood experiments. The simulated and experimental cumulative oil recovery for all six cores and the oil breakthrough times for two cores were comparable within the constraints placed on the data used in the simulations.
4. The core flood experiments showed that a minimum of 11.0-15.0 ppm (0.001-0.015 mg/scc) of JF-2 bio-surfactant was required in a pore volume of surfactant solution to recover any oil through interfacial tension reduction.

5. Based on experimentally measured data, an existing mathematical model to calculate interfacial tension was modified to calculate interfacial tension as a function of JF-2 bio-surfactant concentration. The minimum interfacial tension measured in the presence of the bio-surfactant was 0.1 dynes/cm.
6. The numerical simulator was used to identify gravity segregation as one cause for oil retention near the core outlet. But it was not possible to duplicate the retention process completely with the simulator due to a combination of core geometry effects and gravity segregation. The exact reason for retention was shown and hence not used in modeling the core floods. As a result, experimental injection pressures and the oil slug production were not simulated.
7. The simulator showed that the recovered oil fraction was proportional to bio-surfactant concentration below 21.0 ppm but relative improvements in oil recovery decreased at higher concentrations.
8. A functional form of a tertiary oil recovery model that treats residual oil as a chemical species within a single mobile aqueous phase has been proposed and parameters likely to affect oil mobilization and retention have been discussed.

7.2 Recommendations

1. Experiments to estimate adsorption parameters for JF-2 bio-surfactant are required. Laboratory measured adsorption parameters are essential for two reasons. First, to predict oil recovery during surfactant injection and help design bio-surfactant treatments process. Second, to estimate bio-surfactant consumption and nutrient requirements from bio-surfactant yields because the major cost of MEOR processes are the nutrients and it is critical to have estimate of nutrients requirements.

2. Ternary studies to describe bio-surfactant behavior with crude oil and water are needed. The difference between simulated and experimental oil recovery were attributed to the change in effective end point water permeability and the possible formation of an emulsion between the bio-surfactant, oil and brine. Ternary studies can determine the interactions between the components and identify the properties of the emulsion if formed. This information can be used to develop models to improve upon bio-surfactant based oil recovery simulation.
3. Rock wettability changes and end point effective permeability changes during bio-surfactant/polymer flooding should be investigated. Understanding such changes is important to accurately simulate bio-surfactant and mobilized oil flow in reservoirs and predicting oil recovery.
4. It is recommended that IFT measurements be made using bio-surfactant samples prepared for salinities other than 5.0 % NaCl and at different bio-surfactant concentrations to verify if the changes in IFT were independent of the initial conditions and whether IFT changes are reversible functions of salinity.
5. Fine gridding of reservoir models, especially near the wells and their proper location when simulating the core experiments can help identify causes for oil retention and oil slug production in the core experiments. The effects of flow constriction and divergence on oil displacement can also be explained.
6. Further studies are needed to identify all parameters that affect oil mobilization and retention and combine them into a useful form. The important parameters that should be studied in detail before implementing in a numerical model are; the relationship between interfacial contact area and oil saturation, the change in porosity with oil

saturation and the importance of pore geometry in modeling oil transport and, how to represent pore geometry in the model.

Nomenclature

a_k = Langmuir isotherm constant

a_{k1} = Langmuir isotherm constant parameter

a_{k2} = Langmuir isotherm constant parameter (1/meq)

Ap_1, Ap_2, Ap_3 = Polymer viscosity parameters (wt^{-1}%, wt^{-2}%, wt^{-3}%)

B_o, B_w, B_g = Oil, water, gas formation volume factors (cc/scc, rb/stb, cf/scf)

Bp = Effective salinity parameter

b_{rk} = Permeability reduction parameter

C_t = Total formation compressibility (psi^{-1})

C_i = Concentration of species '*i*' (mass/unit volume)

C_k = Concentration of component k (numbered 1 to 14) (mg/scc, lb/stb)

C_b = Bacteria concentration (mg/scc, lb/stb)

C_{s1}, C_{s2} = Substrate 1 and 2 concentrations (mg/scc, lb/stb)

C_s = Substrate/Nutrient concentration (mg/scc, lb/stb)

C_i = Alcohol inhibitor concentration (mg/scc, lb/stb)

C_7 = Polymer concentration (wt %)

C_{sc} = Critical substrate concentration (mg/scc, lb/stb)

$C_{sf,\max}$, $C_{sf,\min}$, C_{sf} = Bio-surfactant concentration (mg/scc, lb/stb)

C_{sep} = Effective salinity for polymers (meq/ml)

C_{se} = Effective salinity for bio-surfactant (meq/ml)

c_{rk} = Permeability reduction parameter

$\vec{\vec{D}}$ = Dispersion tensor (cm^2/hr, ft^2/day)

$D_{kw,xx}$ = Dispersion in the x direction when flow is in the x direction (cm^2/hr, ft^2/day)

D_k = Diffusion co-efficient (cm^2/hr, ft^2/day)

ES = Interfacial tension parameter

f_5^s = Concentration fraction of alcohol

f_{12}^s = Concentration fraction of calcium ions

g = Acceleration due to gravity

g_c = Gravity constant

$\overrightarrow{\overrightarrow{K}}$ = Absolute directional permeability tensor (md)

K_{rl} = Phase relative permeability

$K_{b/s1}$, $K_{b/s2}$ = Saturation constant for substrates 1 and 2 (mg/scc, lb/stb)

$K_{p/s}$ = Saturation constant for production from substrate (mg/scc, lb/stb)

K_i = Alcohol inhibitor constant (mg/scc, lb/stb)

K_r = Microbe retention factor

K_d = Microbe detachment factor

K_c = Chemotactic co-efficient (cm^2/hr, ft^2/day)

m_s = Maintenance energy (mg/scc, lb/stb)

N_{tl}, N_{tl}^w, N_{tl}^h = Trapping number, high and low trapping numbers.

N_B = Bond number

N_T = Transport number

N_{CP} = Capillary number

N_C = Number of chemical components

N_P = Total number of phases

n = Polymer power law exponent

P_l = Phase pressure (psi)

P_α = Polymer shearing parameter

Q_j = Flow rate of phase 'j' (Vol./Time)

R_{so}, R_{sw} = Gas oil ratio and gas water ratio (scc/scc, scf/scf)

R_p = Product formation rate (hr^{-1}, day^{-1})

R_s = Substrate consumption rate (hr^{-1}, day^{-1})

R_{bf} = Sessile bacteria growth rate (hr^{-1}, day^{-1})

R_{bs} = Planktonic bacteria growth rate (hr^{-1}, day^{-1})

RRF = Residual resistance factor

$R_{k,\max}$ = Maximum permeability reduction factor

r_{is} =

r_{ij} =

S_o, S_w, S_g = Oil, water and gas saturation fractions

S_p = Polymer viscosity parameter

S_{lr}, S_{lr}^h, S_{lr}^w = Residual phase saturation, high and low capillary number residual saturations

S_j = Saturation of phase 'j'

T_{l1}, T_{l2} = Trapping number parameters

t = Time (hr, day)

$\vec{u}_t$ = Total velocity of bacteria (cm/hr, ft/day)

$\vec{u}_c$ = Chemotactic velocity of the aqueous phase (cm/hr, ft/day)

$\vec{u}_w$ = Water phase Darcy velocity (cm/hr, ft/day)

$\vec{u}_j$ = Water phase Darcy velocity (cm/hr, ft/day)

$Y_{b/s}$ = Specific yield of bacteria per mass of substrate (mg/mg, lb/lb)

$Y_{p/s}$ = Specific product yield per mass of substrate (mg/mg, lb/lb)

Greek symbols

μ_l = Phase viscosity (cp)

μ_b = Specific growth rate for bacteria (hr^{-1}, day^{-1})

μ_{bm} = Maximum growth rate for bacteria (hr^{-1}, day^{-1})

μ_{pm} =Maximum product formation rate (hr^{-1}, day^{-1})

$\mu_{\dot{\gamma}}$ = Polymer viscosity at any given shear rate (cp)

μ_0 = Polymer viscosity at infinite shear rate (cp)

μ_∞ = Polymer viscosity at infinite shear rate (cp)

ρ_l = Phase density (mg/scc, lb/ft^3)

ρ_j = Phase density (mg/scc, lb/ft^3)

ϕ = Porosity (fr.)

ψ_l = Phase mobility across a grid boundary face

τ = Formation tortuosity (cm/cm, ft/ft)

α_{lw} = Longitudinal dispersivity (cm, ft)

α_{tw} = Transverse dispersivity (cm, ft)

$\vec{\nabla}\Phi_w$ = Water potential gradient

$\dot{\gamma}$ = Shear rate (sec^{-1})

$\gamma_{\frac{1}{2}}$ = Shear rate where polymer viscosity is half of the zero shear rate viscosity (sec^{-1})

β_{12} = Effective salinity parameter for Calcium

β_5 = Effective salinity parameter for alcohol

$\sigma_{ow}, \sigma_{\min}, \sigma_{\max}$ = Oil water interfacial tension, minimum and maximum IFT (dynes/cm)

σ = Pore space occupied by sessile bacteria (fr.)

ω_{ij} = Mass fraction of species '*i*' in phase '*j*'

ω_{is} = Mass fraction of species '*i*' sorbed on the solid phase '*s*'

θ = Wettability angle (deg.)

REFERENCES

1. *Developments in Petroleum Science,* "*Microbial Enhanced Oil Recovery,*" edited by Donaldson, E.C., Chilingarian, G.V. and Yen, T.F. Elsevier Publications, 1989, p 1-14.
2. Folmsbee, M, Duncan, K., Han, S.O., Nagle, D.P., Jennings, E. and McInerney, M.J.: "Reidentification of Bacillus *licheniformis* JF-2 as Bacillus *mojavensis* strain JF-2," Department of Botany and Microbiology, University of Oklahoma, Norman, OK, (2005).
3. Lin, S., Minton, M.A., Sharma, M.M. and Georgiou, G.: "Structural and immunological characterization of bio-surfactant produced by Bacillus licheniformis JF-2," *Applied Environmental Microbiology*, Vol. 60, Issue 1, (Jan. 1994), p 31-38
4. Donaldson, E.C., Thomas, R.D. and Lorenz, P.B.: "Wettability determination and its effect on oil recovery," *SPEJ* (March 1969) 13-20.
5. Maudgalya, S.: "Development of a bio-surfactant based microbial enhanced oil recovery procedure," MS thesis, The University of Oklahoma, Norman, Oklahoma (2002).
6. Zhang, X.: "Mathematical simulation of transport and growth of microorganisms in porous media and impacts of microbial activities on enhanced oil recovery," PhD dissertation, The University of Oklahoma, Norman, Oklahoma (1994).
7. Healy, R.N., Reed, R.L. and Stenmark, D.G.: "Multiphase microemulsion systems," *SPEJ* (June 1976) 147-160.

8. Mungan, N: “Rheology and adsorption of aqueous polymer solutions,” *Journal of Canadian Petroleum Technology* (1969) **8**, 45-50.

9. Pope, G.A., Wu, W., Narayanaswamy, G., Delshad, M., Sharma, M.M. and Wang, P.: “Modeling relative permeability effects in gas-condensate reservoirs with a new trapping model,” *SPE Reservoir Evaluation and Engineering,* (April 2000) 171-178.

10. John, A., Han, C., Pope, G.A., Sepehrnoori, K.: “A new generation chemical flood simulator,” SPE 89436, presented at the 2004 SPE/DPE Fourteenth Symposium on Improved Oil recovery held in Tulsa, Oklahoma, USA, 17-21 April 2004.

11. Zheng, C. and Bennett, G.D.: “*Applied contaminant transport modeling*,” 2nd Edition, Wiley Interscience Publication, New York, 2002.

12. Crane, M.J. and Blunt, M.J.: “Streamline-based simulation of solute transport,” *Water Resources Research*, Vol. 35, No. 10, (Oct. 1999), p3061-3078.

13. ZoBell, C.E.: “Bacterial release of oil from oil bearing materials, Part I”, *World Oil*, 126(13), pp 1-11.

14. ZoBell, C.E.: “Bacterial release of oil from oil bearing materials, Part II”, *World Oil*, 127(1), pp 1-11,239-187.

15. Yarbrough, H.F. and Coty, V.F.: “Microbially enhanced oil recovery from the upper Cretaceous Nacotoch formation, Union County, Arkansas,” proceedings from the 1982 International Conference on Microbial Enhancement of Oil Recovery, held in Shangri-la, Afton, OK, May 16-21, 1982, p149-153.

16. Lazar, I.: "MEOR field trials carried out over the world during the last 35 years," *Microbial Enhancement of Oil Recovery- Recent Advances*, edited by E.C.Donaldson, Elsevier Science Publishers, 1990, p 485-530.

17. Moses, V.: "MEOR in the field: Why so little?," proceedings from the 1990 International Conference on Microbial Enhancement of Oil recovery, reprinted from: *Microbial Enhancement of Oil Recovery – Recent Advances*, edited by E.C. Donaldson, Elsevier Science Publishers, 1991, p 21-28.

18. Marsh, T.L., Zhang, X., McInerney, M.J., Sharma, P.K. and Jackson, B.E.: "Mechanisms of microbial oil recovery by *Clostridium acetobutylicum* and *Bacillus* strain *JF-2*," proceedings from the 5th International Conference on Microbial Enhanced Oil Recovery and related Bio-technology for solving environmental problems, 1995, p 593-610.

19. Jenneman, G.E., Knapp, R.M., McInerney, M.J., Menzie, D.E. and Revus, D.E.: "Experimental studies of In Situ microbial enhanced oil recovery," *SPEJ*, Vol. 24, (1984) 33-37.

20. Mulligan, C.N., Yong, R.N. and Gibbs, B.F.: "Removal of heavy metals from contaminated soil and sediments using the bio-surfactant surfactin," *Journal of Soil Contamination*, Vol.8, Issue 2, (1999), p 231-254.

21. Rosen, M.J.: "*Surfactants and Interfacial Phenomena*," John Wiley and Sons inc., New York City (1978).

22. Pursley, S.A., Healy, R.N. and Sandvik, E.I.: "A field test of surfactant flooding, Loudon, Illinois," *JPT*, (July 1973), p793-802.

23. Green, D.W. and Willhite, G.P.: "*Enhanced oil recovery*," SPE Text Book Series Volume 6, SPE Richardson, TX (1998), p 793-802.

24. Lake, L.W: "*Enhanced Oil Recovery*," Prentice Hall, Englewood Cliffs, New Jersey (1989), 354-423.

25. Healy, R.N. and Reed, R.L.: "Physiochemical aspects of microemulsion flooding," *SPEJ*, (1976) 491-501.

26. Nelson, R.C. and Pope, G.A.: "Phase relationships in chemical flooding," *SPEJ* (1978) 325-338.

27. Salter, S.J.: "The influence of type and amount of alcohol on surfactant-oil-brine phase behavior and properties," SPE 6843, presented at the 52nd Annual Technical Conference and Exhibition of the Society of Petroleum Engineers, Denver, Colorado, 1977.

28. Meyers, K.O. and Salter, S.J.: "The effect of oil/brine ratio on surfactant adsorption from microemulsion," *SPEJ*, August (1981) 500-512.

29. Wang, F.H.L.: "Effects of anaerobic, reducing conditions on surfactant retention in chemical flooding," *SPERE*, May (1980) 108-116.

30. Smith, L. and Malmberg, E.W.: "Measurement of surfactant loss in porous media," SPE 5306 presented at the 1975 SPE International Symposium on Oilfield Chemistry, Dallas, Jan. 16-17.

31. Lawson, J.B.: "The adsorption of nonionic and anionic surfactants on sandstone and carbonates," SPE 7052 presented at the 1978 Improved Oil Recovery Symposium, Tulsa, April 16-19.

32. Green, D.W. and Willhite, G.P.: "*Enhanced Oil Recovery*," SPE Text Book Series Volume 6, SPE, Richardson, TX (1998) 100-185.

33. Gogarty, W.B.: "Mobility control with polymer solutions," *SPEJ*, June (1967) 161-171.

34. Smith, R.F.: "The behavior of PHPA solutions in porous media," *JPT*, February (1970) 148-156.

35. Dauben, D.L. and Menzie, D.E.: "Flow of polymer solutions through porous media," *JPT*, August (1967) 1065-1073.

36. Hirasaki, G.J. and Pope, G.A.: "Analysis of factors influencing mobility and adsorption in the flow of polymer solution through porous media," *SPEJ*, August (1974) 337-346.

37. Gogarty, W.B.: "Rheological properties of pseudoplastic fluids in porous media," *SPEJ*, (June 1967), p 149-160.

38. Dawson, R. and Lantz, R.B.: "Inaccessible pore volume in polymer flooding," *SPEJ*, June (1972), p 448-452.

39. Martin, F.D. and Kantamukkala, M.S.: "The influence of mechanical degradation on the viscous elastic and elongational flow of polymer solutions used in enhanced oil recovery," proceedings of the 9th International Congress on Rheology, Mexico City, (1984), p 411-419.

40. Camilleri, D., Engelsen, S., Lake, L.W., Lin, E.C., Ohno, T., Pope, G.A. and Sepehrnoori, K.: "Description of an improved compositional micellar/polymer simulator," *SPE Reservoir Engineering*, (Nov. 1987), p 427-432.

41. Knapp, R.M., Civan, F. and McInerney, M.J.: "Modeling growth and transport of microorganisms in porous formations," presented at IMACS, Paris, France, July 18-22, 1998. *Proceedings of 12th World Congress on Scientific Computing* , Edited by R. Vichnevetsky, P Borne and J. Vignes, Vol. 3., (1988), p 676-679.

42. Zhang, X., Knapp, R.M. and McInerney, M.J.: "A mathematical model for microbially enhanced oil recovery processes," proceedings of 1992 International Conference on Microbial Enhanced Oil Recovery, *Developments in Petroleum Science*, Edited by E. Premuzic and A Woodhead, Vol. 39, (1993), p 171-186.

43. Sarkar, A.K., Sharma, M.M. and Georgiou, G.: "Compositional numerical simulation of MEOR processes," Paper No. R-21, presented at the International Conference on Microbial Enhanced Oil Recovery, Norman, OK, May 27-June 1, 1990, *Developments in Petroleum Science*, Edited by E.C.Donaldson, Vol. 31, (1991), p 331-343.

44. Islam, M.R.: "Mathematical modeling of microbial enhanced oil recovery," SPE 20480, presented at the 65th SPE Annual Conference, New Orleans, LA, September 23-26, 1990.

45. Chang, M.M., Chung, F.T.H., Bryant, R.S., Gao, H.W. and Burchfield, T.E.: "Modeling and laboratory investigation of microbial transport phenomena in porous media," SPE 22845, presented at the 66th SPE Annual Conference, Dallas, TX, October 6-9, 1991.

46. Hornof, V. and Morrow, N.R.: "Gravity effects in the displacement of oil by surfactant solutions," *SPERE*, (Nov.1987), p 627-633.

47. Jin, M.: "A study of no-aqueous phase liquid characterization and surfactant remediation," PhD dissertation, The University of Texas at Austin, Texas, (1995), p 121-152.

48. Stegemeier, G.L.: "Relationship of trapped oil saturation to the petrophysical properties of the porous media," SPE 4754, presented at the Improved Oil Recovery Symposium of the Society of Petroleum Engineers, Tulsa, Oklahoma, 1974.

49. Conrad, S.H., Wilson, J.L., Mason, W.R. and Peplinski, W.J.: "Visualization of residual organic liquid in aquifers," *Water Resources Research*, Vol. 28, Issue 2, 1992, p 467-478.

50. Chevalier, L.R. and Jason, R.: "Literature review of 2-D laboratory experiments in NAPL flow, transport and remediation," *Journal of Soil Contamination*, Vol. 8, Issue 1, (Jan. 1999), p149-167.

51. Lake, L.W., Pope, G.A, Carey, G.F. and Sepehrnoori, K.: "Isothermal, multiphase fluid flow in permeable media. 1.," *Insitu. Oil, Coal, Shale, Minerals*, Vol.8, Number 1, 1984, p 1-41.

52. Zheng, C. and Bennett, G.D.: "*Applied contaminant transport modeling*," 2nd Edition, Wiley Interscience Publication, New York, 2002, p 80-106.

53. Kaluarichchi, J.J.: "*Groundwater contamination by organic pollutants: Analysis and remediation*," American Society of Civil Engineers, Vol. 100, American Society of Civil Engineers, Reston, VA, 2001.

54. Thiele, M.R., Batycky, R.P. and Blunt, M.J.: "A streamline based 3D field scale compositional reservoir simulator," SPE 38889, presented at the SPE Annual Technical Conference and Exhibition, held in San Antonio, Texas, Oct. 5-8, 1997.

55. Blunt, M.J., Liu, K. and Thiele, M.R.: "A generalized streamline method to predict reservoir flow," *Petroleum Geoscience*, Vol. 2, (1996), p 259-269.

56. Bang, H.W. and Caudle, B.H.: "Modeling of a micellar/polymer process," *SPEJ* (Dec 1984) p 617-627.

57. Nguyen, T. and Sabatini, D.: "Laboratory study of the variation of *Bacillus mojavensis* JF-2 bio-surfactant lowered IFT and salinity and the determination of optimal salinity," School of Civil Engineering and Environmental Science, The University of Oklahoma, Norman, OK (2005).

58. Malmberg, E.W.: "Characterization and Oil Recovery Observations on a series of synthetic petroleum sulfonates," *SPEJ* (April 1982) p 226-236.

59. Jenneman, G.E., Moffit, P.D. and Yong, G.R.: "Application of a microbial selective-plugging process at the North Burbank unit: Prepilot tests," SPE 27827, presented at the 1994 SPE/DOE Symposium on Improved Oil Recovery, Tulsa, OK, April 17-20.

60. Pfiffner, S.M., McInerney, M.J., Jenneman, G.E. and Knapp, R.M.: "Isolation of a halotolerant, thermotolerant, facultative polymer producing bacteria and characterization of the exopolymer," *Applied and Environmental Microbiology* (June 1986), p 1224-1229.

61. Lake, L.W: "*Enhanced Oil Recovery*," Prentice Hall, Englewood Cliffs, New Jersey (1989), p 314-344.

62. Flory, P.J.: "*Principles of Polymer Chemistry*," Ithaca, New York, Cornell University Press, 1953, p 310.

63. Saad, N.: “Field scale simulation of chemical flooding,” PhD Dissertation, University of Texas, Austin, 1989.

64. Meter, D.M. and Bird, R.B.: “Tube flow of non-Newtonian polymer solutions: Part 1. Laminar flow and rheological models,” *AIChE Journal*, (Nov. 1964), p878-881.

65. Tsaur, K.: “A study of polymer/surfactant interactions for micellar/polymer flooding applications,” MS. Thesis, the University of Texas at Austin, 1978.

66. Martin, F.D., Donaruma, G.L. and Hatch, M.J.: “Development of improved mobility control agents for surfactant/polymer flooding,” 2nd Annual Report, US DOE DOE/BC/00047-13,1981.

67. Muller, G., Laine, J.P. and Fenyo, J.C.: “High molecular weight hydrolyzed polyacrylamides I. Characterization. effect of salts on the conformational properties,” Laboratoire de Chimie Macromoleculaire, ERA 471, Faculte del Sciences del’ Universite de Rouen, 76130 Mont Saint-Aignan, France.

68. Green, D.W. and Willhite, G.P.: “*Enhanced Oil Recovery*,” SPE Text Book Series Volume 6, SPE, Richardson, TX (1998) p105-106.

69. Green, D.W. and Willhite, G.P.: “*Enhanced Oil Recovery*,” SPE Text Book Series Volume 6, p 156.

70. Maudgalya, S., McInerney, M.J., Knapp, R.M., Nagle, D.P and Folmsbee, M.J.: “Development of bio-surfactant based microbial enhanced oil recovery technique,” SPE 89473, presented at the SPE/DOE IOR Conference, held on 19-21 April, 2004.

71. Collins, R.E.: “Flow of fluids through porous media”, 2nd Reprint, Research and Engineering Consultants, Englewood, 1990, p 139-169.

72. Richardson, J.G., Kerver, J.K., Hafford, J.A. and Osoba, J.S.: “Laboratory

determination of relative permeability", *Trans. AIME* (1952) 117-131.

73. Healy, R., N., Reed, R.L and Carpenter, C.W.: "A laboratory study of microemulsion flooding", SPE 4752, presented at the SPE-AIME Improved Oil Recovery Symposium, held in Tulsa, April 22-24, 1974.
74. Green, D.W. and Willhite, G.P.: "*Enhanced Oil Recovery*," SPE Text Book Series Volume 6, p 239-287.
75. Vela, S., Peaceman, D. and Sandvik, E.I.: "Evaluation of polymer flooding in a layered reservoir with cross-flow, retention and degradation", *SPEJ* (April 1976), p 82-89.
76. Brigham, W.E., Reed, P.W. and Dew, J.N.: "Experiments on mixing during miscible displacement in porous media", *SPEJ* (March 1961), p 1-8.
77. Moore, T.F. and Slobod, R.C.: "The effect of viscosity and capillarity on the displacement of oil by water," *Producers Monthly* (Aug. 1956), p 20-30.
78. Dabbous, M.K.: "Displacement of polymers in waterflooded porous media and its effects on a subsequent micellar flood", SPE 6203, presented at the SPE-AIME Annual Fall Technical Conference and Exhibition, held in New Orleans, LA., USA, October 3-6, 1976.
79. Aziz, K. and Settari, A.: "*Petroleum Reservoir Simulation*," Applied Science Publishers, Canada, 2002, p 125-193.
80. Fanchi, J.R., Harpole, K.J. and Bujnowski, S.W.: "BOAST: A three dimensional three phase applied oil simulation tool (Version 1.1), Vol. I: Technical Description and Fortran Code," US DOE Report No. DOE/BC/10033-3, Sept.1982.

81. Corapcioglu, M.Y. and Haridas, A.: "Transport and fate of microorganism in porous media: a theoretical investigation," *Journal of Hydrology*, Vol. 72, (1984), p149-164.

82. Bear, J.: "*Dynamics of Fluids in Porous Media*," New York, Elsevier, (1972), p 605-616.

83. Bu'Lock, J. and Kristiansen, B.: "*Basic Biotechnology*," Academic Press, New York, (1987) p75-131.

84. Pye, D.J.: "Improved secondary recovery by control of water mobility," *Journal of Pet. Tech.* (Aug. 1964), p 911-916.

85. Martin, F.D. and Sherwood, N.S.: "The effect of hydrolysis of polyacrylamide on solution viscosity, polymer retention and flow resistance properties," SPE 5339, presented at the 1975 Rocky Mountain Regional Meeting, Denver, April 7-9.

86. Ward, J.S. and Martin, F.D.: "Prediction of viscosity for PHPA in the presence of calcium and magnesium ions," *SPEJ* (Oct. 1981), p 623-631.

87. Mungan, N.: "Shear viscosities of ionic polyacrylamide solutions," *SPEJ* (Dec.1972), p 469-473.

88. *UT-CHEM Reservoir Simulator Users Manual*, The University of Texas, Austin, 2002.

89. Mungan, N., Thomson, J.L. and Smith, J.W.: "Some aspects of polymer floods," *Journal Pet. Tech.*, (Sept. 1966), p1143-1150.

90. Cernasky, A. and Siroky, R.: "Deep bed filtration of filament layers of particles polydispersed in liquids," *International Chemical Engineering*, Vol. 25, No. 2, (1985) p364-375.

91. Adamson, A.W.: "*Physical Chemistry of Surfaces*," 3rd Edition, John Wiley and Sons Inc., New York, (1976).

92. Salter, S.J.: Selection of pseudo-components in surfactant-oil-brine-alcohol systems," SPE 7056, presented at the 1978 Improved Oil Recovery Symposium, Tulsa, OK, USA April 16-19, 1978.

93. Chang, F.F. and Civan, F: "Modeling of formation damage due to physical and chemical interactions between fluids and reservoir rocks," SPE 22656, presented at the 66th Annual SPE Conference and Exhibition, Dallas, Texas, Oct. 6-9, 1991.

94. Needham, R.B., Threlkeld, C.B. and Gall, J.B.: "Control of water mobility using polymers and multivalent ions," SPE 4747 presented at the 1975 SPE Improved Oil Recovery Symposium, Tulsa, April 22-24.

95. Lake, L.W.: "*Enhanced Oil Recovery*," Prentice Hall, NJ 07632, 1989, p 67-68.

96. Buckley, S.E. and Leverett, M.C.: "Mechanisms of fluid displacement in sand," Trans. AIME, Vol. 146, (1942), p107-116.

97. Collins, R.C.: "Flow of fluids through porous media," Research and Engineering Consultants, Englewood, Colorado, 1976, p 203-206.

98. Lake, L.W.: "*Enhanced Oil Recovery*," Prentice Hall Publishers, New Jersey, (1989), p157-163.

99. Zheng, C. and Bennett, G.D.: "*Applied Contaminant Transport Modeling*," 2nd Edition, Wiley Interscience, John Wiley and Sons Inc. publication, New York, 2002.

100. Brigham, W.E.: "Mixing equations in short laboratory cores," *SPEJ*, (Feb. 1974), p 91-99.

101. Abrams, A: “The influence of fluid viscosity, interfacial tension and flow velocity on residual oil saturation left by waterflood,” *SPEJ*, (Oct. 1975), p 437-447.

102. Schneider, F.N. and Owens, W.W.: “Steady state measurements of relative permeability for polymer/oil systems,” *SPEJ* (Feb. 1982), p 79-86.

103. Morrow, N.R., Chatzis, I. and Taber, J.J.: “Entrapment and mobilization of residual oil in bead packs,” SPERE, Vol. 3, Issue 3, (Aug. 1988), p 927-934.

104. Chatzis, I., Morrow, N.R. and Lim, H.T.: “Magnitude and detailed structure of residual oil saturation,” *SPEJ*, Vol. 23, Issue 2, (April. 1983), p 311-326.

105. Perkins, T.K and Johnston, O.C.: “The review of diffusion and dispersion in porous media,” SPE 480.

106. Saripalli, K.P., Annable, M.D. and Rao, P.S.C.: “Estimation of non-aqueous phase liquid-water interfacial area in porous media following mobilization by chemical flooding,” *Environmental Science and Technology*, Vol. 31, No. 12, 1997, p 3384-3388.

107. Saripalli, K.P., Kim, H., Rao, P.S.C. and Annable, M.D.: “Measurement of specific fluid-fluid interfacial areas in immiscible fluids in porous media,” *Environmental Science and Technology*, Vol. 31, No. 3, 1997, p 932-936.

108. Oostrom, M. and Lenhard, R.J.: “Comparison of relative permeability saturation pressure parametric models for infiltration and redistribution of a light non-aqueous phase liquid in sandy porous media,” Advances in Water Resources, Vol. 21, Issue 2, March 1998, p145-157.

109. Pope, G.A, Carey, G.F. and Sepehrnoori, K.: "Isothermal, multiphase fluid flow in permeable media. 2.," *Insitu. Oil, Coal, Shale, Minerals*, Vol.8, Number 1, 1984, p 41-97.

110. Zheng, C. and Bennett, G.D.: "*Applied contaminant transport modeling*," 2nd Edition, Wiley Interscience Publication, New York, 2002, p109-110.

Appendix

Appendix A

A1. Preparation of bio-surfactant from *Bacillus mojavensis* JF-2

The nutrient medium for *Bacillus mojavensis JF-2* contains the following components per 900.0 cc of solution: 100 mM phosphate buffer with the pH adjusted to 6.8; sodium chloride (50g); sucrose (20 mM); Proteose Peptone (30g); yeast extract (1g); sodium nitrate (g); ammonium sulfate (1g); 100 ml of a metal solution. The metal solution added to this nutrient medium is a modification of Wolin's metal solution[5] and is composed of the following components per 1000.0 cc of Wolin's solution: EDTA (1g); $MnSO_4 \cdot H_2O$ (3g); $FeSO_4 \cdot 7H_2O$ (0.1g); $CaCl_2 \cdot 2H_2O$ (0.1g); $CoCl_2 \cdot 2H_2O$ (0.1g); $ZnSO_4 \cdot 7H_2O$ (0.1g); $CuSO_4 \cdot 7H_2O$ (0.01g); H_3BO_4 (0.01g); $Na_2MO_4 \cdot 2H_2O$ (0.01g); $AlK(SO_4)_2$ (0.01g).

Use a 5000.0 cc preparation bottle to prepare 2000.0 cc of aerobic medium,. Remove 500.0 cc of this solution and place it in a 1000.0 cc bottle and store. This 500.0 cc of solution will be used as uninnoculated control solution. Autoclave both bottles for 20.0 minutes at 16.0 psi. Inoculate 1500 cc of solution with 100.0 ml of an aerobically grown culture of *Bacillus mojavensis* strain JF-2 that is 48 hours old. Incubate the 1500.0 cc of inoculated solution at room temperature on a stir plate with the stir bar set at 300 rpm for 72 hours. After incubation, separate the bacterial cells from the solution by centrifuging the solution at 8000 rpm for 20 minutes in a centrifuge. Store the supernatant solution from which the cells have been removed at 4^0C.

A2. I**nterfacial tension measurement**

1. Experiment procedure.

1.1 The density of the aqueous bio-surfactant solution and crude oil sample were measured with a pycnometer. It is recommended to repeat the measurements at least three times for greater accuracy.

1.2 The aqueous bio-surfactant solution was always prepared in a 5.0% by wt. NaCl solution (Appendix A1). The bio-surfactant concentration in the solution could not be increased nor the salinity of the solution decreased but IFT at lower bio-surfactant concentrations or at higher salinity could be measured.

1.3 A surfactant solution with a bio-surfactant concentration lower than the prepared solution was made by mixing the original surfactant solution with nutrient media. Nutrient media had the same composition as the surfactant solution but had no bio-surfactant. Thus, if the bio-surfactant concentration had to be halved, then equal volumes of the original surfactant solution and nutrient media were mixed.

1.4 A surfactant solution with its salinity higher than the original 5.0% NaCl was prepared by mixing the required amount of NaCl salt to a measured volume of the surfactant solution.

1.5 To measure IFT, two clean high precision-low volume syringes were filled with the bio-surfactant sample and crude oil respectively. The syringes were flushed with the respective fluids two to three times before filling it with clean fluid. This was done to wet the syringe surface.

1.6 A 2.0 mm capillary tube was filled with the surfactant solution with the surfactant syringe. The surfactant solution should completely fill the capillary tube. The

surfactant was slowly injected into the capillary tube to avoid bubble formation. These bubbles could cause the inaccurate measurement of the dimensions of the oil drop. If bubbles are created, hold the tube vertical to allow the bubbles to move up the fluid column towards the tube opening. Use a clean napkin to remove any drops of surfactant from outside the tube.

1.7 Holding the capillary tube horizontal, a small oil drop was carefully injected into the solution in middle of the tube with the oil syringe. The size of the drop should not be very small since that will not spread during the tube rotation or too big, because that will lead to smearing along the walls of the tube.

1.8 Any extra drops of surfactant that were displaced out of the tube were wiped clean with a napkin and the tube inserted into the rotating tube tensiometer.

1.9 Once the tube was fully inserted into its holder, the holder was closed with its cap and the tensiometer motor started.

1.10 Once the motor that rotated the capillary tube at high speeds was running, the stroboscope light was switched on. This would allow the previously calibrated microscope mounted on the tensiometer to observe the oil drop as was got stretched inside the tube under the action of centrifugal force.

1.11 The oil drop would stretch itself like an ellipse being pulled along its major axis. When the length of the drop was approximately four times its height or when the bubble had stopped stretching, the crosshair on the microscope lens was positioned on the top edge of the bubble and the Vernier scale attached to the microscope was recorded. The scale was then rotated till the crosshair was lined on the lower edge of the bubble and the new Vernier reading recorded.

1.12 The speed of the motor was recorded in terms of the rotational frequency (rev.sec^{-1}).

1.13 The temperature at which the recordings were taken was also noted. This must remain constant during measurement. If the machine warmed up, the experiment was stopped to allow the motor to cool before taking new readings.

1.14 After recording the three variables, the light was switched off and the motor stopped. The capillary tube was removed and a new tube with an oil drop suspended in the surfactant solution was inserted into the holder.

1.15 The new tube was rotated at a speed different from the previous trial. The speed could be controlled by a rheostat fixed to the tensiometer.

1.16 Three to four trials were repeated with each sample at different speeds to increase the accuracy of the measurements.

2.0 Observation table

Sample #	**Reading #**	**Oil density (gm/cc)**	**Surfactant density (gm/cc)**	**Speed (sec^{-1})**	**Top edge (µm)**	**Bottom edge (µm)**	**Temperature (^{0}C)**	**IFT (Dynes/cm)**
1	1							
1	2							
1	3							
1	4							
2	1							
2	2							
2	3							

3.0 Formulae

3.1 $\rho_{Liquid}\,(gm/cc) = \dfrac{Mass_{Liquid}}{25.0}$

$P_{Liquid}\,(gm/cc)$ = Liquid density

$Mass_{Liquid}\ (gm)$ = Mass of 25.0 cc of liquid

3.2 $IFT\ (dynes/cm) = 0.52386 \times \dfrac{\Delta\rho \times \Delta h^3}{Speed^2}$

IFT (dynes/cm) = Crude oil- Surfactant interfacial tension

Δh (μ *m)* = Upper edge reading of bubble – Lower edge reading of bubble

Speed (1/sec) = Conversion factor

A3. **Berea core flooding procedure**.

1. Cut and dry Berea sandstone cores

1.1 Berea sandstone cores were selected for the experiments because of the homogenous nature of their permeability and porosity.

1.2 A 1.5 inch diameter drill bit was used to cut the cores from a block of Berea sandstone. The drill bit size selection depends on the core holder's size.

1.3 The cores were cut under a water jet and its end faces smoothed and planed to ensure a proper contact between the injection endplates and the core and a uniform flow profile in and out of the core (A detailed drawing can be observed in **Appendix A4**).

1.4 The wet cores were oven dried at 50-60^0 C for a week.

1.5 Before an experiment, the dried core was weighed and its length and diameter measured.

2. <u>Core placement in the Hassler core holder.</u>

2.1 The core was first placed inside a rubber sleeve and the sleeve with the core was inserted into the core holder. The sleeve grips and squeezes around the core when a confining pressure is applied. The confining pressure is similar to the overburden pressure and forces any injected liquid to flow through the core and not around it. The sleeve dimensions are engineered to fit the core holder and the core while leaving only a small gap between its outer wall and the core holder's inner surface.

2.2 One end plate of the core holder is a fixed plate and the other is a floating type. The core inside the sleeve was placed on the fixed plate before it was inserted into the core holder and the cap was screwed into place. After ensuring that the core rested firmly against the plate, the other cap of the holder with the floating plate was screwed into place. The floating arrangement allows the end plate to adjust its position to the length of the core. In these experiments, the core length was not shorter than six inches.

2.3 The core should fit tightly between the two end plates.

2.4 The space between the sleeve outer wall and the core holder was slowly filled with water using a hand pump. Water was pumped through a tap on the lower side of the cylinder while a tap on the upper side allowed the air to escape. When the air was displaced from the cylinder, the air tap was closed and water pumping continued till the desired confining pressure was reached. The inlet tap was closed and the pump disconnected from the core holder.

2.5 A pressure gauge was attached to the confining pressure tap to continuously monitor the confining pressure. A decrease in confining pressure would indicate a leak inside the cylinder of the core holder.

2.6 To make sure that the core fit properly between the end plates, the core holder inlet and discharge valves were kept open during water injection to build up the confining pressure. If the fit was not proper, water would leak from the valves and pressure would not build up.

2.7 After the confining pressure was at the desired value, the inlet and outlet valves were closed and the core was ready for evacuation.

3. Evacuation. A vacuum was applied on the core to remove the air trapped within the core. This reduced the error in the pressure readings. A carbon dioxide gas flush is recommended because it dissolves readily in water and can be easily removed from the core.

3.1 With the core holder inlet valve closed, a vacuum was applied on the core from the discharge end. The vacuum was maintained for twenty four hours. Following the vacuum, the discharge valve was first closed before disconnecting the vacuum line.

3.2 Carbon dioxide flushing was started by first charging the inlet side tubing of the core holder with the gas before opening the inlet valve and to allow gas into the core. This kept air from the core. The outlet valve was opened so the gas would flow through the core. The gas flush was done for fifteen minutes and the inlet and outlet valves closed.

3.3 A vacuum was again applied. It is recommended to carry out the gas flush – vacuum cycle three times to remove all traces of air from the core. The last step must be a vacuum before brine injection.

3.4 Close the valves and isolate the core. It is now ready for the flood experiment.

4. Brine preparation and filling the brine and crude oil transfer cylinders.

4.1 The required amount of sodium chloride for 5.0% by wt. (50000 ppm) solution was added to deioninzed water. The brine was placed under vacuum for a few hours to remove oxygen dissolved in the solution.

4.2 The brine and crude oil densities and viscosities were measured.

4.3 The transfer cylinders were cleaned and dried before filling with crude oil and brine.

4.4 The transfer cylinders are floating piston type containers. Ordinary motor oil is pumped into one side of the piston which displaces the brine, crude oil or any other liquid from the other side of the piston into the core. Air must not be present on either side of the piston. The cylinders should be filled in the vertical positions and the valves on the end caps kept open when closing vessels to allow any air or excess liquid to come out.

5. Brine injection

5.1 The brine injection rate was set on the constant flowrate Ruska pump. Keeping the core holder isolated from the rest of the system, the inlet tubing was flushed with brine. The pump was started and the flowrate at a tap on the inlet tubing measured to ensure that it was equal to the set flowrate. Once that was confirmed the pump was stopped and the system was ready for injecting brine into the core.

5.2 The volumetric reading on the pump was noted before starting the pump.

5.3 Brine was injected at a low rate initially because the core permeability is unknown. A high flow rate through a low permeability core will damage the tubing and equipment. The flow rate can be changed at anytime during the injection.

5.4 The inlet valve remained closed after starting the pump until the inlet pressure gauge showed a reading of 35.0 psi. A transducer connected to the gauge displayed the pressure on a monitor. When the pressure reading displayed 35.0 psi, the inlet valve was opened to allow brine to flow into the core. The pressure decreased as brine entered the core which was under a vacuum. The core outlet valve was kept closed.

5.5 The outlet valve was opened when the inlet pressure gauge displayed 20.0 psi on the monitor. The pressure was built up to dissolve any carbon dioxide gas remaining in the core in the brine solution and prevent any vapor phase to develop in the dry core.

5.6 The brine produced from the core was collected in a measuring flask.

5.7 Between 100.0 and 120.0 cc (4.0 pore volumes) of was injected into a core.

5.8 The injection pressure was recorded to determine the absolute permeability of the core to brine. Since the discharge valve of the core holder opened into atmospheric pressure, the injection pressure was sufficient for calculating the pressure drop across a core. A back pressure system could be fixed at the discharge to simulate producing well conditions.

5.9 The final volumetric reading minus the sum of the initial reading, the volume of brine collected and the dead volume inside the tubing was the core pore volume. An underlying assumption was that the core was 100% saturated.

6. Crude oil saturation.

6.1 With the inlet and discharge valves closed, the inlet tubing was connected to the oil accumulator with a three way valve. The Ruska pump was started at the required flowrate and the inlet tubing of the core holder flushed with crude oil to remove the brine through the tap on the inlet tubing. The tap was closed after the crude oil filled the tubing.

6.2 The injection pump was started and the outlet and inlet valves of the core holder were opened to inject crude oil into the core. Brine and oil produced from the core was collected in measuring flasks.

6.3 Crude oil injection was continued until less than 1.0 cc of brine was produced with every 20.0 cc of crude oil. At this point, the core was close to residual water saturation. The injection pressure was recorded to calculate the effective oil permeability at residual water saturation.

6.4 Oil injection was stopped and the inlet and outlet valves closed.

6.5 The volume of brine collected minus the tubing holdup volume was used to determine the residual water saturation.

7. Waterflooding.

7.1 With the inlet valve closed, the inlet tubing was connected to the brine accumulator. The Ruska pump flowrate was set to the waterflood rate and started. The inlet side tubing was flushed with brine to remove the crude oil. Once the tubing was free of oil, the pump was stopped and the tap on the inlet tubing closed

7.2 The pump was started and the inlet and outlet valves of the core holder were opened. The oil and water that was produced out of the core was measured.

7.3 The waterflood was continued until negligible oil was produced. This was determined by observing the effluent stream. If there was no oil, the core was at residual oil saturation and waterflooding could be stopped. About fifteen to twenty porevolumes (PVs) of brine were generally needed for the core to reach residual oil saturation.

7.4 The injection pressure was recorded to determine the effective brine permeability of the core at residual oil saturation.

7.5 The inlet and outlet valves were closed and the tubing inlet flushed and filled with the surfactant solution to prepare the core for surfactant injection.

7.6 The volume of oil recovered from the core minus the tubing holdup volume provided the residual oil saturation and the target oil volume for tertiary recovery.

8. Bio-surfactant flooding

8.1 With the inlet valve of the core holder closed, the inlet tubing was connected to the surfactant accumulator (See **Appendix A1** for bio-surfactant preparation details). The Ruska pump flowrate was set to the injection rate and started. The inlet side tubing was flushed. When only surfactant flowed, the pump was stopped and the tap on the inlet tubing was closed.

8.2 The pump was again started and the inlet and outlet valves were opened. The oil, brine, and surfactant that flowed from the core were collected into 25.0 cc measuring flasks.

8.3 Depending on the experiment protocol, the specified volume of surfactant was injected and the pump stopped.

8.4 The injection pressure was recorded continuously during the surfactant injection to determine the permeability reduction factor at the end of the experiment.

8.5 The volume of oil recovered was used to calculate the tertiary oil recovery.

8.6 In flow experiments where a brine postflush was injected, the core inlet valve was closed before connecting the tubing to the brine transfer vessel. The tubing was then flushed before brine was injected into the core.

9. Observation tables**.**

Core property	**Core #**
Dry weight of core, W_D (gm)	
Porosity of core using porosimeter (%)	
Density of brine	
Viscosity of brine (cp)	
Density of crude oil (gm/cc)	
Viscosity of crude oil (cp)	
Pore volume of core (cm^3)	
Length of core (cm)	
Diameter of core (cm)	
Area of cross section of core (cm^2)	

Table 9.1. Core physical data

Readings	**Core #**
Q_w (cc/min)	
ΔP (psi)	
K_{Abs} (md)	
Q_o (cc/min)	
ΔP (psi)	
$K_{o,Eff}$ (md)	
Q_w (cc/min)	
ΔP (psi)	
$K_{w,Eff}$ (md)	

Table 9.2. Flow measurements

Core #	**S_w (%)**	**K_{Abs} (md)**	**S_{wr} (%)**	**$K_{o,Eff}$ (md)**	**$S_{or,Wf}$ (%)**	**$K_{w,Eff}$ (md)**
1						
2						
3						

Table 9.3. Experiment observation summary

Core #	**$S_{or,Wf}$ (%)**	**Q_{Surf} (cc/hr)**	**ΔP (psi)**	**K_{Surf} (md)**	**$Q_{Postflush}$ (cc/hr**	**$K_{Postflush}$ (md)**	**V_{Oil} (cc)**	**Recovery (%)**
1								
2								
3								

Table 9.4 Bio-surfactant flooding summary

10. Formulae.

a. Core Porevolume (cc) = Final reading on pump (cc) – (Initial reading (cc) + Dead vol. (cc) + Vol. of brine collected (cc)).

b. Residual saturation, S_{wr} , $S_{or,\ wf}$ *(%)* = $\frac{V_W, V_O(cc)}{Porevolume(cc)} \times 100$

S_{wr} (%) = Residual water saturation at the end of oil saturation.

$S_{or,\ wf}$(%) = Residual oil saturation after waterflooding.

V_W(cc) = Volume of brine remain inside core at the end of oil injection (cc)

V_O(cc) = Volume of oil inside the core after waterflooding

Porevolume = Porevolume of core (cc).

c. Permeability, K_{abs}, $K_{w,\ Eff}$ (md) = $\frac{Q_{Brine} \times \mu_{Brine} \times L_{Core}}{A_{Core} \times \Delta P}$

$$K_{o,\ Eff,}(\text{md}) = \frac{Q_{Oil} \times \mu_{Oil} \times L_{Core}}{A_{Core} \times \Delta P}$$

K_{abs} (md) = Absolute permeability of core to brine at 100% saturation.

$K_{w,\ Eff}$ (md) = Effective permeability of core to brine at residual oil saturation.

$K_{o,\ Eff}$ (md) = Effective permeability of core to oil at residual water saturation

Q_{Brine} (cc/hr) = Brine injection flowrate

Q_{Oil} (cc/hr) = Oil injection flowrate

μ_{Brine} (cp) = Brine viscosity

μ_{Oil} (cp) = Oil viscosity

ΔP (psi) = Pressure drop across the core

L_{Core} (cm) = Length of core

A_{Core} (cm^2) = Area of cross section of core

d. *Tertiary Recovery* (%) = $\frac{V_O(cc)}{V_{O,Wf}(cc)} \times 100$

$$K_{Surf},\ K_{Postflush}\ (\text{md}) = \frac{Q_{Surfac\,tan\,t,Brine} \times \mu_{Surfac\,tan\,t,Brine} \times L_{Core}}{A_{Core} \times \Delta P}$$

V_O (cc) = Volume of oil recovered after surfactant injection or postflush injection

$V_{O,\,Wf}$ (cc) = Volume of oil remaining inside the core after waterflooding

$Q_{Surfactant}$ (cc) = Surfactant injection flowrate

$\mu_{Surfactant}$(cp) = Surfactant viscosity

A4. **Schematic of the core flooding experiment setup**.

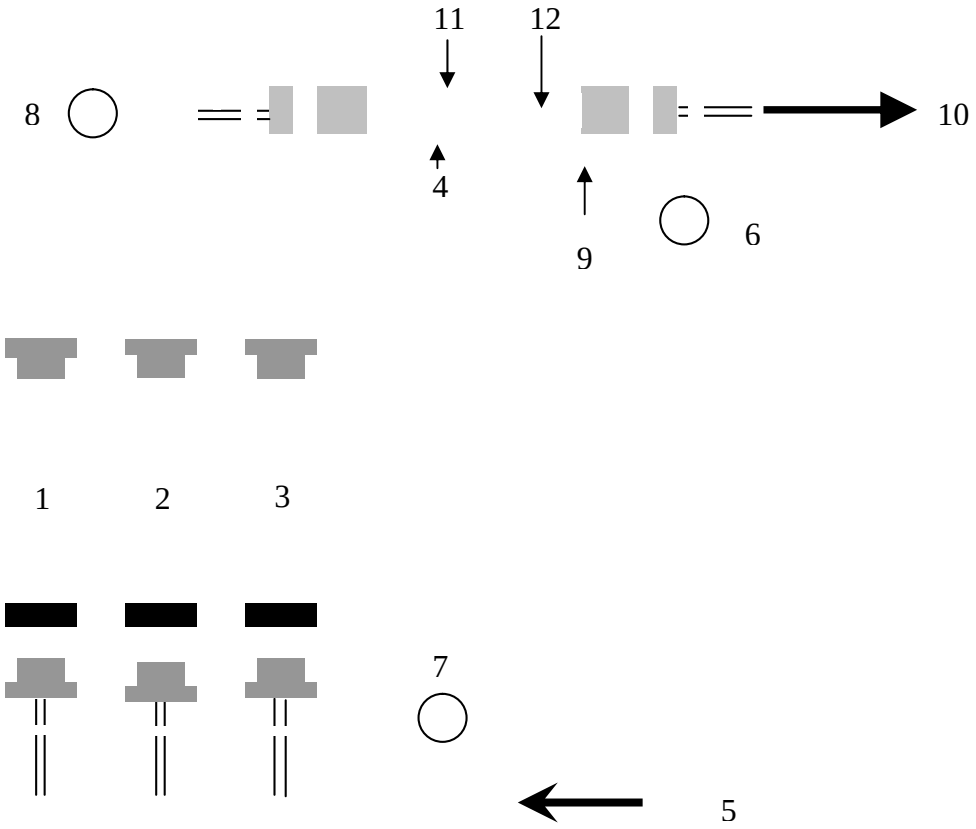

Details:

1, 2, 3 – Accumulators for holding crude oil, brine and surfactant solution.

4 - Hassler® core holder

5 - Ruska pump to inject oil into accumulator (constant injection rate)

6, 7, 8 – Pressure gauges at injection pump, core inlet and overburden pressure

9 – Water injection to build overburden around core

10 – Effluent collection and vacuum connection

11 - Rubber sleeve around core

12 - Berea sandstone core

Appendix B

B1. Verification of simulator output

B1.1. Comparison with analytical Buckley Leverett solution.

Variables	Values
Core dimension: NX x NY x NZ	25,50,100 x 1 x 1
Grid block size: ΔX, ΔY, ΔZ	40,20,10 x 100 x 10 ft
Absolute permeability:	$K_X = K_Y = K_Z$ = 100 md
Porosity	0.2
Reservoir top	8000 ft
Initial pressure:	P_i = 4000 psi
Initial oil saturation	S_{oi} = 0.7
Residual phase saturations	S_{or} = 0.3, S_{wc} = 0.2
Pirson's model for water relative permeability	$K_{rw} = \left(\frac{1 - S_w - S_{or}}{1 - S_{wc} - S_{or}}\right)^2$
Pirson's model for oil relative permeability	$K_{ro} = S_w^{\,3}\left(\frac{S_w - S_{or}}{1 - S_{wc}}\right)^{0.5}$
Phase viscosities:,	μ_o =1.4 cp, μ_w =0.6 cp
Phase densities at surface conditions	ρ_{osc} = 46.244, ρ_{wsc} = 62.24 lb/ft^3
Rock compressibility	$c_r = 5 \times 10^{-6}$ psi^{-1}
Injection/ Production rate	200 and -200 STB/D

B1.2. Comparison of analytical 1 D tracer and diffusion solution.

Variables	Values
Core dimension: NX x NY x NZ	25,50,100 x 1 x 1
Grid block size: ΔX, ΔY, ΔZ	20,10,5 x 50 x 10 ft
Absolute permeability:	$K_X = K_Y = K_Z$ = 100 md
Porosity	0.2
Reservoir top	8000 ft
Initial pressure:	P_i = 4000 psi
Initial oil saturation	S_{oi} = 0.7
Residual phase saturations	S_{or} = 0.3, S_{wc} = 0.2
Longitudinal dispersivity	α_l = 1.0 ft
Tortuosity	τ =1.4
Molecular diffusion	0. cm^2/sec
Water viscosity	μ_w =1.0 cp
Water density at surface condition	ρ_{wsc} = 62.24 lb/ft^3
Rock compressibility	$c_r = 5 \times 10^{-6}$ psi^{-1}
Injection/ Production rate	100 and -100 STB/D

B2. **Verification of new features**.

B2.1 List of variables that are common in all the input data files.

Variables	Values
Brine and oil density at surface conditions	ρ_{wsc} = 1001 mg/scc , ρ_{osc} = 865.4 mg/scc
Longitudinal and transverse dispersivity	α_l =0.1033 , α_t =0.00034
Diffusivity	0.0144 cm^2/sec
Polymer salinity parameters	A_{P1}= 1230 wt^{-1}%, A_{P2}= -1230 wt^{-2}%, A_{P3}= 1300 wt^{-3}%
Viscosity shearing parameters	Sp = -12.0, P_α = 1.9
Fluid viscosity exponent	n= 0.6
Polymer retention parameters	C_{rk} 0.0186 $Darcy^{1/2}$ cp, B_{rk} = 1000 $wt.^{-1}$%
Surfactant adsorption parameters	AA_6 =0.8, AA_{62} = 0.3 , BB_6 = 100.0
Surfactant adsorption parameters	AA_7 =0.8, AA_{72} = 0.3 , BB_7 = 100.0
C_{MAX6}, C_{MCL6}, C_{MCH6}, C_{MEC6}	0.058, 0.011, 0.040, 0.041 mg/scc
E_{S1}, E_{S2}	7.0 , 2.0

Case 5.2.1. JF-2/SP-018 surfactant solution injection.

Table B2.2 JF-2 bio-surfactant and 1000 ppm SP-018

Variables	Values
Core dimension: NX x NY x NZ	100 x 1 x 1
Grid block size: ΔX, ΔY, ΔZ	0.155 x 3.37 x 3.37 cm
Absolute permeability	K_X= K_Y= K_Z= 108 md
Porosity	0.179
Reservoir top	0 cm
Initial pressure	P_i = 14.7 psi
Connate and initial water saturation	S_{wc} = 0.60, S_{wi}= 0.34
Waterflood residual oil saturation	S_{or} = 0.39
Brine and oil viscosity	μ_w = 1.0 cp , μ_o = 6.0 cp
Effective end point water and oil permeability	$K_{o,eff}$ =65 md, $K_{w,eff}$ =30 md
Corey's exponent for water and oil relative permeability	n = 2.5, m= 1.5
JF-2 bio-surfactant concentration, C_6	C_6 = 0.011 mg/scc (0.021,0.031, 0.041 mg/scc)
Polymer concentration, C_7	C_7 = 1.0 mg/scc
NaCl concentration, C_{11}	C_{11}= 50.0 mg/scc
Shear rate at half original viscosity	$\gamma_{1/2}$ = 0.5 sec^{-1}
Surfactant injection rate	Q_{inj} = 5.14 cc/hr
Volume of surfactant treatment	1.0 PV

Case 5.2.2. Plain JF-2 bio-surfactant solution injection.

Table B2.3 11.0 ppm of plain JF-2 bio-surfactant

Variables	Values
JF-2 bio-surfactant concentration, C_6	C_6 = 0.011 mg/scc
Polymer concentration, C_7	C_7 = 0.0 mg/scc
NaCl concentration, C_{11}	C_{11}= 50.0 mg/scc
Surfactant injection rate	Q_{inj} = 5.14 cc/hr
Volume of surfactant treatment	1.0 PV

Case 5.2.3. Plain SP-018 bio-polymer solution injection.

Table B2.4 1000 ppm of plain SP-018 bio-polymer

Variables	Values
JF-2 bio-surfactant concentration, C_6	C_6 = 0.000 mg/scc
Polymer concentration, C_7	C_7 = 1.0 mg/scc
NaCl concentration, C_{11}	C_{11}= 50.0 mg/scc
Surfactant injection rate	Q_{inj} = 5.14 cc/hr
Volume of surfactant treatment	1.0 PV

Case 5.2.4. Effect of increasing bio-surfactant concentration in JF-2/SP-018 flooding (11.0, 21.0, 31.0 and 41.0 ppm).

Table B2.5 Increasing JF-2 bio-surfactant

Variables	Values
JF-2 bio-surfactant concentration, C_6	C_6 = 0.011, 0.021, 0.031and 0.041 mg/scc.
Polymer concentration, C_7	C_7 = 0.0 mg/scc
NaCl concentration, C_{11}	C_{11}= 50.0 mg/scc
Surfactant injection rate	Q_{inj} = 5.14 cc/hr
Volume of surfactant treatment	1.0 PV

Case B2.5. Effect of Sodium Chloride (NaCl) on JF-2/SP-018 flooding to study the effect of salinity on viscosity and adsorption. Core data is the same as listed in **B2.2**. The only variable that changes is the NaCl concentration, C_{11}. The salt concentrations were 2.0 %, 3.0 % and 5% NaCl by wt.

Case B2.6. Effect of Sodium Chloride on JF-2 bio-surfactant flooding to study the effect of salinity on IFT. The core data is the same as that listed in **B2.2**. Two changes were made. The first was a change is in the salinity of the injected surfactant solution,

C_{11}. The concentrations are 3.0 %, 5.0 % and 10.0 %. The second change was the use of 31.0 ppm of plain JF-2 bio-surfactant solution with no bio-polymer added to the solution.

Case B2.7. Effect of Calcium (Ca^{2+}) on JF-2/SP-018 flooding.

Table B2.6. Effect of $Ca2^{+}$ ions in the surfactant.

Variables	Values
JF-2 bio-surfactant concentration, C_6	C_6 = 0.011
Polymer concentration, C_7	C_7 = 0.0 mg/scc
NaCl concentration, C_{11}	C_{11}= 50.0 mg/scc
Ca^{2+} ions concentration, C_{12}	C_{12}= 20 mg/scc
Bp	2.0
Surfactant injection rate	Q_{inj} = 5.14 cc/hr
Volume of surfactant treatment	1.0 PV

Case B2.8 2.0PV's of surfactant solution. The core data is the same as listed in **B2.2**. But instead of 1.0 PV of surfactant injected, 2.0 PV's of surfactant were injected through a core.

B3. **Simulation of core flooding experiments.**

B3.1 List of variables that are common in all the input data files.

Variables	Values
Brine and oil density at surface conditions	ρ_{wsc} = 1001 mg/scc , ρ_{osc} = 865.4 mg/scc
Longitudinal and transverse dispersivity	α_l =0.1033 cm , α_t =0.00034 cm
Diffusivity	0.00001 cm^2/sec
Polymer salinity parameters	A_{P1}= 183.5 wt^{-1}%, A_{P2}= -2339.8 wt^{-2}%, A_{P3}= 15712 wt^{-3}%
Viscosity shearing parameters	Sp = -7.5.0, P_α = 1.9
Fluid viscosity exponent	n= 0.6
Polymer retention parameters	C_{rk} 0.015 $Darcy^{1/2}$ cp, B_{rk} = 1000 $wt.^{-1}$%
Surfactant adsorption parameters	AA_6 =0.8, AA_{62} = 0.3 , BB_6 = 100.0
Surfactant adsorption parameters	AA_7 =0.8, AA_{72} = 0.3 , BB_7 = 100.0
C_{MAX6}, C_{MCL6}, C_{MCH6}, C_{MEC6}	0.058, 0.011, 0.040, 0.041 mg/scc
E_{S1}, E_{S2}	7.0 , 2.0

B3.2 Simulation of core 1

Variables	Values
Core dimension: NX x NY x NZ	100 x 1 x 1
Grid block size: ΔX, ΔY, ΔZ	0.155 x 3.37 x 3.37 cm
Absolute permeability	$K_X = K_Y = K_Z = 108$ md
Porosity	0.179
Reservoir top	0 cm
Initial pressure	$P_i = 14.7$ psi
Connate and initial water saturation	$S_{wc} = 0.60$, $S_{wi} = 0.34$
Waterflood residual oil saturation	$S_{or} = 0.39$
Brine and oil viscosity	$\mu_w = 1.0$ cp , $\mu_o = 6.0$ cp
Effective end point water and oil permeability	$K_{o,eff}$ =65 md, $K_{w,eff}$ =30 md
Corey's exponent for water and oil relative permeability	n = 2.5, m= 1.5
JF-2 bio-surfactant concentration, C_6	$C_6 = 0.011$ mg/scc
Polymer concentration, C_7	$C_7 = 1.0$ mg/scc
NaCl concentration, C_{11}	$C_{11} = 50.0$ mg/scc
Shear rate at half original viscosity	$\gamma_{1/2} = 25$ sec^{-1}
Surfactant injection rate	$Q_{inj} = 5.14$ cc/hr
Volume of surfactant treatment	1.0 PV

B3.3 Simulation of experiment Core 2

Variables	Values
Core dimension: NX x NY x NZ	100 x 1 x 1
Grid block size: ΔX, ΔY, ΔZ	0.155 x 3.37 x 3.37 cm
Absolute permeability	$K_X = K_Y = K_Z = 72.2$ md
Porosity	0.182
Reservoir top	0 cm
Initial pressure	$P_i = 14.7$ psi
Connate and initial water saturation	$S_{wc} = 0.422$, $S_{wi} = 0.61$
Waterflood residual oil saturation	$S_{or} = 0.39$
Brine and oil viscosity	$\mu_w = 1.0$ cp , $\mu_o = 6.0$ cp
Effective end point water and oil permeability	$K_{o,eff}$ =45 md, $K_{w,eff}$ =24 md
Corey's exponent for water and oil relative permeability	n = 2.5, m= 1.5
JF-2 bio-surfactant concentration, C_6	$C_6 = 0.011$ mg/scc
Polymer concentration, C_7	$C_7 = 1.0$ mg/scc
NaCl concentration, C_{11}	$C_{11} = 50.0$ mg/scc
Shear rate at half original viscosity	$\gamma_{1/2} = 25$ sec^{-1}
Surfactant injection rate	$Q_{inj} = 5.14$ cc/hr
Volume of surfactant treatment	1.0 PV

B3.4 Simulation of experiment Core 3

Variables	Values
Core dimension: NX x NY x NZ	100 x 1 x 1
Grid block size: ΔX, ΔY, ΔZ	0.155 x 3.37 x 3.37 cm
Absolute permeability	$K_X = K_Y = K_Z = 103.7$ md
Porosity	0.1841
Reservoir top	0 cm
Initial pressure	$P_i = 14.7$ psi
Connate and initial water saturation	$S_{wi} = 0.632$, $S_{wc} = 0.387$
Waterflood residual oil saturation	$S_{or} = 0.368$
Brine and oil viscosity	$\mu_w = 1.0$ cp , $\mu_o = 6.0$ cp
Effective end point water and oil permeability	$K_{o,eff}$ =65 md, $K_{w,eff}$ =30 md
Corey's exponent for water and oil relative permeability	n = 2.5, m= 1.5
JF-2 bio-surfactant concentration, C_6	$C_6 = 0.011$ mg/scc
Polymer concentration, C_7	$C_7 = 1.0$ mg/scc
NaCl concentration, C_{11}	$C_{11} = 50.0$ mg/scc
Shear rate at half original viscosity	$\gamma_{1/2} = 25$ sec^{-1}
Surfactant injection rate	$Q_{Surf,inj} = 5.14$ cc/hr
Volume of surfactant treatment	2.0 PV

B3.5 Simulation of experiment Core 4

Variables	Values
Core dimension: NX x NY x NZ	100 x 1 x 1
Grid block size: ΔX, ΔY, ΔZ	0.155 x 3.37 x 3.37 cm
Absolute permeability	$K_X = K_Y = K_Z = 40.5$ md
Porosity	0.13
Reservoir top	0 cm
Initial pressure	$P_i = 14.7$ psi
Connate and initial water saturation	$S_{wc} = 0.752$, $S_{wi} = 0.37$
Waterflood residual oil saturation	$S_{or} = 0.248$
Brine and oil viscosity	$\mu_w = 1.0$ cp , $\mu_o = 6.0$ cp
Effective end point water and oil permeability	$K_{o,eff}$ =20.8 md, $K_{w,eff}$ =5.1 md
Corey's exponent for water and oil relative permeability	n = 2.5, m= 1.5
JF-2 bio-surfactant concentration, C_6	$C_6 = 0.021$ mg/scc
Polymer concentration, C_7	$C_7 = 1.0$ mg/scc
NaCl concentration, C_{11}	$C_{11} = 50.0$ mg/scc
Shear rate at half original viscosity	$\gamma_{1/2} = 30$ sec^{-1}
Surfactant injection rate	$Q_{Surf,inj} = 5.14$ cc/hr
Volume of surfactant treatment	1.0 PV

B3.6 Simulation of experiment Core 5

Variables	Values
Core dimension: NX x NY x NZ	100 x 1 x 1
Grid block size: ΔX, ΔY, ΔZ	0.155 x 3.37 x 3.37 cm
Absolute permeability	$K_X = K_Y = K_Z = 26.5$ md
Porosity	0.2289
Reservoir top	0 cm
Initial pressure	$P_i = 14.7$ psi
Connate and initial water saturation	$S_{wc} = 0.551$, $S_{wi} = 0.849$
Waterflood residual oil saturation	$S_{or} = 0.151$
Brine and oil viscosity	$\mu_w = 1.0$ cp , $\mu_o = 6.0$ cp
Effective end point water and oil permeability	$K_{o,eff}$ =14.3 md, $K_{w,eff}$ =8.3 md
Corey's exponent for water and oil relative permeability	n = 2.5, m= 1.5
JF-2 bio-surfactant concentration, C_6	$C_6 = 0.041$ mg/scc
Polymer concentration, C_7	$C_7 = 1.0$ mg/scc
NaCl concentration, C_{11}	$C_{11} = 50.0$ mg/scc
Shear rate at half original viscosity	$\gamma_{1/2} = 35$ sec^{-1}
Surfactant injection rate	$Q_{Surf,inj} = 3.14$ cc/hr
Volume of surfactant treatment	1.0 PV

B3.7 Simulation of experiment Core 6. Plain PHPA solution.

Variables	Values
Core dimension: NX x NY x NZ	100 x 1 x 1
Grid block size: ΔX, ΔY, ΔZ	0.155 x 3.37 x 3.37 cm
Absolute permeability	$K_X = K_Y = K_Z = 240$ md
Porosity	0.187
Reservoir top	0 cm
Initial pressure	$P_i = 14.7$ psi
Connate and initial water saturation	$S_{wc} = 0.439$, $S_{wi} = 0.639$
Waterflood residual oil saturation	$S_{or} = 0.361$
Brine and oil viscosity	$\mu_w = 1.0$ cp , $\mu_o = 6.0$ cp
Effective end point water and oil permeability	$K_{o,eff}$ =160 md, $K_{w,eff}$ =80 md
Corey's exponent for water and oil relative permeability	n = 2.5, m= 1.5
JF-2 bio-surfactant concentration, C_6	$C_6 = 0.0$ mg/scc
Polymer concentration, C_7	$C_7 = 1.0$ mg/scc
NaCl concentration, C_{11}	$C_{11} = 50.0$ mg/scc
Shear rate at half original viscosity	$\gamma_{1/2} = 25$ sec^{-1}
Surfactant injection rate	$Q_{Surf,inj} = 6.4$ cc/hr
Volume of surfactant treatment	1.0 PV

B3.8. The core data for these simulations used data given in **B3.1** and **B3.2**. The only variables that are different are the surfactant injection rate, $Q_{Surf,inj}$, and the number of pore volumes injected. The surfactant injection rate increased from 5.14 to 6.4 and 12.0 cc/hr. The number of pore volumes of surfactant injected in each case was 4.0 PV's.

Variables	Values
Core dimension: NX x NY x NZ	100 x 1 x 4
Surfactant injection rate	$Q_{Surf,inj}$ = 5.14, 6.4, 12.0 cc/hr
Volume of surfactant treatment	4.0 PV